This document is organized as follows:

(1) Author Response to RC1
(2) Author Response to RC2
(3) Marked-up version of manuscript

*Note: The author responses below are the updated versions of the responses posted in the ACP Interactive Discussion, under AC1 and AC2, on 1 May 2020.

**Author Response to RC1**

We appreciate the thoughtful and detailed review from Referee 1. We have taken the comments made by Referee 1 into careful consideration and they have helped improve our manuscript.

The general format of this response is as follows:

- Reviewer comments are in bold and labeled as (N.1), where N is the number of the comment block.
- Author response to comments are in regular, non-bolded text, and labeled as (N.2).
- Modifications in the manuscript are described in italics and labeled as (N.3).

==========

(1.1)

**Unless I have misunderstood something, the core conclusions of this paper regarding coatings with ageing timescales seem to be based on the assumption that both urban and biomass burning BC are emitted with thin coatings. However, there is much evidence to the contrary, as most SP2 measurements of biomass burning at or near source would indicate that they have thick coatings at the point of emission. Furthermore, the thickness of this coating can vary significantly fire to fire (see https://www.atmos-chem-phys.net/14/10061/2014/ https://www.nature.com/articles/ngeo2901, https://www.atmos-chem-physdiscuss. net/acp-2019-157/). It therefore doesn't seem correct to infer conclusions regarding the effect of ageing timescales on coating thicknesses when comparing aerosols from different sources. The authors should review their findings taking this into consideration.**

(1.2)

We agree that that it was presumptive and largely erroneous to make blanket statements about coating thickness without properly taking the emission source(s) into account. As the reviewer noted, we agree that the existing literature shows overwhelming evidence that biomass burning rBC particles are quickly coated after being emitted, and that they are, on

average, significantly more coated than urban rBC particles of comparable atmospheric age. We made major revisions to section 3.7 (formerly section 3.6) and shifted the focus away from the aging timescale. The focus is now on the differences in mixing state during different identifiable source impacts (e.g., biomass burning versus urban). We left some discussion in the manuscript about the effects of aging on mixing state, but we made sure to keep comparisons consistent between the same source or mix of sources.

(1.3)

*See section 3.7 (formerly section 3.6) for major revisions shown in tracked changes. Please also see the Supplement for additional information on source attribution and also new additional analysis including measurements of levoglucosan (i.e., a good tracer for biomass burning) and lidar data from CALIPSO.*

==========

(2.1)

**The conclusions section is long but mainly seems to recap the earlier observations rather than focus on the key scientific advancements being offered by this work. In order to properly judge this aspect of the paper and therefore its suitability for publication, this should be restructured.**

(2.2)

We agree that the conclusion should be restructured and focused on the most salient "key scientific advancements" rather than merely "recapping earlier observations." That being said, we also believe that recapping key observations and details in the conclusion section may be valuable to readers who might be quickly reading through the paper, trying to glean the most important take-away points from the abstract and/or conclusion.

Regarding significant changes to the conclusion, we have added clarification to the key scientific advancements. These key points have been slightly modified in light of comment (1.1) and additional comments from Referee 2. In addition, some extraneous details have been stripped from the conclusion as suggested. The main conclusion points of the manuscript are summarized below.

(2.3)

*Conclusion Point 1: The rBC size distribution was strongly affected by the emission source type. rBC particles measured during periods when biomass burning emissions were dominant ($BC_{bb}$) had larger rBC core diameters (CMD ~ 120 nm) relative to rBC particles measured during time periods dominated by urban emissions ($BC_{ff}$) (CMD ~ 100 nm). rBC particles from well-aged, background air masses ($BC_{aged,bg}$) were characterized by an MMD ~ 115 nm, which likely reflects a mix of large-scale transported BC from unidentified biomass burning and urban emissions.*

*Conclusion Point 2: $BC_{ff}$ were found to be either uncoated or very thinly coated, with mean $CT_{BC}$ less than ~15 nm and average $f_{BC}$ less than ~0.15.*

*Conclusion Point 3: $BC_{bb}$ had thicker coatings overall, with mean $CT_{BC}$ ranging from ~40 to 70 nm and $f_{BC}$ ranging from ~0.23 to 0.47.*

*Conclusion Point 4: $BC_{aged,bg}$ were found to have moderately thick coatings, with mean $CT_{BC}$ of ~60 nm and $f_{BC}$ of ~0.27.*

*Conclusion Point 5: Timescales of less than 24 hours were too short to significantly coat rBC from urban emissions. This is in direct contrast to biomass burning rBC, which has been shown in previous works to acquire thick coatings within hours or even minutes, near the source of emission.*

*Conclusion Point 6: Aged rBC from biomass burning sources were generally more thickly coated, although the time evolution of the mixing state could not be quantified directly over the duration of transport. Periods of "fresh" biomass burning impacts were characterized by slightly thinner $CT_{BC}$ compared to aged biomass burning rBC particles (e.g., L3 vs. L8), but larger $CT_{BC}$ compared to fresh urban rBC particle (e.g., L3 vs. L4). This agrees with previous studies that have also observed thicker coatings in fresh biomass burning rBC relative to fresh urban rBC. The overall larger $CT_{BC}$ for aged biomass burning rBC relative to fresh biomass burning rBC indicates that there is significant coating formation that occurs between the timescale of ~1 day to ~1 week for biomass burning rBC, even after rapid coating formation that occurs soon after emission. An important caveat is that $CT_{BC}$ of biomass burning rBC may not be monotonically increasing over time. Past studies have observed rapid coating of biomass burning rBC within less than one day to more than 100 nm, but we observed a median $CT_{BC}$ of ~48 nm for L3, which suggests that $CT_{BC}$ for biomass burning rBC might decrease at some point during atmospheric transport and then increase later at longer timescales (e.g., median $CT_{BC}$ ~54 nm for L9). We make no definitive claims about the rate of change of $CT_{BC}$ for biomass burning rBC throughout atmospheric transport since we only observed the $CT_{BC}$ from a single discrete point in space, but our measurements do suggest that $CT_{BC}$ for Southern California biomass burning rBC were generally lower than $CT_{BC}$ for Northern California biomass burning rBC.*

*Conclusion Point 7: The high variability of the rBC measurements on Catalina Island during three different campaigns demonstrates how meteorology, emissions source type, and atmospheric aging can drastically affect the physical properties and mixing state of the broader BC population within the same region.*

*See the updated manuscript (with track changes) for comprehensive view of changes made in the Conclusion section.*

==========

(3.1)

**Measurements of coating thickness can become biased if the particles are sufficiently small that the signal-to-noise ratios of the instrument's scattering channels aren't sufficient to successfully retrieve a coating thickness or a delay time. Was the rate of failed retrievals monitored? How was this reflected in the data?**

(3.2)

To minimize the signal-to-noise ratio for the LEO analysis, we only mainly considered LEO-fits for particles with rBC core diameters between 200 and 250 nm (as mentioned in Section 2.7). For the particular SP2 unit used in our study, Krasowsky et al. found that a lower threshold of 200 nm was sufficient to reduce the scattering signal-to-noise ratio (Krasowsky et al., 2018). Previous work by Taylor et al. (2014) defined a lower bound of 135 nm for LEO fitting, which corresponds to a 50% fraction of rBC with detectable split-detector notch position. We chose an even more conservative lower bound of 200 nm in this study to further minimize the scattering signal noise. The 250 nm upper bound is also conservative, considering that previous studies have reported LEO-fit coating thicknesses for particles with rBC core diameters up to 290 nm (Dahlkötter et al., 2014). To check for potential biases due to the saturation of the scattering signal at larger rBC diameters, a subset of the SP2 data (from 7 September 2017) was assessed to see what proportion of the low-gain scattering channel data were saturated. None of the particles (in this subset of data) with rBC core diameters under 250 nm were found to have saturated scattering signals. The fraction of rBC-containing particles that were selected for LEO-fitting (with respect to all rBC particles measured) was not explicitly reported in the manuscript, but the total number of particles analyzed in each LEO period was listed in Table 2. A number of previous studies have also reported only the size range of LEO-fit rBC particles, without explicitly stating the fraction of particles that were LEO-fit versus not LEO-fit. We think that including the size range of the LEO-fit particles and the total number of particles analyzed in the manuscript is sufficient to show that we adequately constrained noise in the scattering signal and also analyzed enough particles to produce robust coating thickness statistics for the L1 to L10 analysis. Other rBC core size intervals were considered and further explanation is provided in the new text shown below (from section 2.7 in manuscript).

For the lag-time (delay time) analysis, a lower threshold of 170 nm was implemented for rBC core diameters. The reasoning for the lower limit is the same as explained above. The only difference is that we relaxed the lower threshold a bit (compared to 200 nm) because the accuracy of the scattering signal is not as crucial to the binary categorization of rBC-containing particles as "thickly-coated" versus "thinly-coated." Previous studies have conducted the delay time analysis with similar size ranges, or even lower thresholds (Krasowsky et al., 2018; Shiraiwa et al., 2007; McMeeking et al., 2011; Moteki and Kondo, 2007; and more).

(3.3)

*A sentence will be added to Section 2.6 to clarify that the lower threshold for rBC core diameter was set to 170 nm for the lag-time (delay time) method.*

*"Only particles with an rBC core diameter greater than 170 nm were included in the calculation of $f_{BC}$ to account for the scattering detection limit of the instrument."*

*"In this study, the LEO "fast-fit" method was used with three points, and particles analyzed were restricted to those with rBC core diameters between 180 and 300 nm. Although the SP2 has been reported to accurately measure the volume equivalent diameter (VED) of scattering particles down to ~170 nm, a more conservative lower threshold of 180 nm was used for our study to reduce instrument noise at smaller VED values near the detection limit (Krasowsky et al., 2018). Specific rBC core diameter ranges were used for different analyses in this study and these ranges are explicitly defined within each respective discussion. One exception was made to the 180–300 nm rBC core diameter restriction in section 3.7. For the analyses and discussion presented in section 3.7, the LEO coating thickness was calculated for all detectable rBC particles with non-saturated scattering signals. The rBC core size was not restricted in this section because the relative comparisons between characteristic coating thickness values were more important for the analysis, rather than the absolute value (which would likely be biased, as discussed further in section 3.8). In other words, the LEO-derived coating thickness values in section 3.7 were not used to report representative averages for selective time periods, but rather were used for comparative and/or qualitative purposes."*

==========

(4.1)

**Setting 'calm' winds as zero on direction on figure 5 makes no sense as this also corresponds to north. The periods should probably be blanked out instead.**

(4.2)

Calm winds have been removed from the wind direction plot as suggested.

(4.3)

*See updated Figure 5.*

==========

(5.1)

**The points plotted on figure S9 should be individually identified according to event.**

(5.2)

Figure S9 (now Figure 12) has been modified to show the scatter between coating thickness and rBC core diameter for all measurements. 1-minute mean values for both coating thickness and rBC core diameter are used for the scatter plot. A statistically significant positive correlation was found and is shown on the figure ($r = 0.5397$ with p-value $<0.001$).

(5.3)

*See updated Figure S9 (now Figure 12 in main manuscript).*

==========

References


Dahlkötter, F., Gysel, M., Sauer, D., Minikin, A., Baumann, R., Seifert, P., Ansmann, A., Fromm, M., Voigt, C. and Weinzierl, B.: The Pagami Creek smoke plume after long-range transport to the upper troposphere over Europe - Aerosol properties and black carbon mixing state, Atmos. Chem. Phys., 14(12), 6111–6137, doi:10.5194/acp-14-6111-2014, 2014.

Krasowsky, T. S., Mcmeeking, G. R., Sioutas, C. and Ban-Weiss, G.: Characterizing the evolution of physical properties and mixing state of black carbon particles: From near a major highway to the broader urban plume in Los Angeles, Atmos. Chem. Phys., 18(16), 11991–12010, doi:10.5194/acp-18-11991-2018, 2018.

McMeeking, G. R., Good, N., Petters, M. D., McFiggans, G. and Coe, H.: Influences on the fraction of hydrophobic and hydrophilic black carbon in the atmosphere, Atmos. Chem. Phys., 11(10), 5099–5112, doi:10.5194/acp-11-5099-2011, 2011.

Moteki, N., Kondo, Y., Miyazaki, Y., Takegawa, N., Komazaki, Y., Kurata, G., Shirai, T., Blake, D. R., Miyakawa, T. and Koike, M.: Evolution of mixing state of black carbon particles: Aircraft measurements over the western Pacific in March 2004, Geophys. Res. Lett., 34(11), doi:10.1029/2006GL028943, 2007.

Shiraiwa, M., Kondo, Y., Moteki, N., Takegawa, N., Miyazaki, Y. and Blake, D. R.: Evolution of mixing state of black carbon in polluted air from Tokyo, Geophys. Res. Lett., 34(16), 2–6, doi:10.1029/2007GL029819, 2007.

**Author Response to RC2**

We appreciate the thoughtful and detailed review from Referee 2. We have taken the comments made by Referee 2 into careful consideration and they have helped improve our manuscript.

The general format of this response is as follows:

- Reviewer comments are in bold and labeled as (N.1), where N is the number of the comment block.
- Author response to comments are in regular, non-bolded text, and labeled as (N.2).
- Modifications in the manuscript are described in italics and labeled as (N.3).

==========

(1.1)

**Major comments regarding source attribution and estimated plume age**

(1.2)

We agree with the reviewer that the source attribution and plume age sections of the manuscript required some major revisions (e.g., section 3.7, formerly section 3.6). We now shift our focus towards comparing the mixing state during different known source impacts, rather than focusing on the plume age. As the reviewer notes, rBC from biomass burning (BB) is coated much more quickly than rBC from urban emissions, and BB rBC has also been observed to have thicker coating overall compared to its urban counterpart.

We would like to address the nuances associated with the specific concerns that the reviewer raises in the comment.

Regarding biomass burning source attribution:

First, we wanted to clarify that we are not definitively attributing ~10 nm coating thickness values to fresh BB rBC particles, and we changed the language in the revised text to make this clear. ~10 nm was the median coating thickness from a population of aerosols that had a larger spread of individual coating thickness values. The coating thickness values on the higher end of the distribution tail (and outliers) are likely attributable to the BB impacts. We clarified in the new text that the peaks in the 2$^{nd}$ campaign (e.g., L4) were likely dominated by urban emissions, but that we could not exclude the likely impact of BB emissions mixing into the broader urban plume. In fact, we still believe that biomass burning did impact our measurements to some degree, even if it was a minor fraction of total sampled rBC. In particular, the Thomas Fire was one of the largest fires in California history, and it was still active during the 2$^{nd}$ campaign (20-22 December 2017). With the center of the Thomas Fire less than 150 km away, and strong atypical Santa Ana winds recorded before and during the time

of measurements, it is hard to imagine BB having no impact on the regional rBC loading at the time. In addition to geographic proximity and meteorology, the air quality monitoring stations in Santa Barbara, Ventura, and Los Angeles all recorded elevated concentrations of $PM_{2.5}$ right around this time period. Additionally, as part of the new supplemental analysis, the HYSPLIT dispersion model was run to simulate the plume dispersion of multiple active fires during the December 2017 campaign. The HYSPLIT dispersion model shows the plumes from the Thomas Fire and several other smaller Southern California fires directly impacting the point of measurement (Catalina Island). These results are included in the revised Supplement. We also added a new qualitative analysis in the Supplement using CALIPSO lidar transects in the Southern California region during the 20-22 December period. From the CALIPSO transects we observed aerosols that were attributed to BB sources present just off the coast of Southern California around this time. This data is also shown in a new section in the Supplement.

Second, since the paper was first submitted, we have obtained levoglucosan data from November 2018 (3rd campaign) that were collected by colleagues at USC who were conducting an independent air quality study in the LA Basin (Soleimanian et al. 2020). Although the reviewer's comment was particularly focused on the L4 period, we would like to point out that the conditions during the 2nd campaign (December 2017) and the first portion of the 3rd campaign (November 2018) were quite similar. Geographically, there were multiple fires throughout the Southern California region in both campaigns (see Figure 3). Both campaigns were also characterized by Santa Ana (i.e., northerly and easterly) winds. The weekly average concentration of levoglucosan between 7 to 14 November and 15 to 22 November was 187.5 ng $m^{-3}$ and 83.89 ng $m^{-3}$, respectively. Note that the 3rd campaign took place between 12 and 18 November 2018. For reference, levoglucosan concentrations during July 2018 (non-wildfire season) ranged between ~4 and 17 ng $m^{-3}$. The elevated concentration of levoglucosan inside the LA Basin during November 2018 removes any lingering doubt that BB aerosols were mixed into the broader regional air mass that was measured on Catalina Island. Given that similar fire and meteorological conditions were present during the 2nd campaign (December 2017), we have high confidence that BB also played at least a minor role in this campaign as well.

Regarding plume age comments:

For the LEO periods mentioned (L3, L8, L9, and L10), the aging timescale range of ~days to a week was meant to serve as a range of possibility rather than an exact aging timescale. We fully acknowledge the limits of HYSPLIT, especially for complex trajectory patterns. That is exactly why we present a very general range of timescales that was based on physical distance from major sources rather than relying on the exact timing of crossovers from the back-trajectories. The reviewer also mentions the loss of rBC coating with aging. This is entirely consistent with the $CT_{BC}$ values measured during periods impacted by long range transport of biomass burning impacted air masses (e.g., L8 and L9). The median $CT_{BC}$ values were within the range of ~60-70 nm during this time period of impact from the Camp Fire. Previous airborne studies have measured average coating thickness values of ~100 nm within hours of emission within the plume. Given that our values are

significantly lower, the rBC measured in our study likely did experience coating loss at some point during transport. We added a short discussion on this topic of coating loss in the coating thickness discussion section and below in the section (1.3). Furthermore, we have added a new section that comprehensively compares our campaign measurements with past mixing state studies conducted with an SP2.

Regarding precipitation comments:

Although the data were not reported, precipitation and cloud cover were monitored throughout the campaigns. There were no precipitation events in the region during any of the measurement days, and most of the days were clear to partly cloudy.

(1.3)

*Major edits were made to section 3.5 (formerly section 3.4) and section 3.7 (formerly section 3.6). A new section 3.8 was added to comprehensively compare our results to past similar studies. Additional evidence (i.e. using CALIPSO lidar data, HYSPLIT dispersion model and levoglucosan measurements) and figures were also added to the Supplement to make our discussion on source attribution more robust. Specifically, please refer to Supplement section S2 and figures S11 through S20.*

*Revised main points regarding variability of coating thickness:*

- *Timescales of less than 24 hours were too short to significantly coat rBC from urban emissions. This is in direct contrast to biomass burning rBC, which has been shown in previous works to acquire thick coatings within hours or even minutes, near the source of emission.*
- *Aged rBC from biomass burning sources were generally more thickly coated, although the time evolution of the mixing state could not be quantified directly over the duration of transport. Periods of "fresh" biomass burning impacts were characterized by slightly thinner $CT_{BC}$ compared to aged biomass burning rBC particles (e.g., L3 vs. L8), but larger $CT_{BC}$ compared to fresh urban rBC particle (e.g., L3 vs. L4). This agrees with previous studies that have also observed thicker coatings in fresh biomass burning rBC relative to fresh urban rBC. The overall larger $CT_{BC}$ for aged biomass burning rBC relative to fresh biomass burning rBC indicates that there is significant coating formation that occurs between the timescale of ~1 day to ~1 week for biomass burning rBC, even after rapid coating formation that occurs soon after emission. An important caveat is that $CT_{BC}$ of biomass burning rBC may not be monotonically increasing over time. Past studies have observed rapid coating of biomass burning rBC within less than one day to more than 100 nm, but we observed a median $CT_{BC}$ of ~48 nm for L3, which suggests that $CT_{BC}$ for biomass burning rBC might decrease at some point during atmospheric transport and then increase later at longer timescales (e.g., median $CT_{BC}$ ~54 nm for L9). We make no definitive claims about the rate of change of $CT_{BC}$ for biomass burning rBC throughout atmospheric transport since we only observed the $CT_{BC}$ from a single discrete point in space, but our measurements do suggest that $CT_{BC}$ for Southern California biomass burning rBC were generally lower than $CT_{BC}$ for Northern California biomass burning rBC.*

==========

(2.1)

**Major comments regarding number size distribution data**

(2.2)

Although we generally acknowledge the concerns about fitting a log-normal distribution to a set of observations without a discernable peak, we also believe that the log-normal fits have value and should be reported (with associated uncertainty clearly described). First, there have been a number of past studies that have also included log-normal fits for their number size distributions, even in cases where the peak in the measured data was ambiguous. At the end of (2.2) is a comprehensive, but not exhaustive, list of studies using the SP2 that have included log-normal fits to rBC number size distributions. Full references are provided at the end of the document.

Second, the physical lower bound on BC core size makes log-normal fitting reasonable in the Aitken range, even if it is below the SP2 detection limit. Single BC nanospheres (i.e., individual spherules) have been observed to be ~20-30 nm in diameter by using TEM imaging techniques (Ellis et al., 2016; Wentzel et al., 2003). Although the detection limit of the SP2 for rBC cores is ~70 nm, it seems reasonable to assume that the peak of the rBC number size distribution in this Aitken range would be between 50 and 80 nm (Kondo et al., 2011b), given that individual BC spherules are unlikely to be smaller than 20 nm. This would naturally imply that most (if not all) BC cores in the ambient air are larger than 20 nm, but smaller than the point at which we observe a sharp increase in the slope on the right-hand side of the number size distribution. This inflection point on the right-hand side is clearly observed from SP2 data, even when the peak is not completely discernable.

Third, even if there was an unmeasured bimodal peak beyond the detection limit of the SP2, the median of the extrapolated log-normal fit would not be a completely useless metric for comparison. As long as the log-normal fitting is consistent between all instances of distributions, it would serve to characterize the Aitken mode of the rBC core size distribution, even if there was another mode lurking in the ultrafine range. This would suggest that the existence of an unknown local maxima in the ultra-fine range is possible, but that it would not invalidate the inter-comparison of Aitken mode distributions for different time intervals.

Fourth and lastly, the appropriateness of the log-normal fit is not entirely contingent upon the explicit observation of a local maxima. It might be entirely inappropriate if we saw that all the observed data points deviated sporadically from the fit curve, but we observe the fit curve describing the observed number size distribution data points very well, with fairly small residuals. We see that the rate of change of the slope is well captured by the fit, which strongly suggests that a log-normal fit is likely representative of the actual distribution. Analogously, we find the LEO-fit for coating thickness quantification as a robust method for mixing state analysis, even though we only use the leading edge of what we expect to be a Gaussian signal. Indeed, the LEO-fit uses an even smaller fraction of the expected Gaussian scattering response compared to the log-normal fits for the number size distribution. Likewise, we are using the existing “edge” of size distribution to fit what we expect to be log-normal.

To address the reviewer's concern with this issue, we made a clear caveat in the text explaining the limitations of the extrapolation, in addition to the already existing disclaimer about the lower detection limit in the first paragraph of section 3.6 (formerly section 3.5). We made it clear and explicit that the peak based on log-normal fits are not definitive measured values, but rather modeled based on reasonable assumptions about the behavior of the distribution in the Aitken range.

The typo in Figure 8 regarding the wrong median value label has also been fixed.

List of publications that have used log-normal fits to the number size distribution data:

Cheng et al., 2018; Kondo et al., 2011a; Kondo, et al., 2011b; Krasowsky et al., 2018; Metcalf et al., 2012; Moteki et al., 2012; Raatikainen et al., 2017; Reddington et al., 2013; Sahu et al., 2012; Schwarz et al., 2008; Shiraiwa et al., 2008

(2.3)

*An additional caveat has been added to section 3.5 (formerly section 3.5) in the manuscript in tracked changes to address the comments and concerns made by RC2.*

*"Figure 10 shows that log-normal fits adequately capture the measured size distributions, though we cannot rule out the possibility of another rBC mode outside the detection limits of the SP2. Although the peak of the observed points is not always discernible (e.g., number size distribution for L5 in Figure 10), it is reasonable to fit these points assuming that a log-normal distribution is a realistic representation of ambient rBC number size distributions in the Aitken mode."*

==========

(3.1)

**Major comments regarding increasing rBC diameter with atmospheric aging**

(3.2)

We agree with the reviewer that the effect of coagulation on the rBC core size is likely overplayed in the manuscript since the rBC number concentration is relatively low in the ambient air at the point of measurement, compared to the rBC number concentration very close to the source of combustion (e.g., in a tailpipe or in a BB flame). We would like to point out, however, that there is a noticeable shift in the rBC size distributions during time periods dominated by urban emissions (e.g., L4 and L5) relative to size distributions that were measured inside Los Angeles near a major highway by Krasowsky et al. (2018). This is a particularly useful comparison because the exact same SP2 was used with the same operating variables. Focusing on the number size distribution, we observe a larger count median diameter during the L4 and L5 periods compared to the count median diameters measured downwind of a highway in a polluted urban environment (Krasowsky et

al., 2018). The size distribution of rBC can only be affected by, (i) the emission source type and/or (ii) coagulation of rBC-containing particles. Related to the reviewer's comment regarding source attribution, we believe that both of these factors likely played some role in the variability of rBC core sizes. We are quite confident that BB sources did contribute, at least in part, to time periods dominated by urban emissions. (see comment block 1 above for details). So, there is likely a source effect. It seems plausible that a mixture of BB impact and coagulation (at least near the source, within the polluted urban basin), contributed to this noticeable shift in the core size distribution.

The reviewer also notes that the cited studies were conducted under higher rBC concentrations than what we encountered in our study. However, while the studies mentioned did have higher campaign-averaged concentrations, the peak concentrations were within the same magnitude, especially for the Shiraiwa et al. study (2008), which took place in the East Asia outflow. The peak magnitudes reported in Shiraiwa et al. reached ~ 1 $\mu g\ m^{-3}$, which is within a factor of two relative to the larger peaks measured in our study (~0.6 $\mu g\ m^{-3}$). Shiraiwa et al. (2008) briefly mention that coagulation could be a potential mechanism that explains why aged particles from China and Korea were larger than particles associated local urban emissions from Japan. While we agree that coagulation at measured concentrations would be slow and possibly negligible, we believe that coagulation could have played a minor role during atmospheric transport from the LA basin to Catalina Island. We make no attempt at quantifying the rate at which coagulation occurs for LA basin dominated air masses, but we qualitatively acknowledge that coagulation likely contributed to the growth of particles, as per the logic above, especially within the first few hours of aging.

(3.3)

*The focus of the paragraph mentioned by the reviewer has been shifted towards an emphasis on source-related impacts rather than impacts from atmospheric processing (i.e., coagulation). A short mention of coagulation still remains, but it serves as a qualitative acknowledgement of its likely minor effect on rBC size distributions. See section 3.6 (formerly section 3.5) for tracked changes.*

*Relevant excerpts from new text in section 3.6:*

*"A survey of past studies that have reported rBC mass median diameter (MMD) and count median diameter (CMD) shows that the source of emissions has a strong influence on rBC core diameter (Cheng et al., 2018). The MMD [CMD] for biomass burning influenced rBC, which has been reported to range from ~130 nm to 210 nm [100 to 140 nm], is generally much larger than the MMD for urban emissions influenced rBC, which has been reported to range from ~100 nm to 178 nm [38 to 80 nm] (Shiraiwa et al., 2007; Schwarz et al., 2008; McMeeking et al. 2010; Kondo et al., 2011a; Sahu et al. 2012; Metcalf et al., 2012; Cappa et al., 2012; Laborde et al., 2013; Liu et al., 2014; Taylor et al., 2014; Krasowsky et al., 2018).*

*The MMD [CMD] for aged air masses in remote regions were reported to range from ~180 nm to 225 nm [90 nm to 120 nm] (Shiraiwa et al., 2008; Liu et al, 2010; McMeeking et al., 2010; Schwarz et al., 2010).*

*Figure 11 shows the rBC MMD and CMD based on the log-normal fits for each LEO period in this study. Based on the source identification discussed in section 3.1 and section S2 in the Supplement, the MMD and CMD values in this study are generally consistent with the ranges reported in past studies. For LEO periods when measurements were strongly influenced by biomass burning emissions (L3, L8, L9, L10), MMD ranged from 149 nm to 171 nm, which is within the range of ~130 nm to 210 nm compiled from past studies. Similarly, when measurements were strongly influenced by urban emissions (L2, L4, L7), the MMD dropped, ranging from 112 nm to 129 nm. This falls within the range of ~100 nm to 178 nm previously reported for measurements of urban emissions from past studies."*

*"Another explanation for varying rBC core size is coagulation (Bond et al., 2013). Shiraiwa et al. (2008) observed an increase in rBC core diameters in aged plumes compared to fresher urban plumes, suggesting that coagulation can alter the rBC size distribution during atmospheric transport (i.e., aging). Although the emissions source type appears to be the dominant influence on rBC core sizes in our study, there is evidence to suggest that coagulation also played a role during transport from the Los Angeles basin to Catalina Island (~70 km away). For example, we observed a $MMD_{fit}$ [$CMD_{fit}$] of 112 nm [53 nm] during L4, when $BC_{ff}$ was measured. This is noticeably larger than values of 93 nm [42 nm] reported in Krasowsky et al. (2018) for measurements conducted 114 meters downwind of a major highway in Los Angeles. Furthermore, Laborde et al. (2013) observed an $MMD_{fit}$ of ~100 nm for $BC_{ff}$ in Paris, which is again lower than the value of 112 nm calculated for L4. Even though it was determined that L4 was characterized by $BC_{ff}$, we cannot rule out the effects of local wildfires influencing the size distribution as well (as explained in the Supplement section S2). While the rBC size distribution from L4 suggests that coagulation plays at least a minor role, both factors (source type and coagulation) likely influence rBC size distributions to varying degrees in areas with varying emissions source types and relatively elevated rBC concentrations (e.g., polluted urban areas).*

==========

(4.1)

**Page 1, line 18, 20. The passive voice exemplified by the use of the word "suspect". Are the author's hedging their bets? Suggest using a different - less passive - word.**

(4.2)

The wording has been changed.

(4.3)

*New text:*

*"In contrast, during periods when measured rBC was dominated by emissions from the Southern California region, both $f_{BC}$ and $CT_{BC}$ were significantly lower, with a mean $f_{BC}$ of ~0.03 and median $CT_{BC}$ ranging from ~0 to 10 nm."*

==========

(5.1)

**Page 1, lines 23-25. The author's write "we conclude that an aging timescale on the order of ~hours is not long enough for rBC to become thickly coated under the range of sources sampled and atmospheric conditions during this campaign." This is misleading as several papers that have studied biomass burning (and those currently under review and data currently being analyzed) have (and are) showing that rBC particle become thickly coated very quickly. While this might be true for urban plumes, it certainly is not for BB (biomass burning) plumes. Please clarify.**

(5.2)

We agree with the reviewer and we have changed the main conclusions of our paper to reflect this. Further response to this specific issue has been discussed in more detail above in comment block 1.

(5.3)

*Any text related to the generalization of thin coatings for particles aged less than 24 hours has either been removed or modified.*

*This was also discussed in greater detail in comment block 1 and applicable changes have been made in sections 3.5 and 3.7 (formerly sections 3.4 and 3.6).*

==========

(6.1)

**Page 2, lines 43-44. The author's write "BC is emitted mostly as an "external" mixture, physically separated from other aerosol species." This is a bit misleading. It is very dependent upon when the plume is sampled. With respect to biomass burning, research has shown that rBC becomes coated within the first few minutes following generation due to the chemical richness of the smoke plumes.**

**Please reword to reflect this.**

(6.2)

We acknowledge that BC can become coated very quickly and that this statement could potentially be misleading. The original intent was to give a conceptual overview of externally versus internally mixed BC. The description has been altered to remove any ambiguities regarding emission point and timescale since emission.

(6.3)

*The text in the introduction (section 1) has been altered to describe the two general types of mixing state without potentially misleading readers into believing that all BC is uncoated in the near-field plume.*

*"A BC particle that is physically separate from other non-BC aerosol species is considered externally mixed. On the other hand, BC is considered internally mixed if it is physically combined with another non-BC aerosol species (Bond et al., 2006; Schwarz et al., 2008a). As freshly emitted BC particles are transported in the atmosphere, they can obtain inorganic and organic coatings from either gaseous pollutants that condense onto the BC, oxidation reactions on the BC surface, or the coalescence of other aerosol species onto the BC, making them more internally mixed (He et al., 2015). In general, the mixing state of BC describes the degree to which BC is internally mixed (Bond et al., 2013). The BC mixing state near the point of emission as well as the evolution during aging in the atmosphere of the mixing state can vary widely, depending on the source of emissions and atmospheric context.*

==========

(7.1)

**Page 3, line 74 and 75. The authors need to be very disciplined in their use of "mixing state", as one can be describing the aerosol mixing state (e.g., external vs internal) or the particle mixing state (e.g., coated or uncoated rBC). Yes, the authors sort of point this out on page 2 (lines 48-50) but then start interchanging "internal mixing state" with mixing state. For example, on the opening sentence of the cited paragraph, are the authors referring to the internal mixing state or the aerosol mixing state? Later in this paragraph, the authors reference internal mixing state of rBC (line 80). Please ensure consistency.**

(7.2) We acknowledge this potential for confusion and changed the language throughout the manuscript to ensure consistency. For the sake of simplicity and consistency, we initially define externally mixed BC as "uncoated BC" and internally mixed BC as "coated BC." Furthermore, we use the general term "mixing state," to refer to the extent to which BC is coated, either at an individual particle level or aggregated (i.e., sample population-wide) level.

(7.3)

*We edited the text to ensure consistency between any language describing the mixing state. This topic was also discussed in comment block 6 above.*

==========

(8.1)

**Page 3, lines 74 - 75. Here are two additional references to the use of microscopy with quantifying rBC mixing state that the authors are encouraged to consider: Adachi, K., Chung, S. H., and Buseck, P. R.: (2010) Shapes of soot aerosol particles and= implications for their effects on climate, J. Geophys. Res. Atmos., 115. Adachi, K., Moteki, N., Kondo, Y., and Igarashi, Y.: (2016) Mixing states of light-absorbing particles measured using a transmission electron microscope and a single-particle soot photometer in Tokyo, Japan, JGR.,121, 9153–9164.**

(8.2)

Thank you for the references and suggestion. They have been added to the manuscript.

(8.3)

*These references have been added to the introduction of the manuscript where microscopy is briefly mentioned.*

==========

(9.1)

**Page 3, lines 80 - 83. Authors are encouraged to review (include) the work by Sedlacek et al., who investigated the utility of the SP2 lagtime methodology [Investigation of Refractory Black Carbon-Containing Particle Morphologies Using the Single-Particle Soot Photometer (SP2) (2015) Aero. Sci. Tech., 49:872]**

(9.2)

Thank you for the suggestion. We have incorporated this reference into our study and expanded on our analysis by including discussion about negative la-times and rBC morphology in the discussion section. See also (11.1) below, which is related to this comment.

(9.3)

*See section 3.4 on negative lag-times and rBC morphology for newly inserted analysis and discussion.*

*Excerpt from new text:*

*"In this study, we observed negative lag-times, although at a relatively low rate, with $f_{lag,neg}$ calculated to be much less than 0.1 throughout most of the measurement periods. We defined $f_{lag,neg}$ to be identical to the "fraction of near surface rBC particles" metric used by Sedlacek et al. (2012), using a lag-time threshold of -1.25 μs to account for uncertainties*

*associated with the lag-time determination. The campaign-wide $f_{lag,neg}$ was 0.017 for the first campaign (September 2017), 0.018 for the second campaign (December 2017), and 0.026 for the third campaign (November 2018). Comparatively, Dahlkötter et al. (2014) observed $f_{lag,neg}$ of ~0.046 during an airborne field campaign measuring an aged biomass burning plume, and additionally calculated a higher fragmentation rate of ~0.4 to 0.5, based on their aforementioned alternative method (Laborde et al., 2012). Sedlacek et al. (2012) reported $f_{lag,neg}$ > 0.6 for ground-based measurements of a biomass burning plume in Long Island, New York, originating from Lake Winnipeg, Canada."*

*See new section 3.4 in manuscript for full details regarding negative lag-times and rBC morphology.*

==========

(10.1)

**Page 3, line 83. The authors are encouraged to review (include) the work by Moteki and Kondo who have also contributed significantly to improving the quantification of the rBC mixing state [Method to measure time-dependent scattering cross sections of particles evaporating in a laser beam (2008) J. Aer. Sci. 39:348].**

(10.2)

Thank you for the suggestion. This study was not initially included in the manuscript because the method described in Moteki and Kondo (2008) was not used for our mixing state analysis. Nevertheless, we have added the reference in the initial description of the LEO method because of its relevance to the Gao et al. (2007) method, which we used in our study.

(10.3)

*The reference has been added to section 2.7 in the manuscript.*

==========

(11.1)

**Page 9, lines 226 - 228. The authors might consider reviewing (including) the work by Sedlacek et al., who looked at the SP2 lagtime for a biomass burn plume. [Determination of and Evidence for Non-core-shell structure of particles containing black carbon using the single particle soot photometer (SP2). (2012) GRL. 39]**

(11.2)

Thank you for the suggested work. We have added an additional short section about the morphology of rBC in the results and discussion section of the manuscript, and we use the same near-surface fraction analysis that Sedlacek et al. (2012) employed in their study. The reference has been added as well.

(11.3)

*See section 3.4 on negative lag-times and rBC morphology for newly inserted analysis. Also see comment block 9 above for related discussion.*

==========

(12.1)

**Page 10, Line 266. As highlighted earlier, please refrain from relying on a passive voice (e.g, "suspect".)**

(12.2)

Passive voice removed.

(12.3)

*The word "suspect" has been removed from referenced text.*

==========

(13.1)

**Page 12: The authors show the back trajectories for each day of the campaign. Why not put this figure in the supplemental and, instead, show those trajectories for the specific periods under discussion. This would make it easier to evaluate the HYSPLIT datasets.**

(13.2)

Thank you for the suggestion. Although we see the value in the suggestion, we prefer to leave Figure 3 in its current state and add a *separate* HYSPLIT figure either in Section 3.7 or in the Supplement. Our reason for showing all the trajectories in Figure 3 is to show the campaign-wide perspective on the source locations of the particles. We also thought it would be useful for visually comparing between the different campaigns, and not just for 10 to 15-minute LEO time periods, which give limited snapshots instead of showing a broader campaign-wide "fingerprint" of trajectories.

(13.3)

*Additional figure with only LEO period back-trajectories has been added to the Supplement. This can also be added to Section 3.7 if it is determined to be more appropriate there.*

==========

(14.1)

**Page 14 line 307. The authors reference Figure S9, but I think they mean S8?**

(14.2)

Thank you for catching this typo.

(14.3)

*Changed from Figure S9 to Figure S8.*

==========

(15.1)

**Page 15, lines 337 - 344. The authors are encouraged to review paper by Subramanian et al., [(2010) Black carbon over Mexico: the effect of atmospheric transport on mixing state, mass absorption cross-section, and BC/CO ratios ACP 10] where attention is drawn specifically to figures 3, 12 and 13.**

(15.2)

Thank you for the paper suggestion. The figures you suggested were carefully reviewed and they were helpful in putting our results in context of past studies like Subramanian et al. (2010). Brief comparisons are made to the results presented in Subramanian et al. (2010) to our results. Reference to the article has also been added to the manuscript.

(15.3)

*See minor additions in Section 3.3 and Section 3.7.*

==========

(16.1)

**Page 22, lines 507 - 508. As highlighted above, this reviewer has concerns regarding the estimated plume ages.**

(16.2)

Appropriate changes have been made to the main conclusions from this paper, as described in more detail in Comment 1.1 above. Most importantly, all blanket statements regarding an aging timescale of more than one day required for thick coating have been altered or removed.

(16.3)

*See revised manuscript for tracked changes. Specifically section 3.7 and section S2 in the Supplement.*

==========

(17.1)

**Supplemental: page 1. As noted earlier, there is no table 3 in the main manuscript.**

(17.2)

The table was accidently omitted. Apologies for any confusion.

(17.3)

*Table 3 has been merged with Table 2. The old Table 3 is now part of Table 2.*

==========

(18.1)

**Supplemental: page 1, line 7. Suggest that the authors review Lund et al., [(2018) Short Black Carbon lifetime inferred from a global set of aircraft observations, npj Climate and Atmospheric Science 1, 31 doi:10.1038/s41612-018-0040-x]**

(18.2)

Thank you for the suggested article. The mean BC lifetime of ~4 days over the Pacific as suggested by Lund et al. (2018) further supports our estimated range of source-to-receptor timescales. We would like to clarify here that our loosely restrained timescales are only meant to give readers an idea of the range of possibilities regarding how long measured particles were transported in the atmosphere. Since the estimated value of ~4 days was meant to represent the mean, individual particles measured during our campaigns could certainly have been aged longer (i.e. ~week).

(18.3)

*Citation added to text.*

==========

(19.1)

**Supplemental: page 7. This is a stylist comment. Would suggest using a different color to denote the sample location on Catalina Island. The currently used green color is hard to discern with the yellow star.**

(19.2)

Style change made as suggested.

(19.3)

*Green circle removed from the figure as it was unnecessary.*

==========

References


Cappa, C. D., Onasch, T. B., Massoli, P., Worsnop, D. R., Bates, T. S., Cross, E. S., Davidovits, P., Hakala, J., Hayden, K. L., Jobson, B. T., Kolesar, K. R., Lack, D. A., Lerner, B. M., Li, S. M., Mellon, D., Nuaaman, I., Olfert, J. S., Petäjä, T., Quinn, P. K., Song, C., Subramanian, R., Williams, E. J. and Zaveri, R. A.: Radiative absorption enhancements due to the mixing state of atmospheric black carbon, Science (80-. )., 337(6098), 1078–1081, doi:10.1126/science.1223447, 2012.

Cheng, Y., Li, S. M., Gordon, M. and Liu, P.: Size distribution and coating thickness of black carbon from the Canadian oil sands operations, Atmos. Chem. Phys., 18(4), 2653–2667, doi:10.5194/acp-18-2653-2018, 2018.

Ellis, A., Edwards, R., Saunders, M., Chakrabarty, R. K., Subramanian, R., Timms, N. E., van Riessen, A., Smith, A. M., Lambrinidis, D., Nunes, L. J., Vallelonga, P., Goodwin, I. D., Moy, A. D., Curran, M. A. J. and van Ommen, T. D.: Individual particle morphology, coatings, and impurities of black carbon aerosols in Antarctic ice and tropical rainfall, Geophys. Res. Lett., 43(22), 11,875-11,883, doi:10.1002/2016GL071042, 2016.

Kondo, Y., Matsui, H., Moteki, N., Sahu, L., Takegawa, N., Kajino, M., Zhao, Y., Cubison, M. J., Jimenez, J. L., Vay, S., Diskin, G. S., Anderson, B., Wisthaler, A., Mikoviny, T., Fuelberg, H. E., Blake, D. R., Huey, G., Weinheimer, A. J., Knapp, D. J. and Brune, W. H.: Emissions of black carbon, organic, and inorganic aerosols from biomass burning in North America and Asia in 2008, J. Geophys. Res. Atmos., 116(8), 1–25, doi:10.1029/2010JD015152, 2011a.

Kondo, Y., Sahu, L., Moteki, N., Khan, F., Takegawa, N., Liu, X., Koike, M. and Miyakawa, T.: Consistency and traceability of black carbon measurements made by laser-induced incandescence, thermal-optical transmittance, and filter-based photo-absorption techniques, Aerosol Sci. Technol., 45(2), 295–312, doi:10.1080/02786826.2010.533215, 2011b.

Krasowsky, T. S., Mcmeeking, G. R., Sioutas, C. and Ban-Weiss, G.: Characterizing the evolution of physical properties and mixing state of black carbon particles: From near a major highway to the broader urban plume in Los Angeles, Atmos. Chem. Phys., 18(16), 11991–12010, doi:10.5194/acp-18-11991-2018, 2018.

Liu, D., Flynn, M., Gysel, M., Targino, A., Crawford, I., Bower, K., Choularton, T., Jurányi, Z., Steinbacher, M., Hüglin, C., Curtius, J., Kampus, M., Petzold, A.,Weingartner, E., Baltensperger,

U., and Coe, H.: Single particle characterization of black carbon aerosols at a tropospheric alpine site in Switzerland, Atmos. Chem. Phys., 10, 7389–7407, https://doi.org/10.5194/acp-10-7389-2010, 2010.

Liu, D., Allan, J. D., Young, D. E., Coe, H., Beddows, D., Fleming, Z. L., Flynn, M. J., Gallagher, M. W., Harrison, R. M., Lee, J., Prevot, A. S. H., Taylor, J. W., Yin, J., Williams, P. I. and Zotter, P.: Size distribution, mixing state and source apportionment of black carbon aerosol in London during winter time, Atmos. Chem. Phys., 14(18), 10061–10084, doi:10.5194/acp-14-10061-2014, 2014.

Metcalf, A. R., Craven, J. S., Ensberg, J. J., Brioude, J., Angevine, W., Sorooshian, A., Duong, H. T., Jonsson, H. H., Flagan, R. C. and Seinfeld, J. H.: Black carbon aerosol over the Los Angeles Basin during CalNex, J. Geophys. Res. Atmos., 117(8), 1–24, doi:10.1029/2011JD017255, 2012.

McMeeking, G. R., Hamburger, T., Liu, D., Flynn, M., Morgan, W. T., Northway, M., Highwood, E. J., Krejci, R., Allan, J. D., Minikin, A. and Coe, H.: Black carbon measurements in the boundary layer over western and northern Europe, Atmos. Chem. Phys., 10(19), 9393–9414, doi:10.5194/acp-10-9393-2010, 2010.

Moteki, N., Kondo, Y., Oshima, N., Takegawa, N., Koike, M., Kita, K., Matsui, H. and Kajino, M.: Size dependence of wet removal of black carbon aerosols during transport from the boundary layer to the free troposphere, Geophys. Res. Lett., 39(13), 2–5, doi:10.1029/2012GL052034, 2012.

Raatikainen, T., Brus, D., Hooda, R. K., Hyvarinen, A. P., Asmi, E., Sharma, V. P., Arola, A. and Lihavainen, H.: Size-selected black carbon mass distributions and mixing state in polluted and clean environments of northern India, Atmos. Chem. Phys., 17(1), 371–383, doi:10.5194/acp-17-371-2017, 2017.

Reddington, C. L., McMeeking, G., Mann, G. W., Coe, H., Frontoso, M. G., Liu, D., Flynn, M., Spracklen, D. V. and Carslaw, K. S.: The mass and number size distributions of black carbon aerosol over Europe, Atmos. Chem. Phys., 13(9), 4917–4939, doi:10.5194/acp-13-4917-2013, 2013.

Sahu, L. K., Kondo, Y., Moteki, N., Takegawa, N., Zhao, Y., Cubison, M. J., Jimenez, J. L., Vay, S., Diskin, G. S., Wisthaler, A., Mikoviny, T., Huey, L. G., Weinheimer, A. J. and Knapp, D. J.: Emission characteristics of black carbon in anthropogenic and biomass burning plumes over California during ARCTAS-CARB 2008, J. Geophys. Res. Atmos., 117(16), 1–20, doi:10.1029/2011JD017401, 2012.

Schwarz, J. P., Gao, R. S., Spackman, J. R., Watts, L. A., Thomson, D. S., Fahey, D. W., Ryerson, T. B., Peischl, J., Holloway, J. S., Trainer, M., Frost, G. J., Baynard, T., Lack, D. A., de Gouw, J. A., Warneke, C. and Del Negro, L. A.:

Measurement of the mixing state, mass, and optical size of individual black carbon particles in urban and biomass burning emissions, Geophys. Res. Lett., 35(13), 1–5, doi:10.1029/2008GL033968, 2008.

Shiraiwa, M., Kondo, Y., Moteki, N., Takegawa, N., Sahu, L. K., Takami, A., Hatakeyama, S., Yonemura, S. and Blake, D. R.: Radiative impact of mixing state of black carbon aerosol in Asian outflow, J. Geophys. Res. Atmos., 113(24), 1–13, doi:10.1029/2008JD010546, 2008.

Soleimanian, E., Mousavi, A., Taghvaee, S., Shafer, M. M. and Sioutas, C.: Impact of secondary and primary particulate matter (PM) sources on the enhanced light absorption by brown carbon (BrC) particles in central Los Angeles, Sci. Total Environ., 705, 135902, doi:10.1016/j.scitotenv.2019.135902, 2020.

Subramanian, R., Kok, G. L., Baumgardner, D., Clarke, A., Shinozuka, Y., Campos, T. L., Heizer, C. G., Stephens, B. B., De Foy, B., Voss, P. B. and Zaveri, R. A.: Black carbon over Mexico: The effect of atmospheric transport on mixing state, mass absorption cross-section, and BC/CO ratios, Atmos. Chem. Phys., 10(1), 219–237, doi:10.5194/acp-10-219-2010, 2010.

Taylor, J. W., Allan, J. D., Allen, G., Coe, H., Williams, P. I., Flynn, M. J., Le Breton, M., Muller, J. B. A., Percival, C. J., Oram, D., Forster, G., Lee, J. D., Rickard, A. R., Parrington, M., and Palmer, P. I.: Size-dependent wet removal of black carbon in Canadian biomass burning plumes, Atmos. Chem. Phys., 14, 13755–13771, https://doi.org/10.5194/acp-14-13755-2014, 2014.

Wentzel, M., Gorzawski, H., Naumann, K. H., Saathoff, H. and Weinbruch, S.: Transmission electron microscopical and aerosol dynamical characterization of soot aerosols, J. Aerosol Sci., 34(10), 1347–1370, doi:10.1016/S0021-8502(03)00360-4, 2003.

# Measurements to determine mixing state of black carbon emitted from the 2017/2018 California wildfires and urban Los Angeles

Joseph Ko[1], Trevor Krasowsky[1,*], George Ban-Weiss[1]

[1]Department of Civil and Environmental Engineering, University of Southern California, Los Angeles, 90089, USA

[*]now at: SpaceX, 1 Rocket Rd, Hawthorne, CA 90250 USA

*Correspondence to*: George Ban-Weiss (banweiss@usc.edu)

**Abstract.** The effects of atmospheric black carbon (BC) on climate and public health have been well established, but large uncertainties remain regarding the extent of BC's impacts at different temporal and spatial scales. These uncertainties are largely due to BC's heterogeneous nature in terms of its spatiotemporal distribution, mixing state, and coating properties. Here, we seek to further understand the size and mixing state ~~evolution~~ of BC emitted from various sources and aged over different timescales using field measurements in the Los Angeles region. We measured refractory black carbon (rBC) with a single-particle soot photometer (SP2) on Catalina Island, California (~70 km southwest of downtown Los Angeles) during three different time periods. During the first campaign (September 2017), westerly winds were dominant~~dominated~~ and ~~this period was largely~~ measured air masses were dominantly aged and representative of well-aged background over the Pacific Ocean~~ measurements were largely characterized by aged rBC particles from mixed continental plumes blowing across the Pacific Ocean ($BC_{aged,bg}$ $BC_{cont}$). thus the sampling location was upwind of the dominant regional sources of BC (i.e., urban emissions from the Los Angeles basin).~~ In the second and third campaigns (December 2017, November 2018), atypical Santa Ana wind conditions ~~caused measured~~allowed us to measured rBC from air masses dominated by ~~to include important contributions from~~ large biomass burning events ~~wildfires~~ in California ($BC_{bb}$) and urban fossil fuel~~urban~~ emissions from the Los Angeles basin ($BC_{ff}$). We observed that emissions source type and aging influenced both the size distribution of rBC cores and rBC mixing state. ~~BC from biomass burning dominated periods ($BC_{bb}$) We observed that biomass burning dominant emissions produced rBC-containing particles with~~had ~~more~~ thicker coatings~~-~~ and larger core diameters ~~than BC from fossil fuel (i.e., urban) dominated periods ($BB_{ff}$).~~ We observed a~~n~~ mean~~average~~ coating thickness ($CT_{BC}$) of ~40–70 nm and count mean diameter (CMD) of ~~fossil fuel (urban) dominant emissions.~~~120 nm for $BC_{bb}$~~,~~. For $BC_{ff}$, ~~while~~ we observed $CT_{BC}$ of ~5–15 nm and CMD of ~100 nm~~ for $BC_{ff}$~~. Generally, our observations provided evidence that aging led to ~~also appears to~~ increased ~~o increased~~ $CT_{BC}$ ~~the coating thickness of~~for both $BC_{bb}$ and $BC_{ff}$. ~~, although the rate of coating accumulationinerease iappears to be highlys non-linear.~~ Aging timescales < ~1 d ~~of less than one day~~ were ~~not~~ insufficient to thickly ~~-~~coat freshly-emitted $BC_{ff}$~~,~~. ~~but~~ However,~~, we found that continental air masses had an urban modean urban mode of the $BC_{cont}$ was identified and characterized by averagea aged~~ $CT_{BC}$ for aged $BC_{ff}$ from ~~mixed continental~~aged background plumes ~~that~~ was ~~of ~70 nm, which is more than>~~ 35 nm thicker than ~~typical the meanaverage~~ ~~fresh~~ $CT_{BC}$ for fresh $BC_{ff}$. ~~observed induring periods impacted by when urban emissions were dominantof fresh urban emissions impact. Comparing~~

between fresh $BC_{bb}$ and aged $BC_{bb}$Likewise, periods of fresh versus aged biomass burning impacts, we found also observed that $CT_{BC}$ for aged $BC_{bb}$ was ~18 nm thicker than $CT_{BC}$ for fresh $BC_{bb}$. The results presented in this study highlight the wide variability in BC mixing state, and further confirmprovide additional evidence howthat emissions source type and aging various external factors drastically could influence BC physical properties.

~~We observed a larger number fraction of thickly coated~~thickly coated ~~particles ($f_{BC}$) and increased coating thickness ($CT_{BC}$) during the first campaign (~ 0.27 and ~ 306 nm, respectively), and during portions of the third campaign when we suspect that rBC was transported long-range from the Camp Fire in Northern California (~ 0.35 and ~ 52 nm, respectively), compared to other time periods. In contrast, during periods when we suspect that measured rBC was dominated by by Southern California fires or urban emissions~~emissonsemissions from the Southern California region~~, both $f_{BC}$ and $CT_{BC}$ were significantly lower, with a mean $f_{BC}$ of ~ 0.03 and median $CT_{BC}$ ranging from ~ 0 to 10 nm. From our rBC measurements and meteorological analyses, we conclude that an aging timescale on the order of ~ hours is not long enough for rBC to become thickly coated~~thickly coated under the range of sources sampled and atmospheric conditions during this campaign. On average, we found that measured rBC had to age more than a day to become thickly coated. Aging timescales for developing thick coatings were found to be longer in this study relative to a number of previous observational studies conducted with an SP2, suggesting that rBC aging is heavily impacted by regional atmospheric context.~~

## 1 Introduction

Atmospheric black carbon (BC) is a carbonaceous aerosol that can result from the incomplete combustion of carbon-containing fuels. Major energy-related sources of BC include vehicular combustion, power plants, residential fuel-use, and industrial processes. Biomass burning, which can be either anthropogenic or natural, is another significant BC source. BC is a pollutant of particular interest for two main reasons: (1) it ~~strongly~~ absorbs solar radiation, which results in atmospheric warming (Ramanathan and Carmichael, 2008), and (2) it is associated with increased risk of cardiopulmonary morbidity and mortality (World Health Organization, 2012). Regarding its effect on climate, BC is widely considered to be the second strongest contributor to climate warming, after carbon dioxide (Bond et al., 2013). Although it has been established that BC is a strong radiative forcing agent in Earth's atmosphere, there remains considerable uncertainty about the extent to which BC affects Earth's radiative budget, from regional to global scale (IPCC, 2013; Bond et al., 2013).

Since the lifetime of BC is relatively short (~days to weeks), the spatiotemporal distribution of BC is highly heterogeneous and thus~~,~~ ~~making it~~ difficult to quantify (Krasowsky et al., 2018). The quantification of where and when BC is emitted around the world is also a challenging task that causes significant ~~uncertainties~~ uncertainty (Bond et al., 2013). In addition to the difficulties that come with tracking the emissions and distribution of BC, there are complex physical and chemical processes that govern the transformation of BC in the atmosphere, which ultimately impact its climate and health effects. These atmospheric processes, ~~influence,~~ in addition to the emissions source type, influence the BC mixing state in a highly

heterogenous and dynamic manner. A hypothetical BC particle that exists completelyis completely, physically separated from other non-BC aerosol species is considered- *externally mixed*~~*emitted mostly as an "external" mixture,* physically separated from other aerosol species~~. On the other hand, BC is considered *internally mixed* if it is physically combined with another non-BC aerosol species (Bond et al., 2006; Schwarz et al., 2008a)~~.~~ . Although BC is likely coated to some extent by non-refractory organic and non-organic compounds at the point of emissions (Johnson et al., 2005), "fresh BC" is generally conceptually considered uncoated. As freshly emitted BC- particles areis transported in the atmosphere, they can it obtains inorganic and organic coatings from either gaseous pollutants that condense onto the BC, oxidation reactions on the BC surface, or the coalescence of other aerosol species onto the BC, making them more ienxternally mixed (He et al., 2015). In short, externally mixed BC is referred to as "uncoated BC" and internally mixed BC is referred to as "coated BC." Aged BC that has acquired coatings is referred to as internally mixed BC (Bond et al., 2006; Schwarz et al., 2008). In general, the *mixing state* of BC describes the degree to whichhow much BC is either externally or internallyinternally mixed~~, with bare uncoated (i.e., , externally mixed) BC particles considered to be externally mixed on the one extremeone end of the mixing state spectrum within a broader aerosol population~~ (Bond et al., 2013). The BC mixing state nearat the point of emission as well as the evolution during aging in the atmosphere of the mixing state can vary widely, depending on the source of emissions as well asand atmospheric processes and conditions.aging processes.context.processes.

The evolution of rBC mixing state as the BC ages in the atmosphere is crucial to understand for two reasons. First, it has been shown that non-refractory coatings on BC can enhance its absorption efficacy, implying that internally mixed BC with thick coatings can have stronger warming potential in the atmosphere compared to uncoated or thinly-coated BC (Moteki and Kondo., 2007; Wang et al., 2014). Second, coatings on BC can alter the aerosol's hygroscopicity and effectively shorten its lifetime by increasing the probability of wet deposition (McMeeking et al., 2011a; Zhang et al., 2015). In short, freshly emitted BC particles are generally hydrophobic, but coatings acquired during the aging process can make BC-containing particles hydrophilic, and therefore, more susceptible to wet deposition. Thus, uncertainties in the evolution of rBC mixing state directly translate to uncertainties regarding BC's impact on Earth's climate due to both the radiative impact per particle mass and spatiotemporal variation of atmospheric BC loading.

Although there have been a number of laboratory experiments (Wang et al., 2018; He et al., 2015; Slowik et al., 2007; Knox et al., 2009) and field campaigns (Krasowsky et al., 2018; Metcalf et al., 2012; Cappa et al., 2012; Schwarz et al., 2008a) studying rBC mixing state, there is considerable variability in results. For example, field studies in China suggest that the mass absorption cross-section (MAC) of BC that has aged for more than a few hours should be enhanced by a factor of ~2 (Wang et al., 2014), while other studies in California reported an absorption enhancement factor of ~1.06 (Cappa et al. 2012) and ~1.03 (~~Cappa et al. 2012;~~ Krasowsky et al., 2016). Preceding these studies, Bond et al. (2006) suggested an enhancement factor of ~1.5 based on a review of laboratory and field studies. The wide range of reported values is not surprising given that rBC mixing state is expected to be influenced by a variety of spatiotemporal factors such as source type, season, and

regional atmospheric composition (Krasowsky et al., 2018). In other words, BC aged in different places and, at different times, may have significantly varying mixing states, resulting in a wide range of absorption and hygroscopicity enhancements in the real world.

Quantifying rBC mixing state is challenging because it requires single-particle analysis (Bond et al., 2006). There are two main methods to measure rBC mixing state: (1) microscopy (Johnson et al., 2005; Adachi et al., 2010, 2016), and (2) real-time, in-situ measurements (Hughes et al., 2000). In our study, we quantify rBC mixing state by taking real-time, in-situ measurements with a single particle soot photometer (SP2). The SP2 uses laser-induced incandescence to measure refractory black carbon (rBC) mass per particle, which can be used to directly compute the mass concentration, number concentration, and mass size distribution, and indirectly compute the number size distribution (Stephens et al., 2003). The SP2 can also measure the internal mixing state of rBC using one of two different methods. In the lag-time method, each sensed rBC-containing particle is deemed as either *thinly-coated* or *thickly-coated* using the measured time difference between the peak of the particle's incandescence and scattering signals induced by the particle (Moteki and Kondo, 2007, 2008). In the leading-edge-only (LEO) method, the actual coating thickness for rBC-containing particles can be explicitly quantified (Gao et al., 2007). Further detail regarding these two methods can be found in section 2.3 and 2.4. In this study, we used both methods to quantify the rBC mixing state.

In this study, we measured rBC with an SP2 on Catalina Island, California (~70 km southwest of Los Angeles) during three different time periods, with the goal of observing how rBC loading and mixing state varied as a function of source type and source-to-receptor timescale. During the first campaign (September 2017), westerly winds dominated and thus the sampling location was upwind of the dominant regional sources of rBC (i.e., urban emissions from the Los Angeles basin). We suspect measurements during this period to represent well-aged particles; evidence suggests that some of which might of the measured particles have originated from wildfires in Oregon and Northern California. In contrast, the second and third campaigns (December 2017, November 2018) were dominated by northerly-to-easterly "Santa Ana conditions", which advected fresh and aged rBC-containing particles from both biomass burning emissions and urban emissions. Several significant wildfires were active in the Southern and Northern California regions throughout the second and third campaigns. In particular, the Thomas Fire, which was active in Southern California during the second campaign, was the second largest wildfire in modern California history. The Camp Fire, which was active in Northern California during the third campaign, was the 16$^{th}$ largest fire in terms of burn area size, and was also considered the deadliest and most destructive wildfire in modern California history. Table 1 lists the two most significant wildfires for each campaign period that we suspect had some impacted on our rBC measurements, along with the total burn area and time period of non-containment for each fire. Mass and number concentrations of rBC-containing particles, rBC size distributions, the number fraction of thickly coatedthickly-coated rBC-containing particles (i.e., using the lag-time method), and absolute coating thickness values (i.e., using the LEO method) are reported. We then evaluate how the rBC loading, size distribution, and mixing state relate to the

meteorology and major sources at the time of measurements in order to further understand the microphysical transformation of BC as it ages in the atmosphere. While a few past studies have investigated the mixing state of rBC in the Los Angeles region using the SP2 (Metcalf et al., 2012; Cappa et al. 2012; Krasowsky et al. 2018), this study is the first to use fixed ground-based measurements off the coast of Los Angeles to focus on how (a) wildfire source-to-receptor travel time, and (b) wildfire versus urban emissions, influence rBC mixing state.

**Table 1.** Major wildfires that were active during the three campaigns. Only the two largest fires from each campaign (in terms of burn area) are listed in the table below. Note that there were numerous other smaller fires that were active during the three campaigns, but not listed in this table.

| Campaign | Wildfire name | Location | Area ($km^2$) | Start date | Containment date |
|---|---|---|---|---|---|
| First (September 2017) | Chetco Bar Fire | Rogue River–Siskiyou National Forest, Oregon | 773 | 12 July, 2017 | 2 November, 2017 |
| | Eclipse Complex | Siskiyou, California | 318 | 15 August, 2017 | 29 November, 2017 |
| Second (December 2017) | Thomas Fire | Ventura and Santa Barbara, California | 1,140 | 4 December, 2017 | 12 January, 2018 |
| | Creek Fire | Los Angeles, California | 63 | 5 December, 2017 | 9 January, 2018 |
| Third (November 2018) | Camp Fire | Butte, California | 620 | 8 November, 2018 | 25 November, 2018 |
| | Woolsey Fire | Ventura and Los Angeles, California | 392 | 8 November, 2018 | 22 November, 2018 |

## 2 Methods

### 2.1 Measurement location and time periods

All measurements reported in this study were conducted at the USC Wrigley Institute for Environmental Studies on Catalina Island (~33°26'41.68"N, 118°28'55.98"W). Catalina Island is located approximately 70 km (43.5 miles) southwest of downtown Los Angeles. Figure 1 shows the location of the sampling site relative to the Los Angeles metropolitan area. The three campaigns were conducted from 7 to 14 September 2017, 20 to 22 December 2017, and 12 to 18 November 2018, Pacific Time (local time).

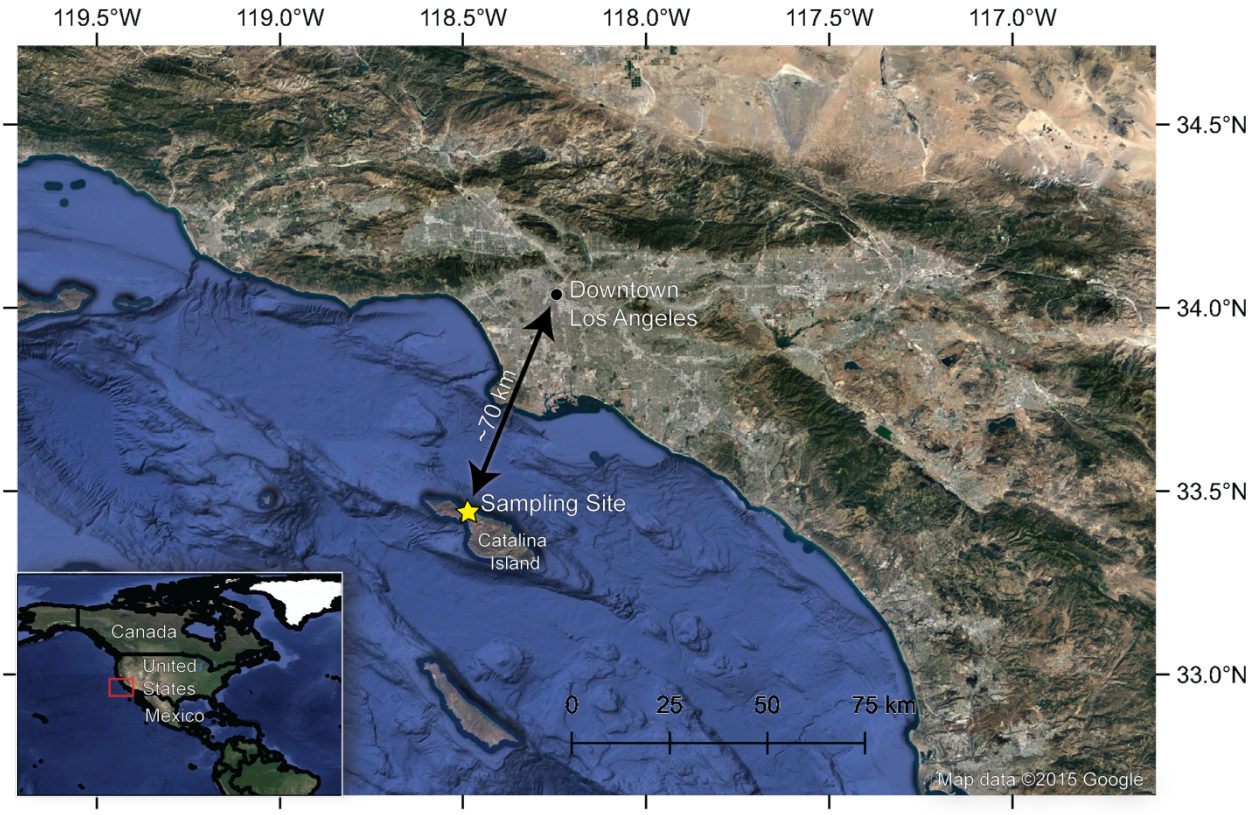


920 **Figure 1.** Overview map showing the location of the sampling site with respect to the Greater Los Angeles (LA) area.

### 2.2 Instrumentation

An SP2 (Droplet Measurement Technologies, Boulder, CO) was used to quantify the physical characteristics of rBC-containing particles for all three campaigns. In short, the SP2 uses laser-induced incandescence to quantify rBC mass on a
925 particle-by-particle basis. The SP2 uses a continuous Nd:YAG laser ($\lambda$ = 1064 nm) that is oriented perpendicular to the flow of air containing rBC-containing particles. As each particle passes through the intra-cavity laser, any coating on the rBC particle vaporizes while the core incandesces and emits thermal radiation. The scattered and thermally emitted radiation is measured by optical sensors and converted to signals that can then be used to obtain information about the mass and mixing state of the sampled rBC-containing particles. In this study, an assumed rBC density of 1.8 g $cm^{-3}$ was used. The SP2 has
930 detection limits from ~0.5 to 50 fg rBC per particle. Further details regarding the governing principles and operation of the SP2 can be found in numerous publications (Stephens et al., 2003; Schwarz et al., 2006; Gao et al., 2007; Moteki and Kondo, 2007; Laborde et al., 2012; Dahlkötter et al., 2014; Krasowsky et al., 2016).

The inlet of the SP2 was positioned on the roof of a three-story research building at the Wrigley Institute as shown in Fig.~~ure~~ S1. The height of the inlet was approximately 15 meters above ground level. A fine mesh was secured to the tip of the inlet to prevent clogging by small insects, and a small plastic cone was also attached to block any potential precipitation from entering the inlet. The inlet tube was fed in through a window of a secure laboratory room on the top floor of the building where the SP2 was housed for the duration of sampling. The SP2 ran continuously for the duration of the three measurement~~sampling~~ periods. Desiccant used to remove moisture from the sample air was replaced on a daily basis, and the data during these replacement periods were subsequently removed during the data analysis.

**2.3 Auxiliary data**

Model simulations and publicly available auxiliary datasets were used to supplement our SP2 measurements.

The National Oceanic and Atmospheric Administration's (NOAA) Hybrid Single-Particle Lagrangian Integrated Trajectory (HYSPLIT) model (Stein et al., 2015) was the primary tool used to identify dominant emissions sources. The HYSPLIT back-trajectories were also used to estimate the age range of measured rBC-containing particles and the path of the air masses carrying these particles. The HYSPLIT trajectory model requires the user to specify the following input parameters: meteorological database, starting point of the back-trajectory, height of source location, run time, and the vertical motion method. A height of 15 meters above ground level was chosen to approximately represent the height of the SP2 inlet positioned on the roof of the laboratory facility. For the first campaign (September 2017), the Global Data Assimilation System (GDAS) meteorology database with 1-degree resolution (~110 km for 1-degree latitude and ~85 km for 1-degree longitude) was selected, and one-week back-trajectories were simulated for every day of the first campaign. For the second and third campaigns (December 2017, November 2018), the High-Resolution Rapid Refresh (HRRR) meteorology database with a 3-km resolution was selected, and 72-hour back-trajectories were simulated starting on every hour. The GDAS database was selected for the first campaign simulations because a 1-degree resolution was sufficient to show that the measured air masses were generally coming from the west. In contrast, the HRRR database was used for the second and third campaigns because a finer resolution helped determine the sources that contributed to measured rBC. The default vertical motion method was selected for all back-trajectory simulations.

Data from local weather stations were used to identify the meteorological regimes during all three campaigns, and to supplement the HYSPLIT back-trajectories used for source characterization. Hourly weather data from Los Angeles International Airport (LAX), Long Beach Airport, Avalon (Catalina Island), Santa Barbara, and Oxnard, during September 2017, December 2017, and November 2018, were obtained using the NOAA National Center for Environmental Information online data tool (https://www.ncdc.noaa.gov/cdo-web/datatools/lcd, last access: 26 August 2019). Five-minute weather data

at the same weather stations and time periods were obtained from the Iowa Environmental Mesonet website (https://mesonet.agron.iastate.edu, last access: 26 August 2019; Todey et al.,2002). Wind data from the USC Wrigley Institute on Catalina Island were also examined when available (7 to 13 September 2017) on the Weather Underground website (https://www.wunderground.com/weather/us/ca/catalina, last access: 26 August 2019), though these data are not validated by NOAA. Data from Santa Barbara, Oxnard, and USC Wrigley Institute were assessed to support conclusions made in this ~~study, but~~study but are not directly presented in any of the analyses here.

In addition to meteorological data, weather information from local news reports, NASA satellite imagery, and global aerosol model data were used in conjunction to explain the variability in rBC concentrations and mixing state during the sampling campaigns. Local weather news reports between 20 December and 22 December 2017 were used to obtain information about the active fires in Southern California and the dominant wind conditions for each day in the second campaign (December 2017) (CBS Los Angeles, 2017a, 2017b, 2017c, 2017d, 2017e, 2017f). There were generally two local weather reports retrievable per day: one in the early morning and one later on in the evening. The information from these reports was used to get a holistic picture of the local fire and weather conditions at the time of sampling. Data from the California Department of Forestry and Fire Protection (https://www.fire.ca.gov/incidents/, last access: 26 August 2019) was also used to verify basic spatial and temporal information about significant fires occurring during sampling periods. The local weather reports were used to cross-validate wildfire timelines, but they are not directly presented here.

NASA satellite imagery and data were accessed through NASA's Worldview online application (https://worldview.earthdata.nasa.gov/, last access: 26 August 2019), which provides public access to NASA's Earth Observing System Data and Information System (EOSDIS). Moderate Resolution Imaging Spectroradiometer (MODIS) images taken from two satellites (Aqua and Terra) were examined for all sampling days. MODIS images were used to identify visible plumes of aerosols, particularly those from large wildfires. The general movement of air masses was also assessed from the visible movement of large-scale clouds from these satellite images. In addition to the MODIS images, aerosol index, aerosol optical depth (AOD), and fires and thermal anomalies data products were examined to supplement the source identification process. For aerosol index, the OMAERUV (Torres, 2006) and OMPS_NPP_NMTO3_L2 (Jaross, 2017) products were used. For AOD, the MYD04_3K MODIS/Aqua and MYD04_3K MODIS/Terra products were used (Levy et al., 2013). For fires and thermal anomalies, the VNP14IMGTDL_NRT (Schroeder et al., 2014) and MCD14DL (Justice et al., 2002) products were used. Examples of NASA data products used for source identification analysis can be found in the Supplement.

An open-source online visualization tool (earth.nullschool.net, last access: 26 August 2019) was used to visually assess the European Centre for Medium-Range Weather Forecasts (ECMWF) Copernicus Atmosphere Monitoring Service (CAMS) model output data (Beccario, 2019; https://atmosphere.copernicus.eu/, last access: 26 August 2019). The CAMS model

provides "near-real-time" forecasts of global atmospheric composition on a daily basis. Specifically, the $PM_{2.5}$ concentration output data from CAMS were examined using earth.nullschool.net. The CAMS output visualizations were particularly helpful for understanding where certain sources were located and when they were likely affecting our measurements. The concentration gradients of $PM_{2.5}$ were examined on the visualization tool on an hourly interval for every day of active sampling in order to supplement the HYSPLIT analysis and confirm the contribution of certain emission sources. Access to the CAMS visualizations for the three campaigns can be found in the Supplement and Video Supplement.

### 2.4 Estimation of source-to-receptor timescale

Characteristic timescales of transport between the sampling site and nearest source(s) were estimated based on the HYSPLIT trajectories simulated for source identification. The approximate source-to-receptor timescale characterizations by HYSPLIT were cross-validated with approximate calculations of transport time performed with representative length scales between sources and the sampling site, and the average wind speeds during the time periods of interest. Further details regarding the calculations of the timescale characterizations are in section S1 of the Supplement. Although we cannot fully capture the intricacies of particle aging timescales with our estimates, they are meant to be conservative approximations based on available meteorological data. These estimated source-to-receptor timescales were used to help categorize different LEO periods by source(s) (see Table 2 and Fig. ~~ure~~ 9~~6~~), and also used in our discussion of how rBC mixing state evolves with particle aging (see Section 3.7~~6~~).

### 2.5 Time series filtering

rBC mass and number concentrations during the first campaign (September 2017) showed anomalous spikes likely due to unexpected local sources. In an effort to obtain representative background concentrations, we filtered these spikes by removing values above a threshold of 0.08 μg $m^{-3}$ and 40 $cm^{-3}$ for mass and number concentrations, respectively. Figure S2 in the Supplement shows the time series for the first campaign before and after removal of spikes. Figure S3 in the Supplement shows the median rBC concentration for the first campaign as a function of the cut-off threshold value. Median rBC mass and number concentrations appeared to asymptote at cut-off values of approximately 0.08 μg $m^{-3}$ and 40 $cm^{-3}$, suggesting that the median rBC concentration values become insensitive to the choice of cut-off threshold above these values.

### 2.6 Lag-time method

The mixing state of rBC was examined using two different methods. The first method used to characterize mixing state is called the lag-time method. This method categorizes each rBC particle as either "thickly-coated" or "thinly-coated" based on a measured time delay (i.e., "lag-time") between the scattering and incandescence signal peaks. This method has been

previously described and used in various studies (Moteki and Kondo, 2007; McMeeking et al., 2011a; Metcalf et al., 2012; Sedlacek et al., 2012; Wang et al., 2014; Krasowsky et al., 2016; Krasowsky et al., 2018). In short, as a coated rBC-containing particle passes through the SP2 laser, the sensors will detect a scattering signal as the coating vaporizes. Shortly after, there will be a peak in the incandescence signal as the rBC core heats up and emits thermal radiation. A probability density function of the lag-time values often results in a bimodal distribution. Based on the data for a particular campaign, a lag-time cut-off is chosen between the two peaks of the bimodal distribution to bin each rBC particle as either thinly or ~~thickly coated~~thickly-coated. The fraction of rBC particles that are thickly-coated ($f_{BC}$) is then determined based on this categorization. For our study, a lag-time cut-off of 1.8~~2~~ µs was chosen to quantify whether an rBC-containing particle was thickly-coated. Only particles with an rBC core diameter greater than 170 nm were included in the calculation of $f_{BC}$ to account for the scattering detection limit of the instrument. As discussed previously by Krasowsky et al. (2018), the lag-time method is inherently susceptible to biases since $f_{BC}$ can depend on the selection of the lag-time cut-off value. For example, Krasowsky et al. selected a cut-off value of 1 µs for a near-highway SP2 campaign in the Los Angeles Basin, which is significantly different than the value of 1.8~~2~~ µs used in this study and others. There remains an unresolved issue of maintaining consistency between different studies utilizing the lag-time method, while simultaneously representing the unique mixing state characterization of each measured rBC population; the definition of "thickly-coated" likely varies by the aerosol population sampled and thus is not necessarily comparable from one study to the next.

### 2.7 Leading-edge-only (LEO) method

BC mixing state was also characterized using the LEO method. In brief, this method reconstructs a Gaussian scattering function from the leading edge of the scattering signal for each rBC-containing particle. The width and location of the reconstructed Gaussian scattering function is determined by a two-element avalanche photodiode. ~~-~~Assuming a core-shell morphology, the rBC coating thickness is subsequently calculated from the reconstructed scattering signal and the incandescence signal (Gao et al., 2007; Moteki and Kondo, ~~et al.~~ 2008). The Paul Scherrer Institute's single-particle soot photometer toolkit version 4.100b (developed by Martin Gysel et al.) was used to perform the LEO method in Igor Pro version 7.09.

~~For our~~In this study, the LEO "fast-fit" method was used with ~~the first~~ three points ~~of the leading edge~~, and particles analyzed were restricted to those with rBC core diameters between 180~~200~~ and 302~~5~~0 nm. Although the SP2 has been reported to accurately measure the volume equivalent diameter (VED) of scattering particles down to ~170 nm, a more conservative lower threshold of 180~~200~~ nm was used for our study to reduce instrument noise at smaller VED values near the detection limit ~~, as done in our previous study~~ (Krasowsky et al., 2018). Specific rBC core diameter ranges were used for different analyses in this study and these ranges are explicitly defined within each respective discussion. One exception was made to the 180–300 nm rBC core diameter restriction~~,~~ in section 3.7. For the ~~analyses analyses~~analyses and discussion

presented in section 3.7, the LEO coating thickness was calculated for all detectable rBC particles with non-saturated scattering signals. The rBC core size was not restricted in this section because the relative comparisons between characteristic coating thickness values were more important for the analysis, rather than the absolute value (which would likely be biased, as discussed further in section 3.8). In other words, the LEO-derived coating thickness values in section 3.7 ~~from this section~~ were not used to report ~~a~~ representative averages for selective time periods, but rather were used ~~more qualitatively for comparison.~~ for comparative and/or ~~qualitative descriptive~~qualitative purposes.~~ (e.g., these values were not incorporated in Table 3). Further details and justification can be found in that section describing why this exception was acceptable for that analysis.the respective analysis.the size restrictions were acceptable for that analysis.~~

## 3 Results and discussion

~~[insert short roadmap of this section]~~This section starts by discussing the major identifiable sources and meteorological patterns in each of the three campaigns (section 3.1)~~s~~. Then, the overall mass and number loading of rBC is discussed and compared to past literature values (section 3.2). Following that, the rBC mixing state results from the lag-time and LEO analyses are discussed (sections 3.3–3.5). The impacts of emissions source type and atmospheric aging on rBC mixing state and core size are subsequently discussed (sections 3.6, 3.7). Section 3 then ends by comparing rBC coating thickness values calculated in this study to ~~those reported in past, similar studies.~~reported values from past studies

### 3.1 Source identification and meteorology

In this section, we summarize the dominant pollutant sources and wind patterns for each of the three campaigns. For all three campaigns, we used HYSPLIT back-trajectories, HYSPLIT dispersion model, CAMS model data, and NASA data products (i.e., satellite imagery, aerosol index products, and AOD products) in conjunction to identify the most likely sources of measured rBC-containing particles. For the first campaign (September 2017), the Oregon wildfires were identified as probable sources of measured rBC. Furthermore, we also identified long-range transport from East Asia and ship/aviation emissions as potential sources contributing to measured rBC. Overall, we expect measured rBC during the first campaign to be aged. For the second campaign (December 2017), fresh urban emissions from the Los Angeles basin and biomass burning emissions from the Thomas Fire in Santa Barbara and Ventura County (along with other smaller Southern California fires) were the main sources identified by our analysis. For ~~our~~ the third campaign (November 2018), fresh urban emissions from the Los Angeles basin and fresh biomass burning emission from the Woolsey Fire in Ventura (along with other smaller Southern California fires) were the main sources identified for approximately the first four days of the campaign. For ~~approximately~~ the last two days of the third campaign, ~~we suspect that~~ the Camp Fire in Northern California (along with other smaller fires in Northern and Central California) ~~had significant contributions~~contributed significantly to measured rBC. Figure 2 displays ~~the percentage of wind coming from different directions,~~wind roses for each campaign~~,~~ at three

different weather station locations (public data provided by NOAA, see section 2.3). Furthermore, Figur.e 3 shows HYSPLIT back-trajectories simulated for each of the three campaigns and further highlights in detail, the differences in wind conditions between the three campaigns. These figures clearly show the distinct meteorological regimes of each campaign. A more detailed description of the source identification process can be found in section S21 of the Supplement.

For the restremainder of the manuscript, we refer to rBC measured when the dominant source was biomass burning emissions will be referred to as $BC_{bb}$, and rBC measured when the dominant source was fossil fuel (i.e., urban) emissions will be referred to as $BC_{ff}$. rBC measured in the first campaign (September 2017), when the measured air masses were dominantly aged and representative of the continental scalewell-aged background over the Pacific Ocean continental background levels, will be referred to as $BC_{Bconaged,bgt.}$ and rBC measured from aged, continental air masses will be referred to as $BB_{cont}$:

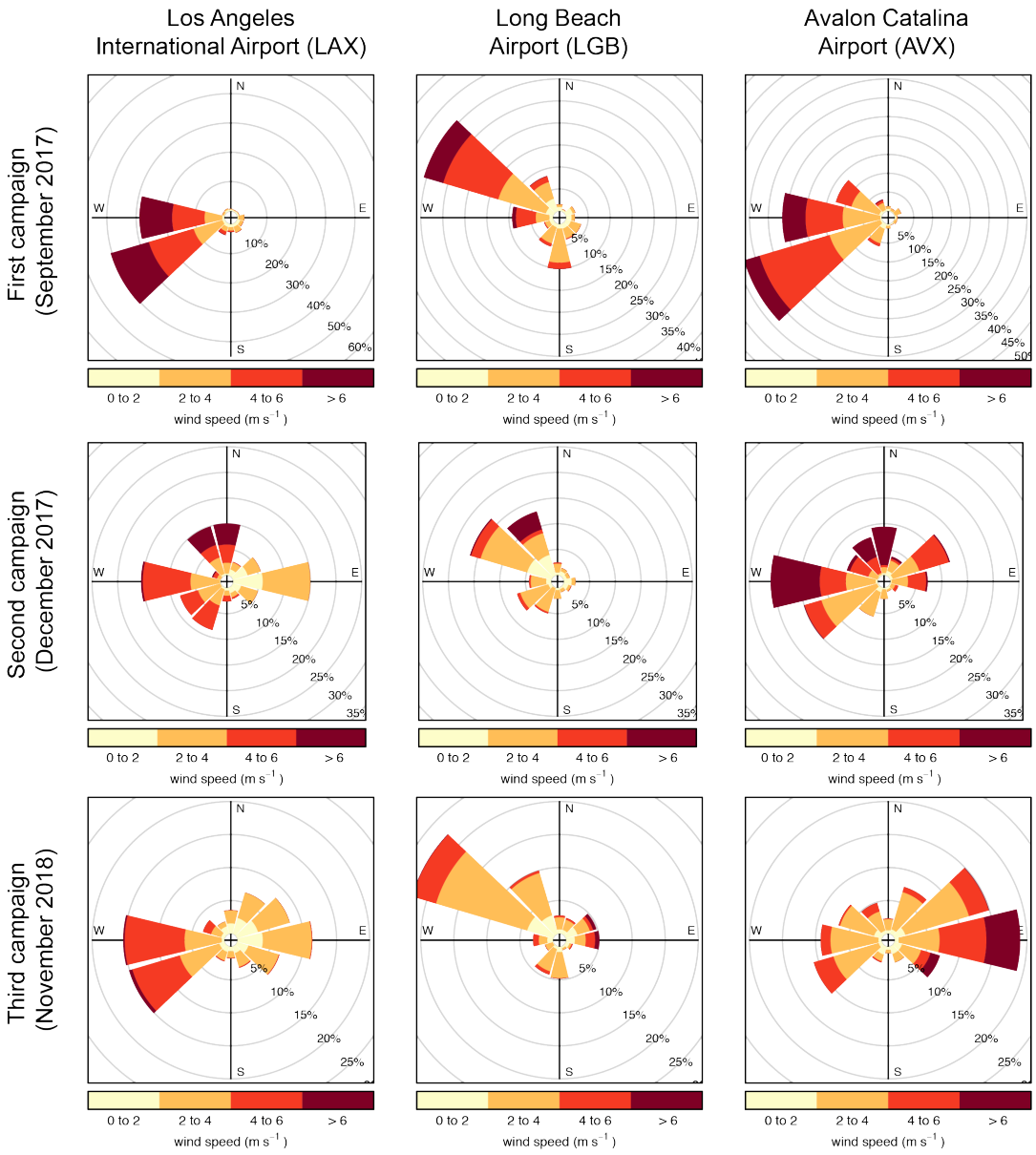


**Figure 2.** Wind roses for the September 2017 (first row), December 2017 (second row), and November 2018 (third row) sampling periods. Wind roses are based on five-minute ASOS airport data from LAX (first column), LGB (second column), and AVX (third column), provided by NOAA.

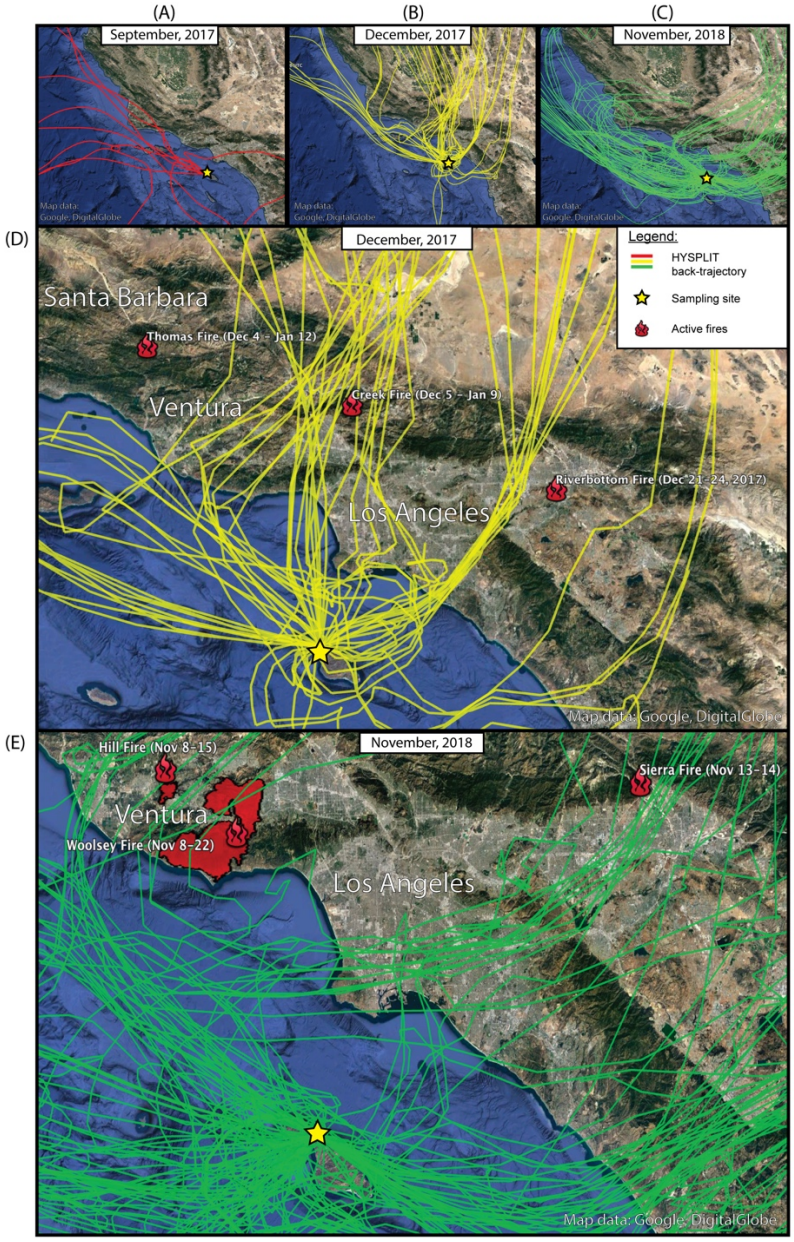


**Figure 3.** HYSPLIT back-trajectories for all three campaigns. The star denotes the start location of each back-trajectory, i.e., the sampling location. The trajectories for the first period (September 2017) (i.e., panel a) represent week-long back-trajectories for each day of the campaign. The trajectories for the (b) second (December 2017) and (c) third (November 2018) periods represent 72-hour back-trajectories for each hour of the campaign. Panels (d) and (e) show more zoomed-in maps of the second and third campaign back-trajectories along with active Southern California fires.

### 3.2 rBC mass and number concentration

Figure 4 shows time series for rBC mass and number concentrations, rBC coating thickness ($CT_{BC}$), number fraction of thickly-coated particles (~~and~~ $f_{BC}$), and rBC count mean diameter (CMD) for all three measurement campaigns. The mixing state ($CT_{BC}$ and $f_{BC}$) and rBC size are discussed in following sections. The mean mass and number concentration (±standard deviation) for the first campaign (September 2017) was 0.04 (±0.01) μg $m^{-3}$ and 20 (±7) $cm^{-3}$, respectively. For the second campaign (December 2017), the corresponding mean concentrations were 0.1 (±0.1) μg $m^{-3}$ and 63 (±74) $cm^{-3}$, with concentrations reaching as high as 0.6 μg $m^{-3}$ and 381 $cm^{-3}$. Likewise, for the third campaign (November 2018), the corresponding mean concentrations were 0.15 (±0.1) μg $m^{-3}$ and 80.2 (±54.5) $cm^{-3}$. The range of observed rBC concentrations is larger for the second and third campaigns compared to the first campaign, and there are distinct prolonged peaks in concentrations that can be observed during these times~~;~~. ~~in~~ In comparison, the first campaign shows relatively stable concentrations.

Given the remote location of the sampling site and the consistent westerly winds during the first campaign (September 2017), the observed rBC concentrations establish an appropriate baseline for ambient conditions away from the broader urban plume in the Los Angeles basin. On the other hand, the concentrations during the second and third campaigns (December 2017, November 2018) were more variable, ~~and the~~with mean concentrations that were ~~were~~ higher than ~~than the mean concentration for~~ the first campaign due to periods of northerly-to-easterly winds driven by Santa Ana wind conditions as described in section 3.1. Figure 5 shows rBC mass and number concentrations along with wind speed and direction during the second campaign. Wind direction was directly related to elevated concentrations for all three peaks shown. Peak P1 is clearly preceded by a prolonged period of northerly winds. Similarly, Peaks P2 and P3 are preceded by periods of easterly winds. An analogous plot for the third campaign is shown in Fig ~~ure~~ S8~~9~~, but the relationship between wind direction measured at LAX and the rBC concentration is not clearly discernible since long distance biomass emissions were impacting the measurements in addition to local sources near the LA basin. The impacts of different sources on measurements during the third campaign are described in detail in section S2 of the Supplement.

~~On average, the~~The mean concentration~~s~~ for the first campaign (September 2017) was~~ere~~ approximately an order of magnitude lower than the ~~average~~ mean concentration of ~0.14 μg $m^{-3}$ observed by Krasowsky et al. (2018) near the ~~outskirts~~ downwind edge (assuming dominant westerly wind flows) of the LA Basin (i.e., ~~, in~~ Redlands, CA). Concentrations during the most polluted time periods in our measurements ~~(i.e. parts of the second and third campaigns)~~ were comparable to recently measured concentrations in the Los Angeles basin (Krasowsky et al., 2018) but at least one to two orders of magnitude lower than average concentrations found in other heavily polluted cities around the world. Mass concentration values of ~0.9 μg $m^{-3}$, ~0.5 to 2.5 μg $m^{-3}$, ~0.9 to 1.74 μg $m^{-3}$, and ~0.6 μg $m^{-3}$ were measured with an SP2 in Paris, Mexico City, London, and Houston, respectively (Laborde et al., 2013; Baumgardner et al., 2007; Liu et al., 2014; Schwarz et al.,

2008a). In urban areas of China, an average mass concentration of ~9.9 μg $m^{-3}$ was reported for a polluted period in Xi'an (Wang et al., 2014).

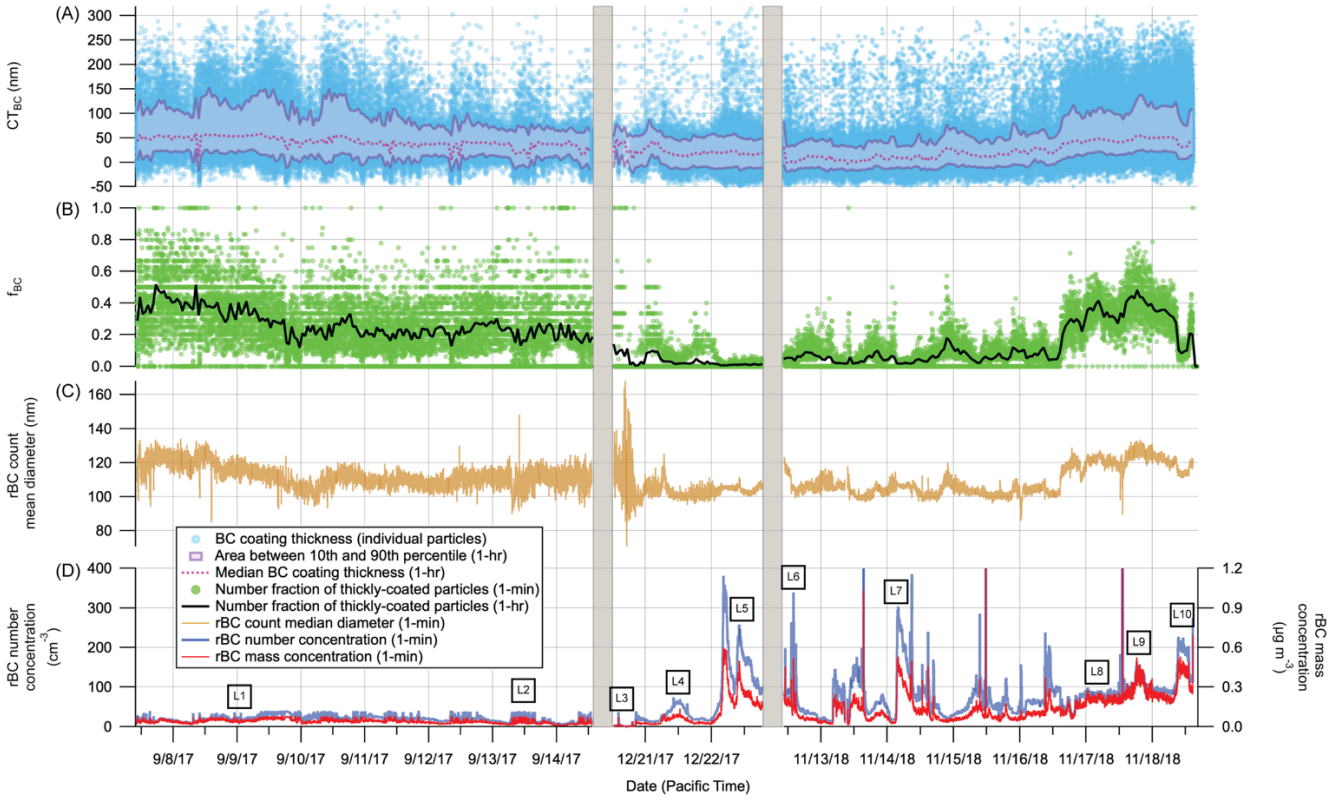


**Figure 4.** Time series of (a) BC absolute coating thickness, (b) number fraction of thickly-coated rBC particles, (c) rBC count median diameter, and (d) rBC concentrations, for all three measurements campaigns. The boxed annotations (i.e., L1 to L10) refer to specific LEO periods, which are further described in Section 3.4. In panel (a), each blue dot represents an individual particle. The hourly median is shown in the dotted pink line, and the corresponding $10^{th}$ and $90^{th}$ percentiles are shown in purple. In panel (b), green dots represent one-minute means while the black curve shows hourly means. Panel (c) shows the one-minute mean for the count mean diameter. Panel (d) shows the one-minute means for rBC concentration.

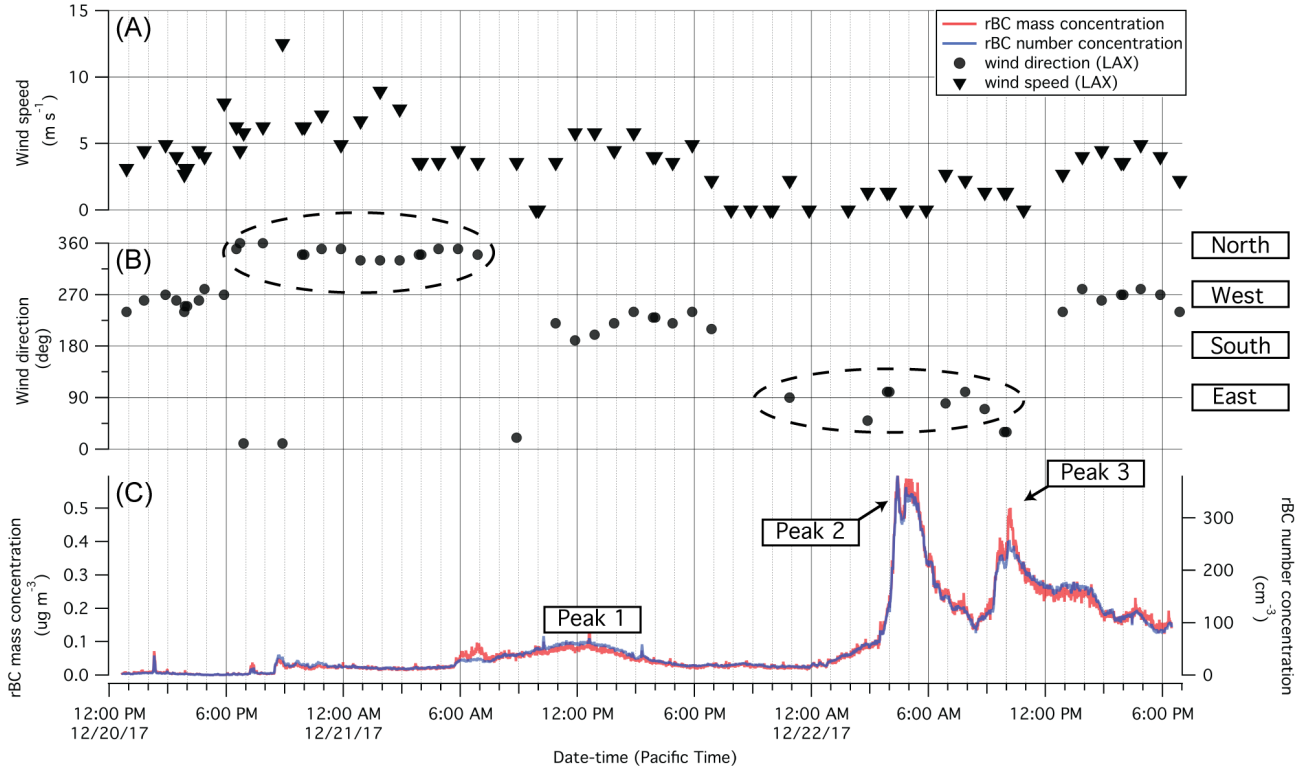


**Figure 5.** Meteorological variables and rBC concentrations during the second campaign (December 2017). Panel (a) shows wind speed and (b) shows wind direction measured by a NOAA weather station located at Los Angeles International Airport (LAX). Panel (c) shows rBC mass and number concentrations and identifies three peaks of interest. The two dashed ovals in panel (b) highlight periods of northerly and easterly winds, which occur ~0.5-1 days before each of the three peaks, suggesting that the elevated rBC concentrations included important contributions from the local Thomas Fire (and other smaller fires) and urban emissions from the Los Angeles basin.

### 3.3 Lag-time analysis: number fraction of thickly-coated rBC-containing particles

Figure 4, panel (b) shows both one-minute and one-hour means ~~averages~~ for $f_{BC}$ over the course of all three campaigns. On average, $f_{BC}$ was larger during the first campaign (September 2017) than during the second and third campaigns (December 2017, November 2018). The mean values (±standard deviation) of $f_{BC}$ were 0.27 (±0.19), 0.03 (±0.09), and 0.14 (±0.15) for the first, second, and third campaigns, respectively. This implies that about one-quarter of the rBC-containing particles that were measured in the first campaign either had sufficient time in the atmosphere to become aged with thick ~~coatings,~~ coatings or originated from biomass burning emission sources, which have been shown to emit more thickly-coated particles compared to fossil fuel emissions (Dahlkötter et al., 2014; Laborde et al., 2013; Schwarz et al., 2008a). M~~while m~~ost of the rBC particles~~rBC~~ measured in the second campaign were~~as~~ thinly-coated, implying ~~the dominant source is impacts from fresh urban emissions~~$BC_{ff}$ ~~was being~~dominated measurements~~d. from the LA basinfresh.~~ The rBC from the third campaign

exhibited mostly thinly-coated rBC for ~~approximately~~ the first ~four days of the campaign and an increased $f_{BC}$ for ~~approximately~~ the last ~two days of the campaign.

Compared to past studies in the Los Angeles region, the mean~~average~~ $f_{BC}$ for the first campaign (September 2017) ($f_{BC}$ = 0.27) is close to the lower end of values from ~~past~~ aircraft measurements ($f_{BC}$ = 0.29) (Metcalf et al., 2012) and the upper end of previous ground-based measurements ($f_{BC}$ = 0.21) (Krasowsky et al., 2016). In contrast, the mean value of $f_{BC}$ for the second campaign (December 2017) is almost an order of magnitude lower than ~~the mean~~average ~~for~~ the first campaign. There are some periods with slightly elevated $f_{BC}$ during the second campaign, but the overall trend suggests that most of the rBC-containing particles in this period are thinly-coated or essentially uncoated. The Santa Ana wind conditions during the second campaign advected fresh (a) urban emissions from the Los Angeles basin, and~~/or~~ (b) biomass burning emissions from active fires in Southern California, as discussed in section 3.1.

The third campaign (November 2018) is unique in that both "fresh" and "aged" ~~rBC-containing aerosols from biomass burning were measured~~$BC_{bb}$, in addition to fresh ~~urban emissions~~$BC_{ff}$ were measured. As shown in Fig~~ure~~ 4, there is a distinct period of relatively higher $f_{BC}$ and rBC concentrations starting at ~~approximately~~ ~noon on 16 November 2018 and lasting through the end of the campaign on 18 November 2018. This is the only period from all three measurement campaigns where we observed both high ~~an elevated~~ rBC mass/number loadings and high $f_{BC}$ values. In section 3.1, we identified the Camp Fire to be the ~~pre~~dominant source during this time period within the third campaign. Thus, ~~This time period of direct impact~~with strong contributions from biomass burning emissions, and without the strong ~~impact~~contributions of local urban emissions, ~~shows~~shows ~~shows that~~the biomass burning rBC ~~are~~particles measured in this portion of the third campaign are more thickly-coated than our measured ~~its~~ urban ~~counterpart~~rBC. Previous~~This confirms what many previous laboratory and field~~field studies have reported~~found~~ that ~~xx yy zz~~$BC_{ff}$ generally have a lower $f_{BC}$ relative to $BC_{bb}$ (Schwarz et al., 2008a; Sahu et al., 2012; Laborde et al., 2013; McMeeking et al., 2011b; Akagi et al., 2012~~2~~)~~urban emissions to be mosin both laboratory and field experiments~~. For example, Schwarz et al. (2008a) reported that $f_{BC}$ ~ 10% for urban emissions and ~~compared to~~ $f_{BC}$ ~ 70% for biomass burning emissions~~(Schwartz)~~. The impact of source type on rBC mixing state will be further discussed in section 3.7.~~, and it will be further discussed in section 3.7.~~ ~~This implies that rBC-containing particles from the Camp Fire were contributingcontributed to the elevated rBC mass/number loadings and had sufficient time in the atmosphere to acquire thick coatings and thus increase $f_{BC}$.~~

## 3.4 Negative lag-times and rBC morphology

A number of previous studies (Moteki and Kondo., 2007; Sedlacek et al., 2012; Moteki et al. 2014; Dahlkötter et al. 2014; Sedlacek et al., 2015) reported negative lag-times from both laboratory and field measurements of rBC. ~~In short,~~It has been hypothesized that a negative lag-time is observed when rBC fragments ~~"disintegrates" (i.e., fragments)~~ from its ~~rBC-free~~

coating material, resulting in a scattering signal that follows an incandescent signal. Dahlkötter et al. (2014) summarized that this phenomenonnegative lag times can occur when either: (i) rBC is very thickly coatedthickly-coated in a core-shell configuration, (ii) rBC is thickly coatedthickly-coated and the core is offset from the center in an eccentric arrangement, or (iii) rBC is located on or near the surface of an rBC-free particle. The morphology of rBC-containing particles is of importance because the enhancement of BC light absorption can vary widely depending on whether the morphology more closely resembles a core-shell configuration or near-surface attachment (Moteki et al., 2014). Although the fraction of negative lag-times ($f_{lag,neg}$) cannot definitively identify the morphology of individual rBC-containing particles (Sedlacek et al., 2015) or accurately quantify the actualactual percentage of all fragmentingdisintegrating rBC-containing particles (Dahlkötter et al. 2014), it can offer some general insights about rBC morphology, especially when it is paired with other information, like the emissions source typetype and population averagedconcurrent rBC coating thickness mixing state. $f_{lag,neg}$ is a conservative lower-bound estimate for the fragmentation rate since there may be rBC particles with positive lag-times that still fragment in the SP2 (Dahlkötter et al., 2014). Dahlkötter et al. (2014) used a method examining the tail end of the time-dependent scattering cross-section in order to determine if a rBC-containing particle was fragmenting or not, thereby calculating a higher fragmentation rate relative to $f_{lag,neg}$. Details of the time-dependent scattering cross-section method can be found in Laborde et al. (2012) and Dahlkötter et al. (2014). This method to calculate a refined fragmentation rate was not used in Sedlacek et al. (2012), nor in and this study.

Furthermore, Sedlacek et al. (2012, 2015) suggest that $f_{lag,neg}$ and the lag-time distributions may provide assist ininsight into source attribution. More specifically, Sedlacek et al. (2012) measured a confirmed biomass burning plume in August 2011, and they found high positive correlation between biomass burning tracers and $f_{lag,neg}$ during the period of impact, suggesting that $f_{lag,neg}$ may be a useful indicator of biomass burning influence. biomass burning rBC may have a high frequency of fragmentation, and therefore higher $f_{lag,neg}$ may be uniquely identifiable using $f_{lag,neg}$. .

In this study, we observed negative lag-times, although at a relatively low rate, with $f_{neg,lag,neg}$ calculated to be much less thanmuch less than 0.1 throughout most of the measurement periods (see Fig. 6). We defined $f_{lag,neg}$ to be identical to the "fraction of near surface rBC particles" metric used by Sedlacek et al. (2012), using a lag-time threshold of -1.25 µs to account for uncertainties associated with the lag-time determination. The campaign-widewide averaged $f_{lag,neg}$ was 0.017 our campaigns we for the first campaign (September 2017), 0.018 for the second campaign (December 2017), and 0.026 for the third campaign (November 2018). Comparatively, Dahlkötter et al. (2014) observedreported $f_{lag,neg}$ of ~0.046 during an airborne field campaign measuring an aged biomass burning plume in Germany, and additionally calculated a a much highern overall, much higher fragmentationdisintegration rate of ~0.4 to 0.5, based on a method that examines the tail end of

~~the time-dependent scattering cross-section~~their aforementioned alternative method (Laborde et al., 2012). ~~Details of the time-dependent scattering cross-section method can be found in Laborde et al. (2012) and Dahlkötter et al. (2014).~~ Sedlacek et al. (2012) reported $f_{lag,neg}$ > ~~of more than~~ 0.6 for ground-based measurements of a biomass burning plume in Long Island, New York, originating from Lake Winnipeg, Canada~~;~~. ~~and t(The scattering cross section method used by Dahlkötter et al. (2014) was not used to calculate a modified n additional disintegrationfragmentation rate in either this study or Sedlacek et al. (2012)..)~~

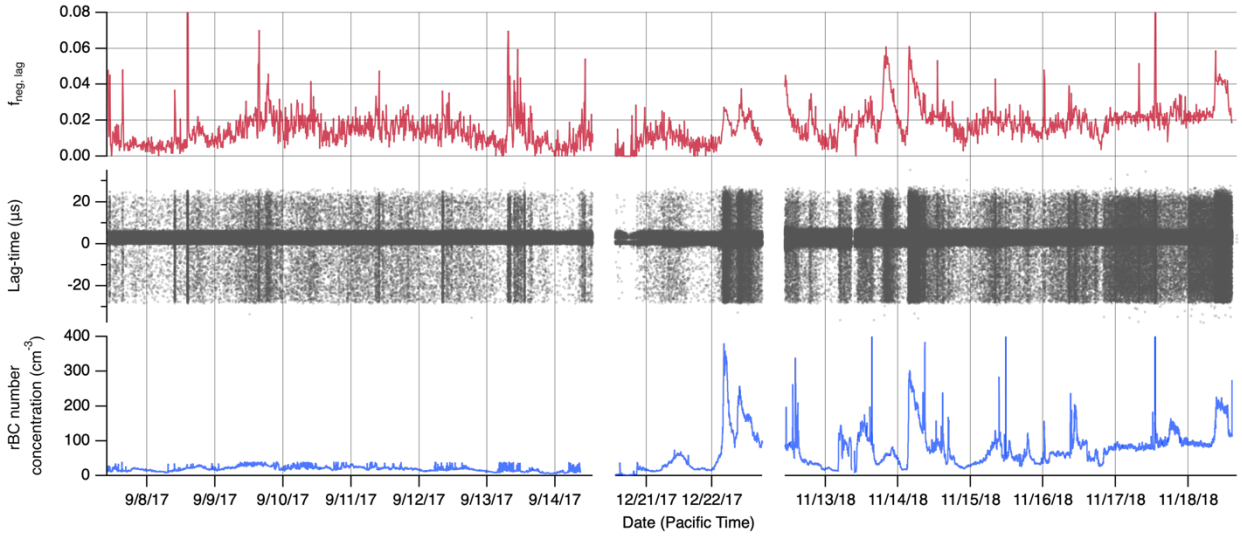


**Figure 6.** Panel (a) shows the 10-minute mean time series for number fraction of rBC particles with negative lag-times ($f_{neg, lag}$). The threshold for negative lag-times was set to -1.25 µs to account for uncertainties in the lag-time determination (Sedlacek et al., 2012). Panel (b) shows the time series of lag-time values for each individual particle, corresponding to individual dots on the graph. Panel (c) shows the one-minute mean rBC number concentration for reference.

The widely varying $f_{lag,neg}$ between these different studies (including ~~this~~our ~~and this~~ study) ~~(including this study)~~ suggests that ~~the absolute magnitude of~~ $f_{lag,neg}$ may not be a ~~helpful~~useful metric when comparing between studies. ~~In fact, this confirms~~ O~~o~~ne of the key findings from Sedlacek et al. (2015) shows that~~t~~ SP2 operating conditions ~~can~~ strongly affects the frequency of negative lag-times, and suggests that inter-study comparisons of ~~the magnitude of~~ $f_{lag,neg}$ could ~~prove fruitless~~be meaningless, or at worst misleading, if the laser power and sample flow rate are not reported. See the section S3 in the S~~s~~upplement for more details. ~~According to Sedlacek et al. (2015) higher laser power and higher sample flow rates result in more rapid rBC heating, and therefore higher rates of fragmentation (i.e., larger $f_{lag,neg}$). In this study, a laser current of 1600 mA was used for the first and second campaign, and a laser current of 1850 mA was used for the third campaign. The sample flow rate was set to 120 $cm^3$ $min^{-1}$. Comparatively, Sedlacek et al. (2012) reported a laser current of 3000 mA and sample flow rate of 120 $cm^3$ $min^{-1}$. Given that Sedlacek et al. (2015) found reports a six-fold increase in $f_{lag,neg}$ by increasing the laser current from 2000 mA to 3000 mA (with the same sample flow rate), it starts to make sense whywas expected that $f_{lag,neg}$ in this study was so much would be much lower than $f_{lag,neg}$ reported by Sedlacek et al. (2012). Taking the this~~

~~differenceoperating conditions into account and multiplying the $f_{lag,neg}$ in this study by an adjustment factor of ~7 (1850 mA versusto 3000 mA), the November 2018 peaks observed in the $f_{lag,neg}$ time series in Fig.ure 6 would increase from ~0.06 to ~0.41, which is much closer to the 0.6 value reported by Sedlacek et al. (2012).~~

The higher mean value of $f_{lag,neg}$ (0.026) during the third campaign (November 2018), relative to the first (0.017) and second (0.018) campaigns, shows that $f_{lag,neg}$ could potentially be a useful as a supplemental metric when identifying impacts from biomass burning sources, as mentioned by Sedlacek et al. (2012, 2015). Figure 7 also shows that the 10-minute mean~~averaged~~ negative lag-times increase in magnitude with increasing rBC core diameter between the range of ~100 to 115 nm (i.e., higher rates of fragmentation with increasing core size). This follows a similar trend observed by Sedlacek et al. (2012, 2015), who attributed this trend to increased heat dissipation to surrounding gases for smaller rBC cores, which in turn decreases the particle heating rate and consequently decreases the fragmentation rate. ~~This~~Our observations ~~trend confirms~~add to the limited past observations that show that the fragmentation rate of rBC particles in the SP2 depend on physical factors like the core size. This further complicates the practical use of $f_{lag,neg}$ as a biomass burning indicator.

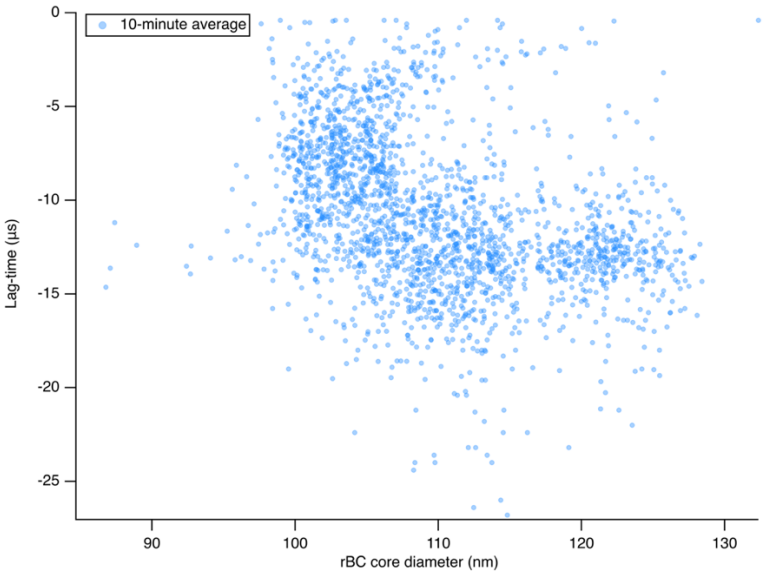


**Figure 7.** Scatter plot of 10-minute mean negative lag-times versus 10-minute mean rBC core diameters.

~~Our data also indicate that~~Certain trends in $f_{lag,neg}$ for this study further indicate that it should ~~likely cannot~~ not be used in isolation~~alone~~ to verify the relative abundance of biomass burning aerosol versus non-biomass burning aerosols. There are peaks in the $f_{lag,neg}$ time series (Fig. ~~ure~~ 6) that do not follow the expected trends based on identifiable source impact time periods. For example, the two peaks on 22 December 2017 (~~urban emissions dominated peaks~~$BC_{ff}$ periods) correspond to $f_{lag,neg}$ values exceeding 0.02, but $f_{lag,neg}$ hovers around 0.02 on 17 November 2018, when we ~~confirmed~~had expected direct

impact from the Camp Fire. ~~We know~~As evidenced from the meteorology (Section 3.1), mixing state (Section 3.3), rBC concentrations (Section 3.2)~~meteorology~~, and rBC core size (to be discussed in Section 3.6),~~ and rBC mass loading concentrations,~~ measurements on~~ measurements on~~$BC_{bb}$ ~~was measured on~~ ~~that~~ 17 November 2018 were dominated by biomass burning emissions~~was clear~~, ~~ywere more dominated by biomass burning emissions,~~ but $f_{lag,neg}$ fails to show that independently. These anomalous observations show that $f_{lag,neg}$ needs to be used with caution, and that ~~measurements~~future studies are necessary~~ should be conducted~~ to extensively quantify the relationship between $f_{lag,neg}$ and source type.

The ~~direct~~ observations of negative lag-times in this study confirm~~s~~ that ambient rBC likely do not ~~strictly~~ adhere strictly to core-shell morphology. The exact morphology of measured rBC cannot be ~~commented on~~quantified based on our measurements~~ alone~~, but the presence of negative lag-times in this study highlights the need to further understand rBC morphology and its effect on absorption enhancement in future studies, as well as~~t~~ the potential for $f_{lag,neg}$ to be used as a supplemental source identification tool.~~ GEORGE LEFT OFF HERE.~~

~~In addition to calculating $f_{BC}$, we also examined the fraction of negative lag-times ($f_{lag, neg}$) as shown in Figure 6, panel (a). Sedlecak et al. (2012, 2015), as well as others (Moteki and Kondo., 2007; Moteki et al. 2014and Kondo, 2007; Dahlkötter et al. 2014), observed negative lag-times both in ambient field and laboratory settings. Sedlacek et al. (2012) observed $f_{lag,neg}$ of more than 0.6 during field measurements of a biomass burning plume. Biomass burning tracer measurements were conducted simultaneously in the Sedlacek et al. (2012) study to confirm the source of the plume. A high correlation was observed between the biomass burning tracer and $f_{lag,neg}$, suggesting that $f_{lag,neg}$ could be a potential tool for identifying biomass burning influenced plumes. Following that study, Sedlacek et al. (2015) conducted laboratory experiments to investigate the phenomena of negative lag-times and its implication on the morphology of rBC-containing particles. In short, Sedlacek et al. (2012, 2015) concluded that negative lag-times were attributable to fragmentation of near surface coating material from the rBC particle caused by a non-core-shell morphology.~~

### 3.~~5~~4 Leading-edge-only (LEO) fit analysis: rBC coating thickness

To further examine the mixing state of rBC-containing particles, the leading-edge-only (LEO) fit method was used to quantify rBC coating thickness ($CT_{BC}$) ~~during various time periods of interest~~on a particle-by-particle basis. Figure 4 shows the time series of $CT_{BC}$ throughout all three campaigns. The time series of $CT_{BC}$ shows that each campaign was characterized by different mixing states~~a distinct mixing state distribution~~, and that ~~certain trends emerged within campaigns.~~there are distinct trends within each campaign~~ as well~~. ~~$f_{lag,neg}$~~

The inter-campaign differences are ~~further~~ highlighted~~s~~ in Fig.~~ure~~ 8, which shows the $CT_{BC}$ distribution for each ~~distinct~~ campaign, as well as the ~~cumulative~~ distribution including rBC from all campaigns. For both rBC core diameter ranges (180–220 nm and 240–280 nm), we ~~clearly~~ observe that the first campaign has the largest mean~~average~~ $CT_{BC}$, followed by the third and second campaign, respectively. The mean~~average~~ $CT_{BC}$ (± standard deviation) for the first, second, and third campaign was 52.5 (± 45.5) nm, 22.3 (± 25.0) nm, and 40.3 (± 41.5) nm, respectively, for particles with a rBC core diameter between 180 and 220 nm.

Comparing the time series of $CT_{BC}$ to the time series of $f_{BC}$ (Fig.~~ure~~ 4~~6~~), we observe similar trends over time, which is expected and also reported in past studies that have employed both the lag-time and LEO methods (Metcalf et al., 2012; Laborde et al., 2012; McMeeking et al., 2011a). Figure S9 shows that there is a statistically significant correlation between 10-minute mean $CT_{BC}$ and $f_{BC}$ throughout all three campaigns ~~(r = 0.82 and τ = 0.62)~~. The Pearson correlation test (i.e., linear correlation test) was conducted to quantify the linear correlation between the two variables and to infer the statistical significance of the potential correlation. For the test, $\alpha = 0.05$ (i.e., 95% confidence level)~~, which means there is a 5% chance of rejecting the null hypothesis (i.e., no significant correlation) when it is true.~~ The test ~~returned~~resulted in ~~a pp value of ~ 0~~<0.001, ~~which means that we could reject the null hypothesis with near 100% confidence, and that we could~~suggesting ~~strongly infer~~ a statistically significant correlation. The sample Pearson correlation (r) was 0.82~~, where -1 implies perfectly negative correlation and +1 implies a perfectly positive correlation~~. The statistically significant, positive~~This~~ correlation confirms that these two methods are in general agreement ~~with each other~~, and that they can be used together to robustly describe the rBC mixing state. ~~from a broad, time-averaged perspective.~~

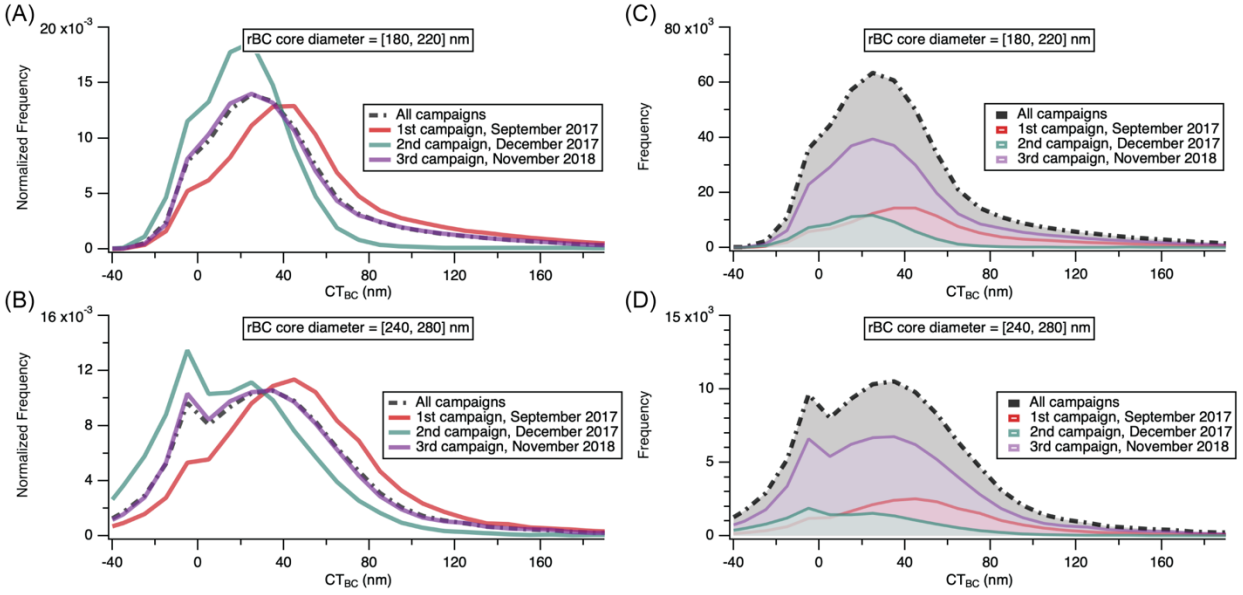

**Figure 8.** Distributions of BC coating thickness ($CT_{BC}$) aggregated by campaign are shown in red (1st campaign), green (2nd campaign), and purple (3rd campaign). The combined distributions for all campaigns are shown in black. Panels (a) and (b) show the normalized frequency distributions, while panels (c) and (d) show the absolute frequency distributions. The distributions are also distinguished by the rBC core diameter ranges included in the LEO analysis. The top panels (a) and (c) show distributions for particles with rBC core diameters between 180 and 220 nm. The bottom panels (b) and (d) show distributions for particles with rBC core diameters between 240 and 280 nm.

In addition to aggregating $CT_{BC}$ by campaign, we also examined ten ~~-~~discrete time periods of interest ~~within in campaign~~ to get~~explore~~ a more ~~fine-grained~~detailed understanding of the mixing state ~~variability, and~~variability ~~and explore how they were dependent dependingit depends on a variety of external factors can influenced the mixing state.~~ Two time periods from the September campaign, three time periods from the December campaign, and five time periods from the November campaign were selected to represent a diverse range of meteorological conditions, emission sources, and age of aerosols. Table 2 lists the ten LEO-fit periods, and their median and mean $CT_{BC}$. The LEO-fit periods are also annotated on the rBC concentration time series (see Fig~~ure~~ 4) to show when they occurred in the context of all three campaigns. The median $CT_{BC}$ for the LEO periods ranged from –0.43 to 54~~5~~.0~~9~~ nm. L6 had the lowest median $CT_{BC}$ (–0.43 nm), while L9 had the highest median $CT_{BC}$ (54~~5~~.0~~9~~ nm).

**Table 2.** Details of the ten different LEO time periods. Further details about the source-to-receptor characteristic timescales can be found in the Supplement, section S1.

| LEO Time Period | Date/Time (Pacific Time) | Period Length (mins) | Total number of rBC particles analyzed[a] | Mean coating thickness (nm) | Median coating thickness (nm) | Characteristic timescale |
|---|---|---|---|---|---|---|
| L1 | 9 Sep. 2017, 12:00-1:00am | 60 | 397 | 62.2 | 53.5 | ~days to week |
| L2 | 13 Sep. 2017, 11:59-12:58pm | 59 | 467 | 28.1 | 23.6 | ~minutes to hours |
| L3 | 20 Dec. 2017, 12:59-2:00pm | 61 | 79 | 49.3 | 47.7 | ~days to week |
| L4 | 21 Dec. 2017, 12:29-1:00pm | 31 | 318 | 14.3 | 12.0 | ~3 hours |
| L5 | 22 Dec. 2017, 9:59-10:15am | 16 | 1,176 | 14.6 | 12.2 | ~12 hours |
| L6 | 12 Nov. 2018, 12:00-1:00pm | 60 | 1,752 | 5.6 | -0.4 | ~8 hours |
| L7 | 14 Nov. 2018, 5:00-6:00am | 60 | 2,879 | 10.7 | 8.2 | ~17 hours |
| L8 | 17 Nov. 2018, 5:00-6:00am | 60 | 2,712 | 57.2 | 48.4 | ~days to week |
| L9 | 17 Nov. 2018, 7:00-8:00pm | 60 | 1,254 | 67.2 | 54.0 | ~days to week |
| L10 | 18 Nov. 2018, 10:00-11:00am | 60 | 4,778 | 40.6 | 31.2 | ~days to week |

[a] LEO coating thickness calculations shown in the table only include rBC-containing particles with core sizes between 200 and 250 nm.

Figure 96 illustrates the $CT_{BC}$ distributions and statistics of each LEO period. L1 and L2 were from the first campaign (September 2017). L1 is representative of ambient background rBC-containing particles from the first campaign. A period that did not exhibit any anomalously large rBC mass concentration values was chosen so that contributions from possible nearby sources would not skew the meanaverage $CT_{BC}$. On the other hand, L2 intentionally spans a period with many anomalously high rBC mass concentration values. Although these anomalous values were removed from the concentration time series discussed previously in section 2.4, the values were *not* removed for the LEO analysis of L2 in order to examine the relationship between $CT_{BC}$ and possible nearby emissions. As hypothesized, the rBC-containing particles from L2 were generally more thinly coatedthinly-coated than those from L1. The median $CT_{BC}$ from L2 was ~was 3062.5 nm lowerthinner than that for L1, which corroborates our hypothesis that the anomalously high mass concentration values in the first campaign included contributions from nearby, unidentified fossil fuel sources.

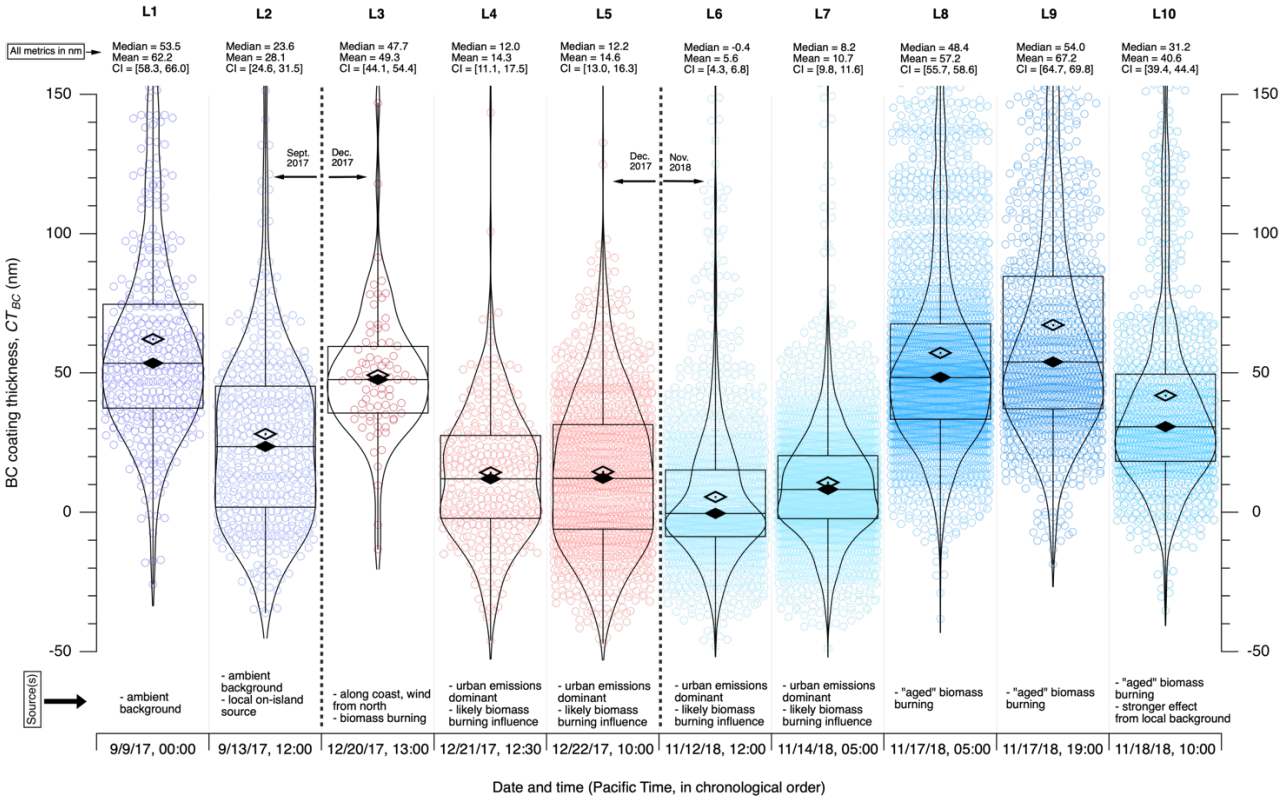


**Figure 9.** Violin plots that show the distribution of rBC coating thickness values calculated for each LEO time period, L1 through L10. Each circle marker in the plot represents a particle analyzed by the LEO analysis and the curves for each "violin" shape represents the normalized probability density function of the coating thickness for each LEO period. The violin shape results from mirroring each probability density distribution along a vertical axis. Box-and-whiskers plots are also overlaid to show the quartiles (25$^{th}$, 50$^{th}$, and 75$^{th}$ percentiles) of the coating thickness distributions. The 95% confidence intervals (CI) based on Student's t-distribution are shown above each violin plot to demonstrate when the mean coating thickness values are statistically distinguishable from one another. The mean (unfilled diamond) and median (solid diamond)

coating thicknesses are also indicated above each violin plot, and a brief description of sources for each LEO period is annotated below each distribution.

L3 through L5 are time periods from the second campaign (December 2017). L3 represents a period near the start of the second campaign (December 2017). The predominant wind direction during L3 was westerly, with a~~n~~ mean~~average~~ wind speed of ~4.5 m $s^{-1}$. HYSPLIT back-trajectories and CAMS data show that L3 likely included important contributions from the Thomas Fire in Santa Barbara and Ventura County. The $PM_{2.5}$ concentration gradient from CAMS was examined over time to track the movement of plumes that influenced the measurements during this time period. A few days prior to the start of the second campaign, the Thomas Fire ~~emitted~~ resulted in a large aerosol plume westward over the Pacific Ocean. From visually tracking $PM_{2.5}$ concentration gradients, it appears that a large-scale, clockwise, atmospheric circulation brought aerosols from the Thomas Fire to Catalina Island around the time of L3 (see video 2 of Video Supplement). The average concentration during L3 was about an order of magnitude lower than the average concentration for the September campaign. This could be partially attributed to the fact that L3 was around 1 to 2 pm, when the planetary boundary layer would be expected to increase in height, causing pollutant~~s~~ concentrations to decrease due to dilution. The median $CT_{BC}$ for L3 was 47.7~~2~~ nm, which is slightly ~~thicker than the median~~lower ~~$CT_{BC}$~~ than ~~found~~ for L1, which is representative of the ambient background conditions. The slightly larger $CT_{BC}$ for L3 likely~~might~~ reflects the fact that mixing state is sensitive to the source of emissions. In this time period, urban emissions were likely mixed into the ~~plume~~regional air mass, slightly lowering the median $CT_{BC}$ ~~slightly~~. A number of previous studies have suggested that rBC from biomass burning emissions are generally more ~~thickly coated~~thickly-coated (Sahu et al., 2012; Schwarz et al. 2008a; Dahlkötter et al., 2014). In this case, we have evidence to ~~suspect~~ support that a larger fraction of measured rBC during L3 came from the local Thomas Fire, while L1 represents a mix of influences, including, but not limited to, aged biomass burning aerosols. The effect of emissions sources on rBC mixing state is ~~thoroughly~~ discussed in section 3.7.

L4 through L7 represent periods ~~of time~~ when the Los Angeles basin, ~~and~~ Santa Barbara/Ventura counties, ~~(which includes both biomass burning and urban emissions),~~ and San Diego county (to a lesser degree) were identified as major sources. Air masses measured during these periods likely contained a mixture of both urban emissions and biomass burning emissions (see Supplement section S2 and accompanying figures), although urban emissions were likely dominant~~. The HYSPLIT back-trajectories for these periods pass near several significant local fires in the Southern California region. We also expect urban emissions (i.e., mostly vehicular emissions) to be contributing to the measurements during these periods, when trajectories are generally traversing through urban areas of Southern California~~. Overall, these LEO periods exhibit the lowest median $CT_{BC}$, ranging from -0.4 to 12.2 nm. The potential relationship between aging time and $CT_{BC}$~~, especially for these urban emissions influenced periods,~~ is discussed further in section 3.7~~6~~.

L8, L9, and L10 are the unique LEO periods from the third campaign (November 2018) with concurrently ~~elevated~~ increased rBC concentrations and $f_{BC}$ (discussed in the previous section). We also observed ~~the highest median~~significantly higher $CT_{BC}$ values during these periods compared to ~~urban emissions influenced periods~~BC~~s~~ L4–L7, with median $CT_{BC}$ ~~values~~ ranging from 31.2 to 54.0 nm~~. L8 and L9 were both periods of stable elevated $f_{BC}$ and rBC concentrations~~. We have strong evidence to support that the sampled particles include important contributions from aged rBC from the Northern California fires, particularly the Camp Fire (see section S2 in Supplement). The relatively high $CT_{BC}$ values in L8 and L9 (compared to other LEO periods) further support our claim that rBC-containing particles from Northern California fires were dominating our measurements during this time. L10 has a median $CT_{BC}$ of 31.2 nm, which~~that~~ is ~23~~0~~ nm lower~~smaller~~ than the median value for ~~s in L8 and~~ L9. This reduction in the median $CT_{BC}$ is also reflected in the decrease of the $f_{BC}$ values near the end of the campaign. Meteorological data, MODIS satellite images, and CAMS data during this time period suggest that sources from the Southern California (and possibly Central Valley) region contributed more to measurements during L10 than they did during L8 and L9, explaining the lower $CT_{BC}$ and higher overall concentrations. Wind speeds were lower on average for L10 compared to L8 and L9. The mean wind speed for L10 at LAX, based on 5-minute NOAA data, was ~1.3 m $s^{-1}$, while the mean wind speeds for L8 and L9 were ~2.1 m $s^{-1}$ and 1.6 m $s^{-1}$, respectively. There was also a general shift of wind direction from westerly to north-easterly, approximately a half day before L10 (see Fig.~~figure~~ S~~8~~9 in Supplement). MODIS satellite imagery and CAMS data also confirm that local to regional sources were likely impacting the measurements more during this period (see video 3 and 4 of Video Supplement), compared to L8 and L9. The ~~stagnant~~ meteorology, in addition to local to regional sources of emissions from the Los Angeles basin and Southern California ~~more broadly~~, likely explain the reduction in $CT_{BC}$ and the near doubling of the rBC concentration level.

### 3.6~~5~~ rBC core size ~~distributions~~

The number- and mass-based size distributions for rBC cores were assessed for periods L1 to L10. Similar to past studies, rBC core mass equivalent diameters between 70 and 450 nm are reported (Gao et al., 2007; Moteki and Kondo, 2007; Dahlkötter et al., 2014; Krasowsky et al., 2018). Figure 10~~7~~ shows both log-normal fits of the rBC core size distributions and measured rBC core diameters for three LEO periods (L1, L5, and L10); we investigated these three LEO periods to assess whether log-normal fits adequately represent the actual rBC size distributions before presenting log-normal fits for all LEO periods. Previous studies have shown that rBC core size distributions ~~in nature~~ are generally log-normal in the accumulation mode (Metcalf et al., 2012). Figure 10~~7~~ shows that log-normal fits adequately capture the measured size distributions, though we cannot rule out the possibility of another rBC mode outside the detection limits of the SP2. Although the peak of the observed ~~points~~size distribution is not always discernible (e.g., number size distribution for L5 in Fig.~~ure~~ 10), it is reasonable to fit these points assuming that a log-normal distribution is a realistic ~~reasonable~~ representation of ambient rBC number size distributions in the Aitken mode. ~~The rate of change of the observed points is also captured very well qualitatively by the log-normal fits, further indicating its appropriateness.~~

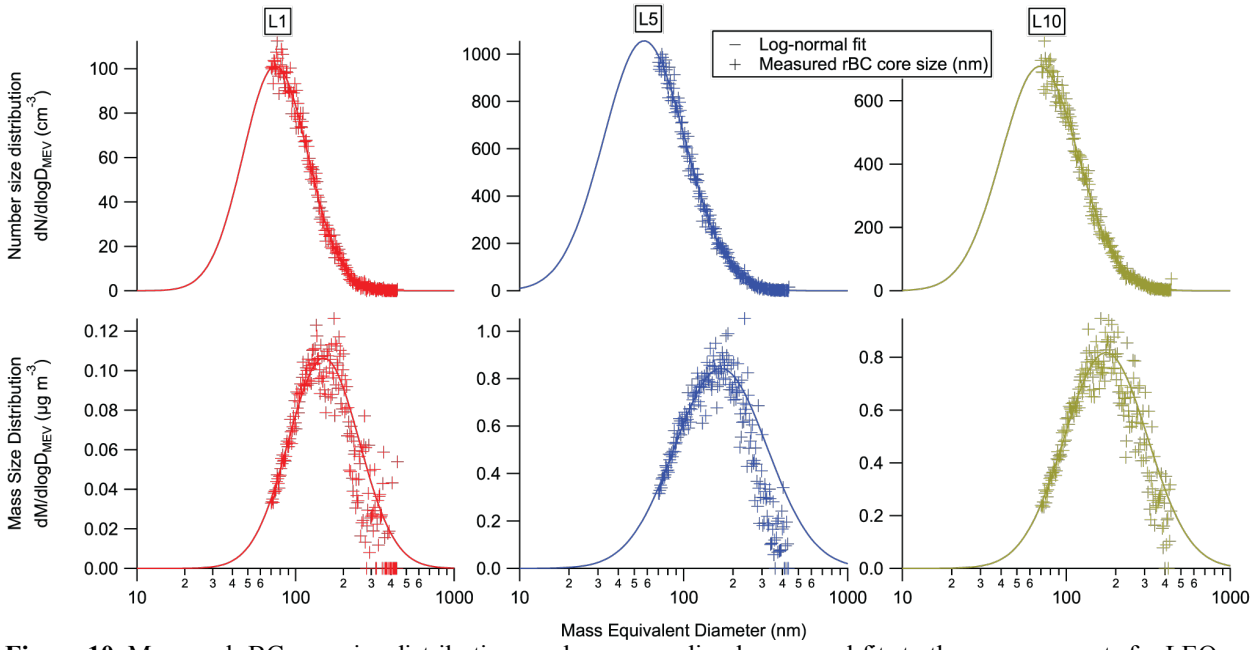


**Figure 10**. Measured rBC core size distributions and corresponding log-normal fits to the measurements for LEO periods L1, L5, and L10.

A survey of past studies that have reported log-normal fit rBC mass median diameter ($MMD_{fit}$) and count median diameter ($CMD_{fit}$) shows that the source of emissions has a strong influence on rBC core diameter (Cheng et al., 2018). The $MMD_{fit}$ [$CMD_{fit}$] for ~~biomass burning influenced rBC~~$BC_{bb}$, which has been reported to range from ~130~~52~~ nm to 210 nm [100 to 140 nm], is generally ~~much~~ larger than the $MMD_{fit}$ [$CMD_{fit}$] ~~MMD~~ for ~~urban emissions influenced rBC~~$BC_{ff}$, which has been reported to range from ~100 nm to 178 nm [38 to 80 nm] (Shiraiwa et al., 2007; Schwarz et al., 2008a; McMeeking et al. 2010; Kondo et al., 2011; Sahu et al. 2012; Metcalf et al., 2012; Cappa et al., 2012; Laborde et al., 2013; Liu et al., 2014; Taylor et al., 2014; Krasowsky et al., 2018). The $MMD_{fit}$ [$CMD_{fit}$] for well-~~aged air masses in remote regions BC~~$_{cont}$aged background BC were reported to range from ~180 nm to 225 nm [90 nm to 120 nm] (Shiraiwa et al., 2008; Liu et al, 2010; McMeeking et al., 2010; Schwarz et al., 2010).

Figure 11~~8~~ shows the ~~median rBC core diameter~~rBC $MMD_{fit}$ and $CMD_{fit}$ ~~based on the log-normal fits~~ for each LEO period in this study. Based on the source identification discussed in section 3.1 and section S2 in the Supplement, the $MMD_{fit}$ and $CMD_{fit}$ values in this study are generally consistent with the ranges reported in~~mentioned from~~ past studies. For ~~LEO periods when measurements were strongly influenced by biomass burning emissions~~$BC_{bb}$ (L3, L8, L9, L10~~, L10~~), M~~M~~MD ranged from 149 nm to 171 nm, which is within the range of ~130 nm to 210 nm ~~compiled from~~reported in past studies. F~~Similarly,~~ or $BC_{ff}$ ~~when measurements were strongly influenced by urban emissions~~ (L2, L4, L7~~, L2~~), the $MMD_{fit}$ dropped, ranging

from 112 nm to 1293 nm. This falls within the range of ~100 nm to 178 nm previously reported for measurements of urban emissions from past studies. LEFT OFF

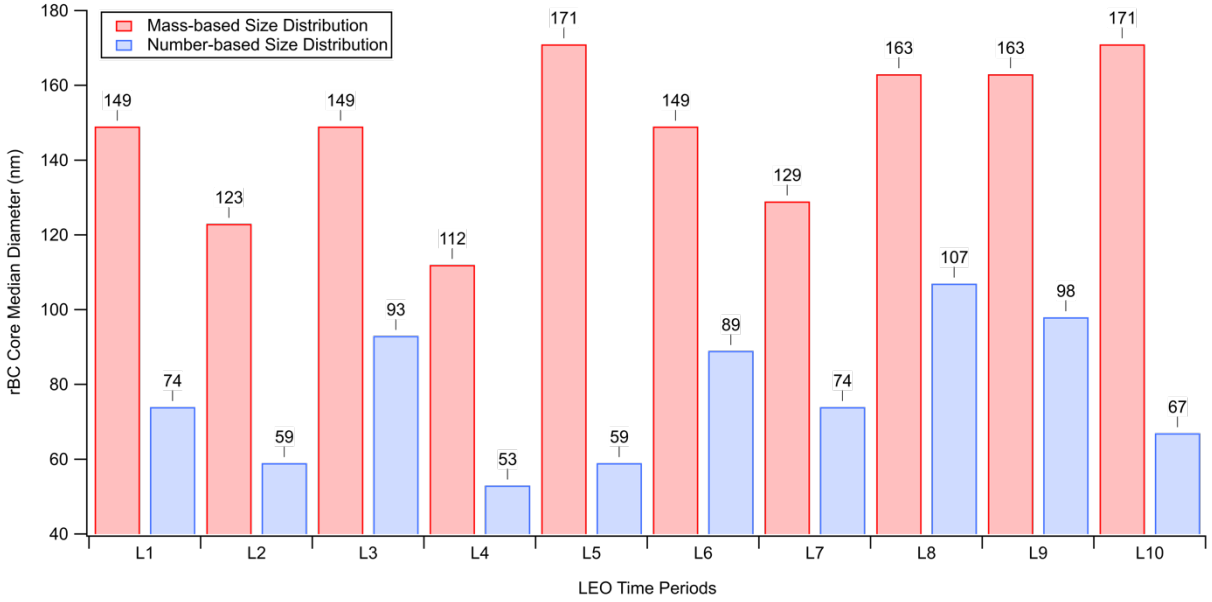


**Figure 11.** Median rBC core diameter for both mass and number size distribution lognormal fits.

We assert that Tthe CMD and MMD can be used together to help qualitatively determine when plumes are mixed and impacted by multiple source types, as opposed to using only one overmedian metric or the other.There were some periods in which we observed a relative increase in the $MMD_{fit}$, but concurrent decrease in the $CMD_{fit}$. For example, L5 exhibits a relatively high $MMD_{fit}$ (~171 nm), which might suggests that this was a biomass burning dominated nt time period, but the $CMD_{fit}$ is the second lowest fromof all the LEO periods (~53 nm). L10 also exhibits a similar pattern. In these types of such ambiguous seemingly contradictory situations, it could be useful to consider thea hypothetical scenario in whichit is likely that biomass burning aerosols are entrained into a broader urban plume (e.g., from Los Angeles basin). An urban plume with no biomass burning influence will likelyis expected to exhibit a very low $CMD_{fit}$. As a biomass burning influence starts to mix with to increase within that initially "pure" urban plumeaerosol gets entrained, an incremental increase in biomass burning aerosol load will have a much larger effect on the $MMD_{fit}$ is expected to change more than on the $CMD_{fit}$ due to its larger rBC core size relative to urban rBC cores. (For a unit increase in diameter, the mass weighting will increase proportionally to the third power, while the size weighting will increase proportionally on a first order basis.) This may explains why inn some cases we observe somesee relatively high $MMD_{fit}$ values simultaneouslyalong with relatively low $CMD_{fit}$ values,. This highlightings the need to examine both the number and mass size distributions for rBC core size analysisWith a more refined quantitative approach and methods, the combined analysis of number and mass size distributions may potentially assist in identifying periods of mixed source impacts and quantifying the relative impacts of

from the different sources in future studies.with source apportionment of mixed plumes in future studies with the SP2. For example,

In addition to varying source type,The otherAnother explanation for varying rBC core size is coagulation is the only physical mechanism that increases rBC core size (Bond et al., 2013). Shiraiwa et al. (2008) observed an increase in rBC core diameters in aged plumes compared to more fresher urban plumes, suggesting that coagulation can alter the rBC size distribution during atmospheric transport (i.e., aging). Although the emissions source type appears to be the dominant influence on rBC core sizes in thisour study, there is evidence to suggest that coagulation did occuralso played a role during transport from the Los Angeles basin to Catalina Island (~70 km away) in this study. For example, we observed an $MMD_{fit}$ [$CMD_{fit}$] of 112 nm [53 nm] during L4, when $BC_{ff}$ was measured.which was dominated by , when we know that urban emissions were dominant, butand tThis is noticeably larger than values of 93 nm [42 nm] reported in Krasowsky et al. (2018) for measurements conducted 114 meters downwind of a major highway in Los Angeles. Furthermore, Laborde et al. (2013) observed an $MMD_{fit}$ of ~100 nm when impacted measuring by fresh traffic emissionsfor $BC_{ff}$ in Paris, which is again lower than the value of 112 nm calculated for L4. Even though it was determined that L4 was predominantly urban emissions influencedwas characterized by $BC_{ff}$, we cannot rule out the possibility ofthe effects of local wildfires influencing the size distribution as well (as explained in the Supplement section S2). While the rBC size distribution from L4 suggests that coagulation plays at least a minor role, both factors (source type and coagulation) likely influence rBC size distributions to varying degrees in areas with heterogenousvarying emissions source profilestypes and relatively elevated rBC concentrations (e.g., polluted urban areas).

There is variability in the median core diameters of both the mass-based and number-based size distributions. Looking specifically at the mass size distribution, the median diameter ranges between 112 nm (L4) and 171 nm (L5, L10). A study by Laborde et al. (2013) discusses the relationship between rBC core diameter and air mass type. According to Laborde et al., an average rBC core diameter of ~100 nm was observed for fresh urban emissions, while diameters of ~200 nm were observed for "continental air masses," which would be expected to be include a larger contribution of aged rBC. The mass size distributions from our LEO periods do not strictly adhere to a positive correlation between aging time and average rBC core diameter as reported by Laborde et al. (2013). In fact, sometimes we observe the opposite relationship. For example, as discussed in the previous section, L5 includes important contributions from freshly emitted rBC, but the mass median diameter is the largest out of all LEO periods (171 nm). Moteki et al. (2012) found negative correlation between aging timescale and rBC core size due to the fractal morphology of the rBC collapsing into a spherical morphology. This mechanism is in direct contrast to the coagulation mechanism described by Laborde et al. (2013), which would serve to increase the mass median rBC core diameter.

~~In our study, we observed a mix of rBC core diameters for different periods. For example, L8 and L9 exhibit higher mass median diameters than L4, L6, and L7. We assert that rBC measured during L8 and L9 are more aged than for L4, L6, and L7. As mentioned previously, L5 is inconsistent with the pattern of higher mass median diameter~~ MMD ~~with greater contributions of aged particles.~~

## 3.7 Impact of emissions source and aging on rBC mixing state

~~The dominant drivers for increased rBC core size (i.e., emission source type and aging) are also the driving factors influencing main drivers for increased CTBC. Figure 12 shows a scatter plot as a function of CTBC and rBC core diameter. The statistically significant correlation ($r = 0.55$, $\tau = 0.43$) confirms that there is an in direct relationship between these two physical characteristics of BC. In other words, biomass burning (as opposed to fossil fuel) and longer aging generally seem to increase both the rBC core size and as well as the BC coating, and vice versa. Figure 13 shows the CTBC distributions for different rBC core size ranges, and a similar relationship between the two variables can be observed. As the core size increases (lighter to darker curves), a broader right hand side tail is observed in the biomass burrBC, and it confirms that similar factors influence these attributes in~~ As seen in Figure ~~12S10, we see a statistically significant, moderate positive correlation ($r = 0.55$, $\tau = 0.43$R2 = 0.36) between median one minute mean CTBC and one minute mean rBC core diameter the median number based diameter for rBC. This is consistent with the coagulation mechanism increasing core size with increasing age, as suggested by previous studies (Krasowsky et al., 2018; Laborde et al., 2013; Shiraiwa et al., 2008). In other words, since CTBC generally increases with atmospheric aging, the positive correlation between CTBC and number based diameter found in this study supports previous suggestions that rBC core sizes increase with atmospheric aging. Additionally, we observe that changes in the mass median diameter are not consistent with the changes in number median diameter, although the figure is not presented here. Although previous studies, like Laborde et al. (2013), have focused on the mass median diameter, our results suggest that the number median diameter could be a more useful metric when correlating core diameters to mixing state metrics since the SP2 measures characteristics of individual rBC particles on a number basis and the CTBC is calculated for each measured particle.~~

~~CTBC distributions for each campaign, implying larger average CTBC for particles with larger rBC cores.~~

~~Source type (e.g., urban versus biomass emissions, and different types of fuels burned) can also play a significant role in determining rBC core size (Sahu et al., 2012; Pan et al., 2017; Laborde et al., 2013; Moteki et al., 2012; Metcalf et al. 2012; Wang et al. 2018). Past studies suggest that rBC cores from biomass burning emissions are larger. For~~

~~example, Metcalf et al. (2012) reported a mass median diameter of ~122 nm for rBC from urban emissions in Los Angeles, while Sahu et al. (2012) reported a mass median diameter of ~190 nm for rBC from biomass burning emissions in various regions around California. Our measurements are in general agreement with previous studies. The mass median diameter of rBC cores measured during periods of strong biomass burning influence (L8-L10) are larger than those calculated for other LEO periods, with the exception of L5 (see Figure 8). This provides further confirmation that rBC core size is influenced by the source of emissions.~~

### ~~3.~~3.6 ~~Particle age and rBC mixing state~~Evolution and variety of~~Impact of emission source and aging on rBC mixing state~~state

The dominant ~~drivers for increased~~ factors that influence rBC core size (i.e., emission source type and aging) also influence~~are also the driving factors~~the same factors influencing rBC mixing state. Figure 12 shows a scatter plot of ~~count as a function of~~one-minute mean $CT_{BC}$ versus one-minute mean~~and~~ rBC core diameter. A statistically significant, positive correlation ($p < 0.001$) was found, with $r = 0.55$. ~~PLEASE ADD P VALUE … THAT'S WHAT DETERMINENS SIGNIFICANCE.~~ - Further details regarding the statistical tests used to calculate the correlation coefficients and to conduct the hypothesis testing can be found in section 3.5. ~~Both the a Pearson correlation test (i.e., linear correlation test) and Kendall tau correlation test were conducted to quantify the correlation between the two variables and to infer the statistical significance of a possible correlation using hypothesis the potential correlationtesting. For both tests, $\alpha = 0.05$ (i.e., 95% confidence level), which means there is a 5% chance of rejecting the null hypothesis (i.e., no significant correlation) when it is true. Both tests returned a p-value of ~ 0, which means that we could reject the null hypothesis with near 100% confidence, and that we could strongly infer a statistically significant correlation. The sample Pearson correlation (r) was calculated to be 0.55, where the possible -1 implies is interpreted as a perfectly negative correlation and +1 is interpreted as aimplies a perfectly positive correlation. The Kendall τ was 0.43, where 0 implies no relationship and 1 implies a perfect relationship.~~

The ~~statistically significant~~significant correlation ~~($r = 0.55$, $\tau = 0.43$)~~ confirms ~~that there is an indirect relationship between these two physicalthese two physicals characteristics characteristicsproperties are related.s of BC. In other words,~~ that larger contributions from biomass burning (as opposed to fossil fuel) and longer aging timescales ~~generally~~are associated with ~~seem to~~ increases in both the rBC core size and the BC coating thickness~~, and vice versa~~. Figure 13 shows the $CT_{BC}$ distributions for different rBC core size ranges, and a similar relationship between the two variables can be observed. As the core size increases (lighter to darker curves), a broader right-hand side tail is observed in the $CT_{BC}$ normalized distributions for each campaign, implying higher mean~~higherlarger average~~ $CT_{BC}$ for particles with larger rBC cores.

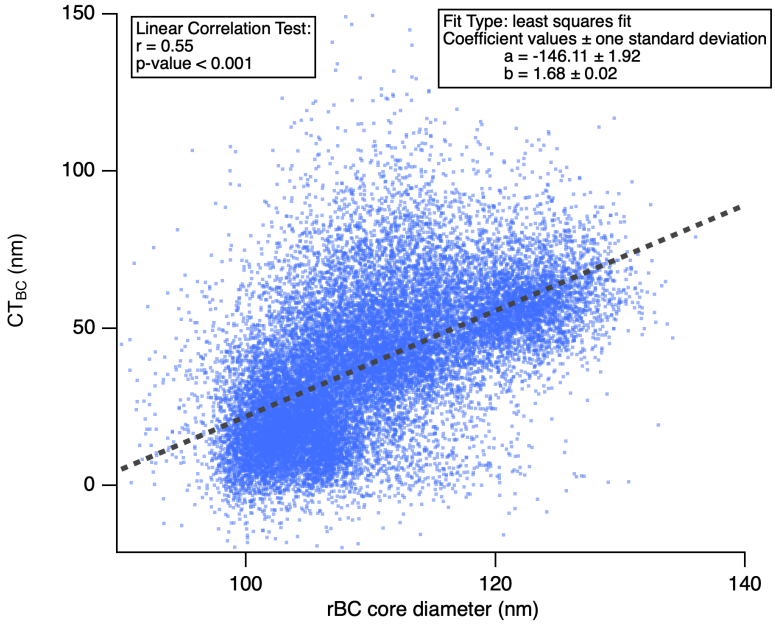


**Figure 12.** rBC coating thickness versus rBC core diameter. Each point on the plot represents a 1-minute mean. Data from all three campaigns are shown. $CT_{BC}$ values are calculated for particles with rBC core diameters between 200–250 nm. The line represents the least-squares linear regression to the one-minute mean data points. There is a statistically significant positive correlation shown between $CT_{BC}$ and rBC core diameter, as shown in the summary box in the top left corner.

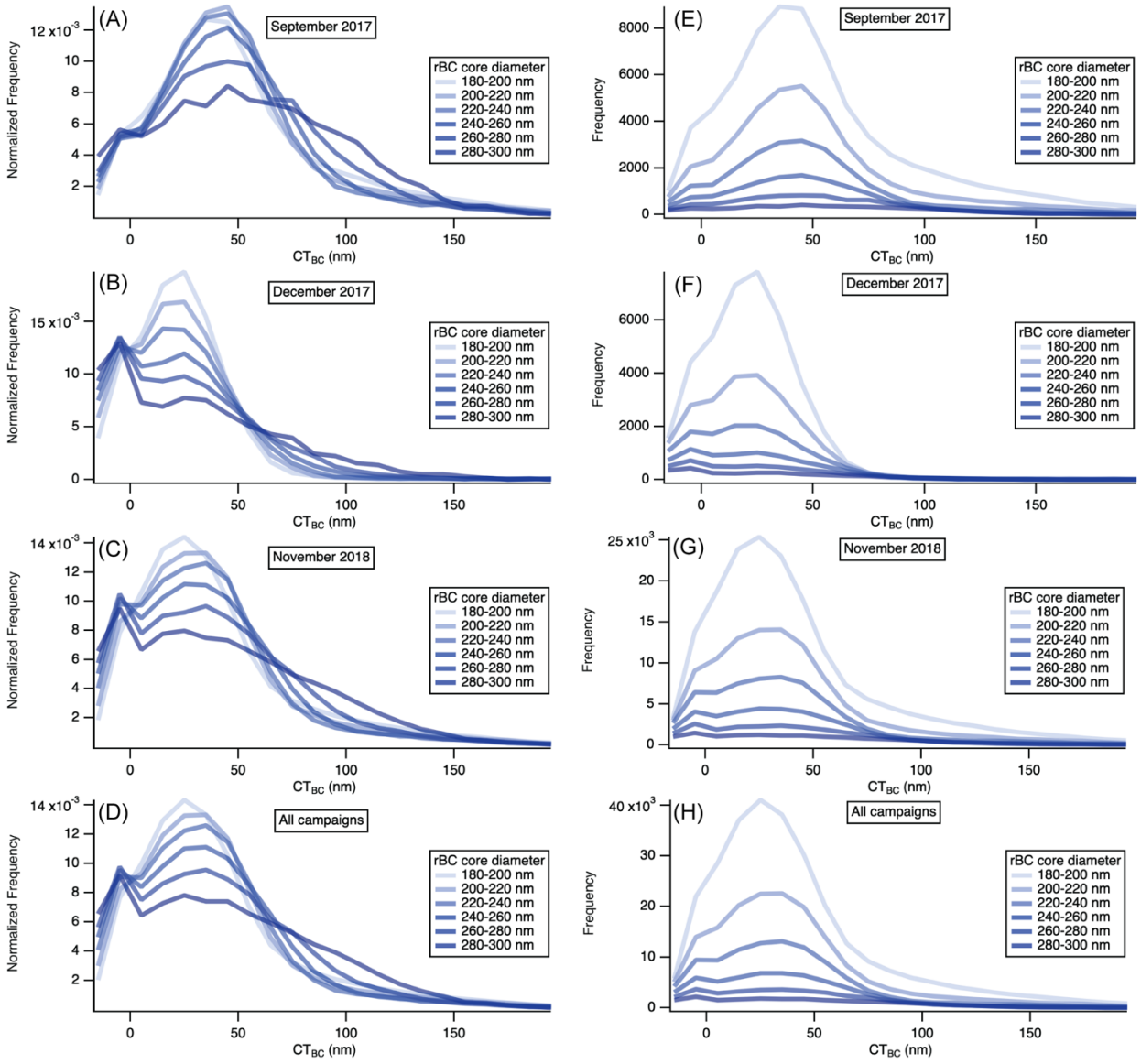


**Figure 13.** Distributions of BC coating thickness ($CT_{BC}$) aggregated by campaign and varying rBC core diameter ranges used in the LEO analysis. Panels (a) through (d) in the left column show the normalized frequency distributions, while panels (e) through (h) in the right column show the absolute frequency distributions. Within each panel, each line represents a distribution for a particular rBC core diameter range, with darker lines representing larger diameter ranges and vice versa.

The time evolution of both $CT_{BC}$ and rBC core size is represented in a series of scatter plots in Fig. 14~~5~~ and 15~~6~~. In each of the figures, the scatter between one-minute mean $CT_{BC}$ and rBC CMD ~~count mean diameter~~ are grouped into six-hour time intervals for both the second (December 2017) and third (November 2018) periods, respectively. In these figures, the time evolution of the rBC physical properties can be examined in detail and compared to periods of known emissions source impacts. There are a few significant patterns worth mentioning here. First, the influence of BC~~B~~$_{bb}$ can be ~~clearly~~ observed

between 16 and 18 November 2018 in Fig. 15. Both $CT_{BC}$ and CMD drastically increase for a prolonged period of time, implying an ~~clear~~ impact from the Camp Fire plume from Northern California. Second, the scatter plots for 20 to 22 December 2017 and 12 to 15 November 2018 show that there is some variability over time ~~time in the rBC mixing state and size~~in the cluster shapes, which can be explained by the local wildfires that were confirmed to influence the broader LA basin plume (see ~~Supplement~~ section S2 for details regarding source attribution). Although the scatter plots during these time periods support that $BC_{ff}$ was~~ere~~ largely dominant, there are some periods where the CMD spread deviates quite noticeably (e.g., Fig. 14, 06:00 21 Dec. 2017), or even periods that show two distinct clusters (e.g., Fig. 15, 12:00 12 Nov. 2018), supporting our claim that local ~~biomass burning influence~~wildfires were indeed~~as~~ influencing our measurements.

A similar figure for the first campaign (September 2017) is included in the Supplement as Fig. S23, but not shown here because of the relatively stable mixing state and size of $BC_{aged,bg}$~~$BC_{cont.}$~~. ~~-~~ These figures confirm the general patterns noted in previous sections ~~above~~ regarding the effects of different sources on rBC mixing state.~~biomass burning versus urban emissions on the mixing state.~~

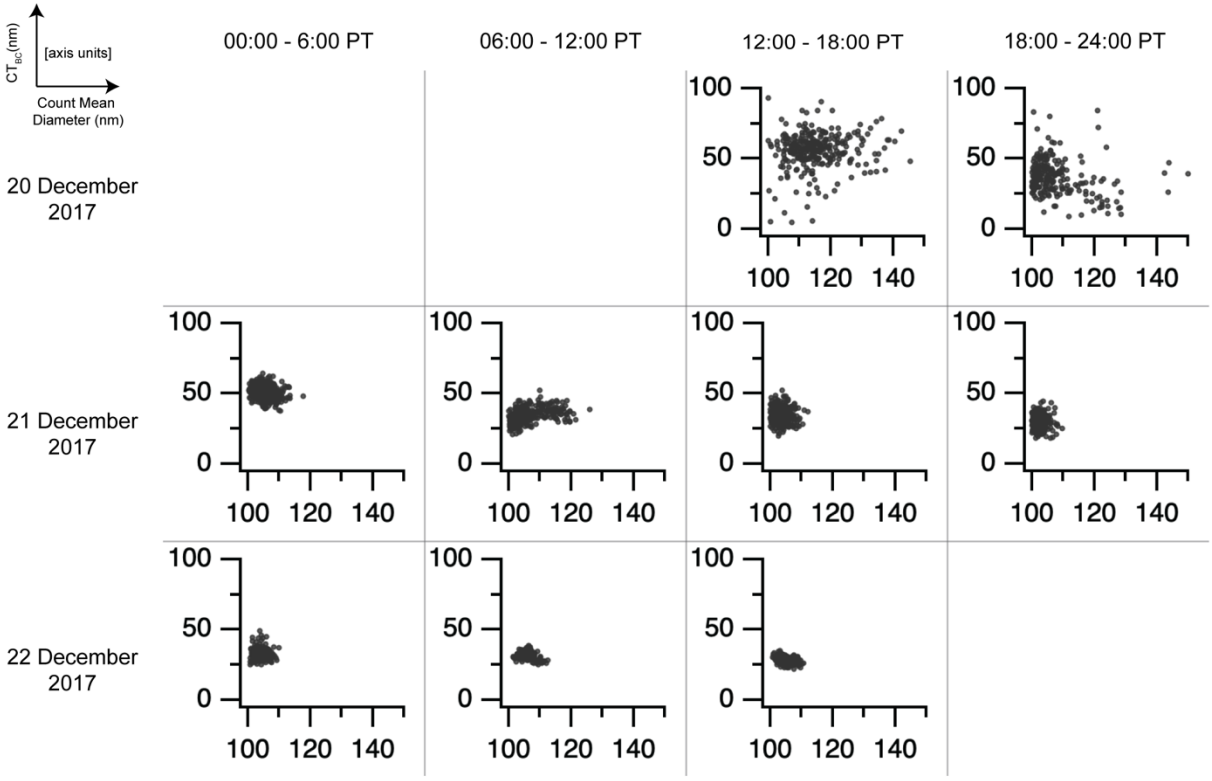


**Figure 14.** Matrix of scatter plots showing the time evolution of $CT_{BC}$ (nm) and rBC count mean diameter (nm) for the second campaign (December 2017). Axes labels are shown in the upper left. A scatter plot is shown for each six-hour time interval of the day, starting at 00:00 Pacific Time, and for each day of the campaign. The columns of the matrix denote the time interval of the day, and the rows of the matrix denote the days of the campaign. Each point within a plot represents a one-minute mean value for both $CT_{BC}$ and count mean diameter.

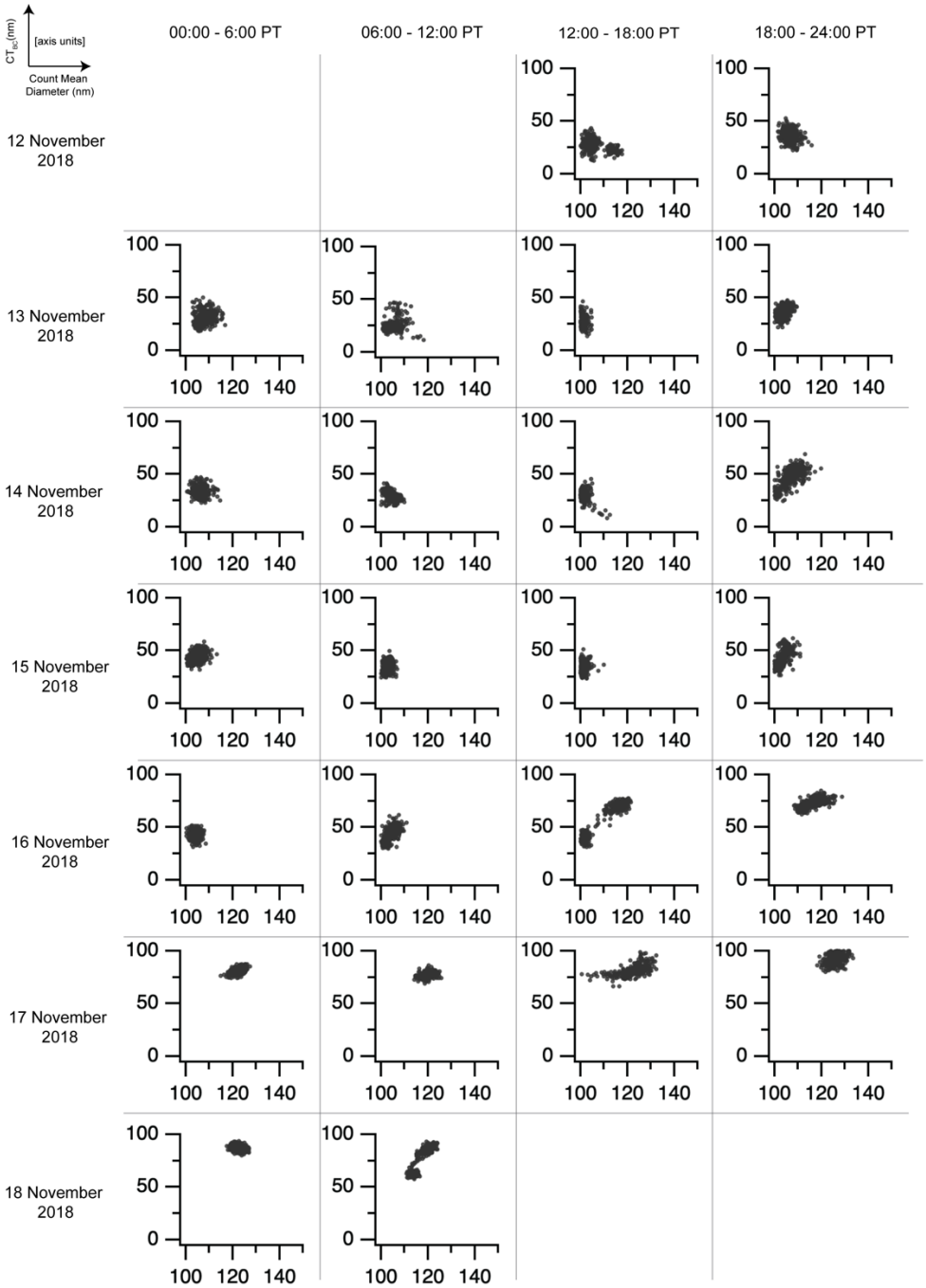


**Figure 15.** Matrix of scatter plots showing the time evolution of $CT_{BC}$ (nm) and rBC count mean diameter (nm) for the third campaign (November 2018). Axes labels are shown in the upper left. A scatter plot is shown for each six-hour time interval of the day, starting on 00:00 Pacific Time, and for each day of the campaign. The columns denote the time interval of the day, and the rows denote the day of the campaign. Each point within a plot represents a one-minute mean value within that six-hour interval for both $CT_{BC}$ and count mean diameter.

When the scatter plots of one-minute mean $CT_{BC}$ and rBC mean diameter~~CMD core diameter~~ are ~~further~~ aggregated~~groupedaggregated~~ by campaign, distinct ~~modes (i.e.,or "clusters")~~patterns emerge. Contour plots ~~of count as a function of these~~representing the 2-d joint histograms of these two variables are shown in Fig.~~ure~~ 164. Each campaign exhibits a~~as a~~ distinct ~~"fingerprint"~~pattern ~~and some inferences can be made about the ewhich~~that is representative of the emissions sources and relative age of the measured air masses. ~~Identical clustering patterns are also observed in Figure 15, where en one-minute mean lag times are plotted against $CT_{BC}$.~~ Figures 16~~4~~b and 16~~4~~e show a single cluster for the second campaign (September 2017) characterized by relatively thin coatings and smaller rBC core diameters, ~~compared~~compared to the other campaigns. Figures ~~1~~416c and ~~1~~416f on the other hand show~~s~~ two ~~separatedistinct~~ distinct clusters for the third campaign (November 2018). One cluster represents thickly-coated particles with larger rBC core diameters, and the other represents more thinly-coated particles with smaller rBC core diameters. The thinly-coated/smaller rBC core cluster for the third campaign exhibits some similarities to the single cluster for the second campaign. Figures ~~1~~416a and ~~1~~416d show two overlapping clusters for the first campaign (September 2017), which fall loosely~~somewhat~~ in between the thickly-coated and thinly-coated clusters from the third campaign~~ modes.clusters~~ ~~fgagagfagafgafg~~For easy reference, a cluster characterized by thin coatings and smaller rBC cores will be referred to as a~~the~~ "$BC_{bbff}$~~thinly-coated~~ cluster," a cluster with thick coatings and larger rBC cores will be referred to as a~~the~~ "-$BC_{bb}$ ~~thickly-coated~~ cluster," and the bimodal, mixed cluster ~~for aged air masses~~ will be referred to as the~~a the~~ "$BC_{aged,bg}$~~BC$_{cont}$ aged~~ cluster."

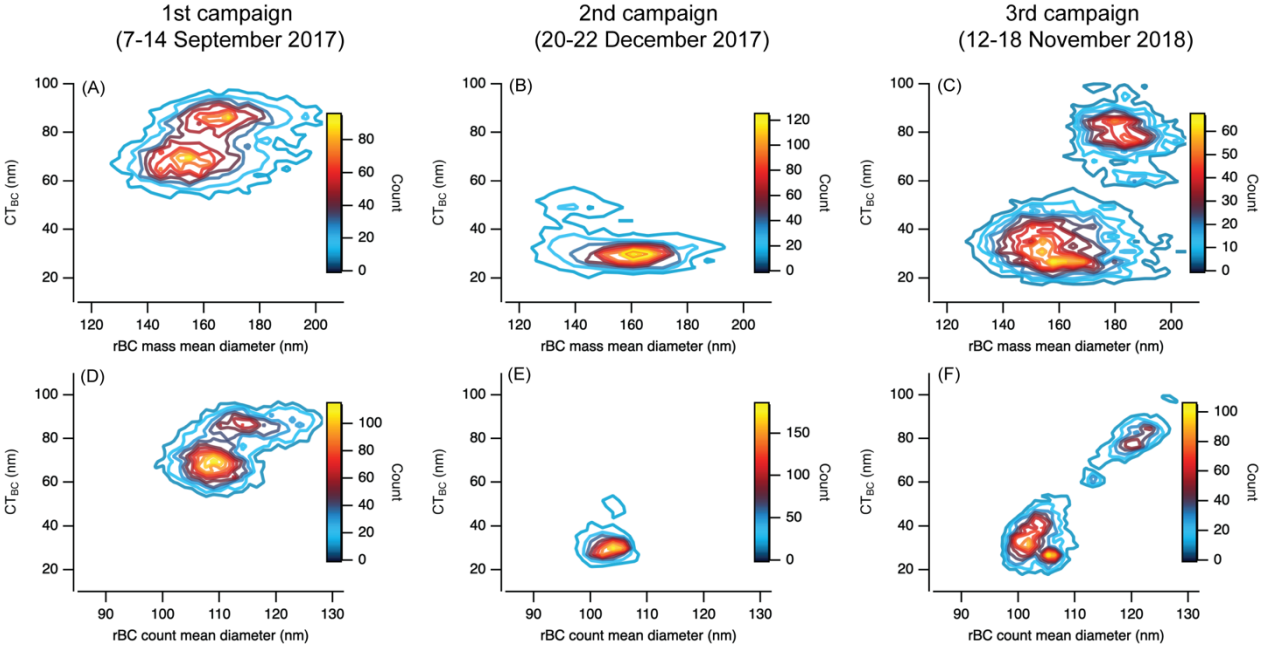


**Figure 16.** Contour plots of count as a function of one-minute mean BC coating thickness ($CT_{BC}$) and one-minute mean rBC core diameter. This figure can be interpreted as a 2-d joint histogram, converted to a contour plot. Each count represents a single one-minute mean data point. The contours are created based on the 2-d joint histogram that is calculated using a

50x50 grid within the range of all one-minute mean data. Panels (a), (b), and (c) in the first row show mass mean diameter on the horizontal axes, while panels (d), (e), and (f) in the second row show count mean diameter.

~~Combining statements made in previous sections with the campaign "fingerprints" shown in Figure 14, it is clear that~~ ~~emissions source strongly influences the physical characteristics of BC.~~ Within the context of ~~all the statements made in previous sectionssource identification discussed in previous sectionsthe identifiable~~identifiable sources discussed in previous sections (section 3.1 and S2), it is evident~~clear~~ that these distinct clusters in Fig. ~~14~~16 are ~~largely driven~~strongly influenced by emissions source type. A~~The~~ $BC_{bb}$ ~~thickly coatedlarge~~ cluster is ~~only~~ present in the third campaign (November 2018)~~,~~ when impacts from long-range transported biomass burning emissions were ~~confirmed~~identified, but not in the second campaign (December 2018). Furthermore, a $BC_{ff}$ ~~a thinly coated~~ cluster is present in both the second (December 2017) and third campaign, but not in the first campaign (September 2017). This ~~definitively showsimpliesshows~~~~confirms~~ that fresh (age < 1 d), urban~~-dominated~~ emissions from the LA basin and the surrounding southern California region ~~result inlead to a distinct cluster characterized by~~are characterized by thin coatings and smaller core size, confirming what has also been observed in other past field studies (Laborde et al., 2012; Liu et al., 2014; Krasowsky et al., 2018).

The $BC_{aged,bg}$~~$BC_{cont}$~~~~aged~~ cluster (Fig. ~~14~~16a, ~~14~~16d) exhibits two distinct modes within the same cluster. One ~~upper~~ mode is characterized by a peak $CT_{BC}$ [~~(~~CMD]~~)~~ that is ~20 nm [~~(~~~10 nm]~~)~~ larger~~higherlarger~~ than the other mode~~, and a peak count mean diameter that is ~10 nm larger than the other mode~~. Within the context of $BC_{aged,bg}$~~$BC_{cont}$~~, this mode is referred to as the larger mode, while the other mode with smaller $CT_{BC}$ and CMD is referred to as the smaller mode. This ~~shows~~suggests that ~~aged, continental , ambient air~~ $BC_{aged,bg}$~~$BC_{cont}$~~ ~~masses blowing~~advecting ~~towards California~~over the Pacific Ocean during typical meteorological conditions contain rBC from both biomass burning and fossil fuel (i.e., urban) emissions sources. ~~Continental scale~~ Aged background air masses are likely to contain aerosol from a mix of ~~both~~ sources~~, as various plumes are entrained into one another throughout long range transport.~~.

~~Furthermore, t~~The time evolution of both $CT_{BC}$ ~~and rBC core size is represented in a matrix series of scatter plots in Fig. 156 and 167. In each of the figures, the scatter between $CT_{BC}$ and rBC count mean diameter are grouped into six-hour time intervals for both the second (December 2017) and third (November 2018) periods, respectively. A similar plot for the first campaign (September 2017) is included in the Supplement as Fig. S23. This way~~In these figures, the time evolution of the ~~BC physical properties can be examined in detail and compared to periods of known emissions source impacts. A similar plot~~figure ~~for the first campaign (September 2017) is included in the Supplement as Fig. S23. These figures confirm the general patterns noted above regarding the effects of biomass burning versus urban emissions on the mixing state.~~.

In addition to emissions source type, atmospheric aging also appears to have an observable~~ed~~ effect on the mixing state. ~~discernible effect on the physical attributes of BC.~~

Table 3 lists the range of estimated "source-to-receptor" timescales for rBC-containing particles measured during LEO time periods L1 to L10. In short, the first campaign (September 2017) is broadly characterized by source-to-receptor timescales on the order of days to a week. The second campaign (December 2017) is characterized by timescales of less than one day. ~~Finally~~And~~,~~ the third campaign (November 2018) is characterized by timescales of less than one day for the first four days of the campaign, and timescales of approximately days to a week for the last two days of the campaign.

With regards to aging, we ~~can~~ first observe~~conclude~~ that ~~rBC fromwithin fresh, urban emissions dominated air masses~~$BC_{ff}$ particles do not develop~~exhibit~~ thick coatings within the timescales observed in this study~~on average, in this study~~. This suggests that a timescale of less than one day is not sufficient to thickly coat urban rBC-containing particles in the lower boundary layer, in the Los Angeles~~A~~ region. Although a modestly higher $CT_{BC}$ is observed during urban-dominated time periods, relative to $CT_{BC} \sim 0$ nm observed by Krasowsky et al. (2018) inside the LA basin, this is likely due to the effects of local biomass burning emissions mixing into the broader urban plume in both December 2017 and November 2018, as discussed above (also see section S2). While we observed mostly thinly-coated ~~r~~BC from these urban-dominated time periods ~~in this study~~, ~~it must be~~we acknowledge~~d~~ that the timescale required to acquire coatings on BC will likely ~~this timescale ( < 1 d) cannot be applied as a blanket conditionstatement for all urban BC. The rate of coating is largely a function of~~differ by location because of variations in local meteorology, pollution concentrations, and emission source profiles~~, which can widely vary from region to region~~.

~~Regarding the aging of for~~On the other hand, ~~biommass burning BC~~$BC_{bb}$~~biomass burning sources rBC, aAged rBC from biomass burning sources~~ were generally more ~~thickly coated~~thickly-coated, although the time evolution of the mixing state could not be quantified directly in this study ~~over the duration of transport~~. ~~Periods with of "fresh" biomass burning~~Fresh $BC_{bb}$ ~~impacts were characterized by~~had slightly lower~~thinner~~ $CT_{BC}$ ~~CTBC~~ compared to that of aged ~~biomass burning rBC particles~~$BC_{bb}$ (e.g., L3 vs. L9~~8~~), but higher~~higherlarger~~ $CT_{BC}$~~CTBC~~ compared to ~~fresh urban rBC particle~~that of fresh $BC_{ff}$ (e.g., L3 vs. L4). ~~This agrees with previous studies that have also observed thicker coatings in fresh biomass burning rBC relative to fresh urban rBC.~~ The overall higher~~larger~~ $CT_{BC}$ ~~CTBC~~ for aged ~~biomass burning rBC~~$BC_{bb}$ relative to fresh ~~biomass burning~~$BC_{bb}$ ~~rBC~~ indicates that ~~there is some ignificant~~ significant coating~~coating~~ formation ~~that~~can occur ~~s between the~~within timescales of ~1 day to ~1 week for ~~biomass burning rBC~~$BC_{bb}$, even after rapid coating formation that occurs soon after emission. An important caveat is that $CT_{BC}$ ~~CTBC~~ of $BC_{bb}$ ~~biomass burning rBC~~ may not be ~~simply~~ monotonically increasing over time.

Past studies have observed rapid coating of ~~biomass burning rBC~~$BC_{bb}$ within ~~the first few hours~~one day to more than 100 nm (Perring et al., 2017; Morgan et al., 2020), but we observed a median $CT_{BC}$ ~~CTBC~~ of 47.7~~2~~ nm for L3, which suggests that

$CT_{BC}$ ~~CTBC~~ for $BC_{bb}$ ~~biomass burning rBC~~ might decrease ~~at some point~~ during atmospheric transport ~~(~~under certain conditions~~)~~ and could ~~then~~again increase later at longer timescales (e.g., median $CT_{BC}$ ~~CTBC~~ of 54.0~~68.6~~ nm for L9), although we would need simultaneous measurements near the point of biomass burning emissions in order to confirm this ~~hypothesis theory with certainty~~for a specific plume. Previous studies have noted that the competing processes of dilution-driven evaporation and oxidation-driven condensation determine the ~~decrease or increase of~~abundance of~~relative change in~~ organic aerosol relative to carbon monoxide (ΔOA/ΔCO) in biomass burning plumes (Garofalo et al., 2019). Although the time evolution of ΔOA/ΔCO is not necessarily indicative of rBC mixing state evolution, the same physical processes (i.e., evaporation and condensation) must apply to OA rBC coating formation~~,~~ and loss ~~possiblypotential evaporationloss~~. The conflicting observations from various studies showing ΔOA/ΔCO either increasing, decreasing, or staying relatively stable in the near-field (timescale of ~hours) suggest~~s~~ that rBC coating in dense fresh biomass burning plumes may ~~also be influenced by~~undergo similar competing physical mechanisms. Preliminary results from ~~Emerging~~d~~D~~eveloping research showed~~s~~ that well-aged $BC_{bb}$ (>7 days) ~~may in certain cases be thinnerhave~~had thinner coatings~~gs~~ than ~~very~~ fresh $BC_{bb}$ (< 5 h), providing emerging evidence that rBC coating may not always monotonically increase (Sedlacek et al., 2019). Further research is necessary to confirm this process in more field measurements, and to determine the various mechanisms that may be driving the loss of rBC coating in biomass burning plumes. We make no definitive claims about the rate of change of $CT_{BC}$ ~~CTBC~~ for ~~biomass burning rBC~~$BC_{bb}$ throughout atmospheric transport since we ~~only observed~~measured ~~the~~ $CT_{BC}$ ~~CTBC from a single discrete point in space~~at one location. Nonetheless,~~,~~ ~~but~~ our measurements ~~do~~ suggest that $CT_{BC}$ ~~CTBC~~ for fresh Southern California ~~biomass burning (fresh biomass burning) rBC~~ $BC_{bb}$ were generally lower than $CT_{BC}$ ~~CTBC~~ for aged Northern California ~~biomass burning (aged biomass burning) rBC.~~$BC_{bb}$.

The contour plots for the first campaign (September 2017), shown in Fig. ~~1~~4~~1~~6a and ~~1~~4~~1~~6d, offer additional perspective on how aging ~~could be affecting~~can affect ~~rmight be affecting~~ BC mixing state within ~~mixed source air massescontinental~~ well-aged background air masses over longer aging time~~s~~ scales (~days to week). The first notable feature of the $BC_{aged,bg}$ ~~BC~~$_{cont\ aged}$ cluster is that the ~~lower mode~~smaller mode is significantly more coated than the ~~thinly coatedthinly coated~~$BC_{ff}$ clusters found in ~~the~~ Fig. 16~~figures~~ for the second (December 2017) and third (November 2018) campaigns~~continental scale transport.~~. The peak of the ~~lower mode~~smaller mode of the $BC_{aged,bg}$ ~~BC~~$_{cont}$ ~~aged~~ cluster is at least 3~~2~~5 nm higher than the peak of the ~~thinly coatedthinly coated~~respective $BC_{ff}$ clusters in Fig. 16b, 16c, 16e, and 16f. Assuming that this ~~lower mode~~smaller mode represents fossil fuel influenced BC (i.e., urban BC), this confirms that while urban BC may not become thickly-coated within a~~a~~ day, they seem to~~do~~ acquire coatings over ~~long range transport on the timescale of days to a week~~longer timescales.

Another prominent feature of the $BC_{aged,bg}$ ~~BC~~$_{contaged}$ cluster is the shift in mass mean diameter (MMD) (Fig. ~~1~~4~~1~~6a) and count mean diameter (CMD) (Fig. ~~1~~4~~1~~6d) peaks, relative to the ~~thinly coated~~$BC_{bb}$ and ~~thickly coated cluster~~$BC_{ff}$ clusters in the December 2017 (Fig. 16b, 16e) ~~-~~and November 2018 (Fig. 16c, 16f) plots ~~in Fig. 16. Assuming that this lower mode is~~

~~representative of fossil fuel influenced (urban) BC.~~~~Specifically examining the~~Comparing peaks of the ~~lower mode~~smaller mode of the $BC_{aged,bg}$~~$BC_{cont}$~~ cluster in both Fig. ~~14~~16a and ~~14~~16d to the respective peaks of the $BC_{ff}$ clusters in Fig. 16b, 16c, 16e, and 16f~~,~~, we observe that the MMD is generally lower ~~decreases~~ for the smaller mode of $BC_{aged,bg}$~~$BC_{cont}$~~ while the CMD is generally higher ~~increases, relative to the respective peaks of the thinly coated clusters~~. The ~~seemingly contradictory~~apparent lower MMD in $BC_{aged,bg}$~~$BC_{cont}$~~ compared to $BC_{ff}$~~decrease in the MMD with age~~ can be explained by the impact of local~~fresh~~ biomass burning sources ~~BC~~ in both the second (September 2017) and third (November 2018) campaigns~~-~~, ~~, combined with the much larger rBC loading in the last two campaigns,~~ as previously mentioned in section 3.6. On the other hand, the overall ~~increase in the~~higher peak CMD for the lower mode of the $BC_{aged,bg}$~~$BC_{cont}$~~ cluster implies ~~this implies~~ that either (i) urban BC is coagulating over long aging timescales (days to week), (ii) source-specific variables like fuel type and combustion conditions are influencing the initial core size distribution~~er time scale~~, or (iii) the urban area in which the rBC is emitted contains a much higher concentration of rBC, ~~permitting more~~leading to more coagulation in the near-field before continental-scale transport. Any combination of these three explanations could contribute to the overall increase~~d~~ in the peak rBC diameter of the urban mode. We do not attempt to quantify the extent to which each factor ~~explanation~~ contributes to~~his~~ core size increases in this study, though (i) is unlikely to be important given the dependence~~t~~ of coagulation rate on number concentrations. ~~how much each explanation is responsible for the s~~ Further research needs to be conducted to accurately characterize the relative importance of each factor.

Shifting ~~our focus now~~focus to the ~~upper mode~~larger mode in the $BC_{aged,bg}$~~$BC_{cont}$~~ cluster in Fig. ~~14~~16a and ~~14~~16d, which we~~is likely~~ attribute to~~representative of~~ biomass burning BC, we notice lower ~~a decrease in both the~~ CMD and MMD, relative to the ~~thickly coated~~$BC_{bb}$ clusters ~~mode~~ in Fig. ~~14~~16c and ~~14~~16f. Based on the assumption that the initial rBC size distribution of the biomass burning rBC from the first campaign and third campaign are similar, selective wet deposition and/or increased hygroscopicity of thickly-coated rBC ~~can~~~~may~~could explain this apparent decrease in the overall rBC core size. Moteki et al. (2012) found that larger rBC particles were more effectively removed through wet deposition. McMeeking et al. (2011a) ~~also~~ reported that more thickly-coated particles were more hygroscopic, which would in turn lead~~s~~ to a higher likelihood~~probability~~ of wet scavenging. Either, or both, of these mechanisms ~~can~~could explain why the peak rBC diameter ~~is lower~~ of~~for a well~~more ~~aged rBC in~~ the ~~biomass burning mode~~larger mode in the $BC_{aged,bg}$~~$BC_{cont}$~~ cluster is lower than the peak rBC diameter of the $BC_{bb}$ cluster.~~s. could~~

~~For the first campaign (September 2017), source identification analysis suggests that the measured rBC-containing particles were likely from aged biomass burning emissions and other unidentified sources of aged rBC-containing particles. The fact that all regional emissions were downwind of the sampling site during the first campaign suggests that measured rBC included negligible contributions from fresh emissions from the Los Angeles basin. There were no active wildfires in the~~

Southern California region at the time of the first campaign, but there were significant wildfires in the Pacific Northwest and the northern tip of California (near the California-Oregon border) around the time of measurements, as discussed in section 3.1. We suggest that measured rBC included contributions from these wildfires (see section 3.1), though we make no attempt to quantitatively determining the relative contribution from these wildfires to our measurements.

**Table 3.** Estimated source-to-receptor timescales for rBC containing particles measured during the different LEO periods. Further detail on the methodology to determine these estimates can be found in the supplemental section S1.

| LEO time period | Characteristic timescale |
|---|---|
| L1 | ~days to week |
| L2 | ~minutes |
| L3 | ~days to week |
| L4 | ~3 hours |
| L5 | ~12 hours |
| L6 | ~8 hours |
| L7 | ~17 hours |
| L8 | ~days to week |
| L9 | ~days to week |
| L10 | ~days to week |

For the second campaign (December 2017), there was a more diverse range of source types and locations. This was expected, based on the more variable meteorology with respect to the first campaign (September 2017), especially the presence of the less common Santa Ana winds. Fresh urban and biomass emissions influenced air masses (L4 and L5) contained particles with a characteristic age ranging from ~3-12 hours, with an associated median $CT_{BC}$ of ~11 nm. In contrast, L3 had vastly longer aging timescale (~days to week), and an associated median $CT_{BC}$ that was approximately four times higher than that of L4 and L5. The concentrations during L3 were also comparable to the average concentration of the first campaign, which further supports that fresh urban emission sources from the Los Angeles basin were not contributing to the aerosols being measured during the L3 period. The difference in $CT_{BC}$ between periods within the same campaign highlights the relationship between aging timescale and $CT_{BC}$.

By comparing periods L4-L7 and L8-L9, we estimate a conservative minimum aging timescale for rBC particles to acquire significant coatings. For L4-L7, we observed relatively low values of $CT_{BC}$ and $f_{BC}$, corresponding to fresh biomass and urban emissions from the Southern California region. In contrast, we observed the highest values of $CT_{BC}$ and $f_{BC}$ for L8 and

~~L9, when synoptic winds were blowing aged biomass burning aerosols along the coast of California from the Camp Fire (Northern California) plume. We estimate that source-to-receptor transport from the Camp Fire to Catalina Island is approximately one week. In comparison, all characteristic timescales for L4-L7 were less than 24 hours. Based on these observations, we can make a conservative statement that rBC-containing particles that are aged less than one day in the Los Angeles basin (either from biomass burning or urban emissions) are not likely to be thickly coated~~thickly coated~~. This is in contrast to other previous SP2 measurements that have been made in other regions, which have suggested that timescales of less than one day are sufficient to thickly coat rBC-containing particles (Moteki and Kondo, 2007; Akagi et al., 2012; Baumgardner et al., 2007; Cheng et al., 2018; Dahlkötter et al., 2014; Kondo et al., 2011; Laborde et al., 2013; Metcalf et al., 2012; Pan et al., 2017; Perring et al., 2017; Schwarz et al., 2008a; Shiraiwa et al., 2007; Wang et al., 2014, 2018). However, results reported here are consistent with a recent study by Krasowsky et al. (2018) in the Los Angeles basin that also suggests that rBC-containing particles in the Los Angeles region are not significantly coated within timescales less than one day. Our findings add to a growing body of evidence that suggests that regional differences, like atmospheric context and emission sources, play a significant role in the evolution of rBC mixing state, and more specifically, the rate at which rBC-containing particles acquire coatings.~~

T~~T~~he evolution of rBC mixing state and rBC size distribution has important implications on accurately assessing the regional climate benefits of black carbon reductions, particularly in California, and also reducing uncertainty in global radiative forcing of BC~~ in climate models~~. Understanding the ~~time scales for rBC-containing particles to acquire coatings~~impact of varying emissions source types and atmospheric aging in different regional contexts~~regions~~ is crucial~~important~~ for accurately quantifying the enhancement of BC light absorption, and also for determining BC lifetime in the atmosphere since hygroscopic coating material can enhance the particle's susceptibility to wet deposition (Zhang et al., 2015). The rBC mixing state results from this study add to a growing body of evidence that suggests that biomass burning emissions and longer aging timescales generally lead to more thickly-coated rBC particles. These results also emphasize the need for more ~~future~~ field measurements of rBC mixing state in various regions around the world to ~~clarify the~~ further understand how ~~relationship between~~ different emissions source profiles~~types~~ and ~~,~~atmospheric aging ultimately effect rBC physical properties in various, real-world ~~ying~~ atmospheric contexts. ~~The rBC mixing state results from this study add to a growing body of evidence that suggests that BC$_{bb}$ biomass burning emissions and longer aging timescales generally produclead toproducee more thickly-coated rBC particles. LEFT OFF/, and rBC physical properties., in order to understand its spatial and temporal differences, and consequently its effect on climate forcing on both a regional and global scale.~~

### 3.87 Comparison to past studies quantifying $CT_{BC}$ using the SP2 the LEO method

Overall, the range of $CT_{BC}$ calculated in this study agree wellgeneral agreement are in general agreement with reported values from past studies. Table 3 presents a comprehensive list of $CT_{BC}$ values from various studies, categorized by dominant emissions source type and sorted alphabetically by first author name. [insert body of text]

For periods dominated by strong biomass burning emissions$BC_{bb}$ influence, the mean $CT_{BC}$ ranged between ~40–70 nm in this study. This range overlaps with the range of values reported by Morgan et al. (2020), Pan et al. (2017), Sahu et al. (2012), Schwarz et al. (2008a), and Sedlacek et al. (2012).

For periods dominated by strong fossil fuel (i.e., urban) emissions$BC_{ff}$s influence, the mean $CT_{BC}$ ranged between ~5–15 nm in this study. This range overlaps with the range of values reported by Krasowsky et al. (2018), Laborde et al. (2012), Liu et al. (2014), Sahu et al. (2012), and Schwarz et al. (2008a).

For periods dominated by aged/continental air masses$BC_{aged,bg}$BC$_{cont}$, the mean $CT_{BC}$ was ~60 nm in this study. This value falls within the range of values reported by Laborde et al. (2013), Schwarz et al. (2008a), and Shiraiwa et al. (2008).

An important observation to notecaveat to notebe noted when making inter-study comparisons is that the studies that reported higher $CT_{BC}$ ranges (,–relative to this study), tended to have a lower value for the lower rBC core diameter threshold. For example, Gong et al. (2016) reports a $CT_{BC}$ range of 110–300 nm for biomass burning emissions using an rBC core diameter range of 80–180 nm. Since the scattering detection limit is accurate down to ~170 nm for the SP2, this implies that includingthat the inclusion of particles with rBC core sizes smaller than 170 nm will bias the average $CT_{BC}$ values higher becausesince smaller rBC particles (< 170 nm core diameter) with thin coatings will not be included in the overall averagingthe coating on smaller rBC particles may not be detected and the coating thickness on many smaller rBC particles will not be included in the overall averagingonly smaller rBC particles with optical diameters below the scattering detection will not be included in the LEO analysis. limit will may be inaccurately characterized as uncoated (e.g., a particle with a 100 nm rBC core and 630 nm coating will be characterized by LEO as having a $CT_{BC}$ of ~ 0 nm)with thick coatings will be optically detectibleonce the rBC core size drops below the scattering detection limit ~ 170 nm.. Dahlkötter et al. (2014), Gong et al. (2013), Perring et al. (2017), Taylor et al. (2014), Cheng et al. (2018), Metcalf et al. (2012), Raatikainen et al. (2015), and Sharma et al. (2017) all reported $CT_{BC}$ for rBC-containing particles in a size range that includes rBC cores smaller than 170 nm. There is value in reporting $CT_{BC}$ for rBC particles with core sizes smaller than 170 nm because it will show the relative abundance of coated rBC-containing particles exceeding ed the lower scattering detection limit, but care must be taken when comparing $CT_{BC}$ values calculated with varying rBC core size restrictions.—ca

For future studies using the SP2, we suggest that at a minimum, the rBC core size range be explicitly stated if $CT_{BC}$ is being quantified and reported. Furthermore, it would be useful to establish some standardized guidelines for~~regarding~~ reporting ~~of~~ $CT_{BC}$ so that future inter-study comparisons can serve as reliable benchmarks. ~~For example, one might conduct LEO analysis for a whole host of rBC diameter ranges, but future guidelines might suggest that the authors report the $CT_{BC}$ for the hypothetically standard rBC core diameter range, in addition to any other size ranges additional ranges they want to analyze or report in their study.~~ As shown ~~clearly~~ in Figure 13 and discussed earlier, the range of rBC core diameters used for the calculation of $CT_{BC}$ has a significant effect on the $CT_{BC}$ statistics. These ranges must be considered in order to accurately represent the physical parameterization of BC mixing state and ~~rBC core size~~size distributions in models.

**Table 3.** Summary table of rBC coating thickness values reported in previous studies using the SP2.

| Dominant source | Coating thickness (nm) | rBC core diameter (nm) | rBC age | Description | Time period | Reference |
|---|---|---|---|---|---|---|
| Biomass burning emissions | ~40–70[a] | 200–250 | ~days–wk | Ground-based measurements on Catalina Island (~70 km SW of Downtown LA) | 17–18 Nov 2018 | This study |
| | 105–136 | 140–220 | ~3–4 d | Airborne measurements of the Pagami Creek Fire plume (Minnesota, US) conducted over Germany | 16 Sep 2011 | Dahlkötter, 2014 |
| | 110–300 | 80–130 | – | Ground-based measurements in Shanghai, China | 5–10 Dec 2013 | Gong, 2016 |
| | 11–15 | 200–260 | – | Ground-based measurements in Paris, France | 15 Jan–15 Feb 2010 | Laborde, 2013 |
| | 100–300 | – | – | Ground-based measurements in London, during periods significantly influenced by solid fuel burning | 22–24 Jan 2012 | Liu, 2014 |
| | < 30 | – | – | Ground-based measurements near central Manchester, UK | 3–16 Aug 2010 | McMeeking, 2011 |
| | 40–120 | – | < 3 h | Airborne measurements across the Amazon and Cerrado | Sep and Oct 2012 | Morgan, 2020 |
| | 11–54 | 190–210 | < 10 s | Burning experiments in laboratory combustion chamber | – | Pan, 2017 |
| | 90–110 | 160–185 | < 2 d | Airborne measurements of the Yosemite Rim Fire, CA | Aug 2013 | Perring, 2017 |
| | 20–80 | 200 | – | Airborne measurements over California during ARCTAS-CARB campaign | 15–30 Jun 2008 | Sahu, 2012 |
| | 65±12 | 190–210 | 0.5–1.5 h | Airborne measurements over Houston and Dallas, TX | 20–26 Sep 2006 | Schwarz, 2008a |
| | 40–70 | – | ~days | Ground-based measurements of a wildfire plume from the Lake Winnipeg area in Canada, conducted in Long Island, NY | 2 Aug 2011 | Sedlacek, 2012 |
| | 79–110 | 130–230 | 1–2 d | Airborne measurements over wildfires in eastern Canada and North Atlantic | Jul–Aug 2011 | Taylor, 2014 |
| Fossil fuel emissions | ~5–15[a] | 200–250 | < 1 d | Ground-based measurements on Catalina Island (~70 km SW of Downtown LA) | 17–18 Nov 2018 | This study |
| | 22–40 | 130–160 | < 3 h | Airborne measurements over the Athabasca oil sands in Canada | 13 Aug–7 Sep 2013 | Cheng, 2018 |
| | 17–39 | 160–190 | | | | |
| | 50–130 | 60-80 | – | Ground-based measurements in Shanghai, China | 5–10 Dec 2013 | Gong, 2016 |
| | ~0–24 | 240–280 | < 7 h | Ground-based measurements in the Los Angeles basin | Aug–Oct 2016 | Krasowsky, 2018 |
| | 2±10 | 200–260 | – | Ground-based measurements in Paris, France | 15 Jan–15 Feb 2010 | Laborde, 2013 |
| | 0–50 | – | – | Ground-based measurements in London, during periods dominated by traffic sources | 31 Jan–1 Feb 2012 | Liu, 2014 |
| | 99±20 | 90-260 | – | Airborne measurements in the Los Angeles Basin and surrounding outflows | May 2010 | Metcalf, 2012 |
| | 88±4[b] | 180 | ~hours | Ground-based measurements in Gual Pahari, India | 3 Apr–14 May 2014 | Raatikainen, 2015 |
| | 0–40 | 200 | – | Airborne measurements over California during ARCTAS-CARB campaign | 15–30 Jun 2008 | Sahu, 2012 |
| | 20±10 | 190–210 | 2–3.5 d | Airborne measurements over Houston and Dallas, TX | 20–26 Sep 2006 | Schwarz, 2008a |
| | 30–40 | 200 | ~ 6 h | Ground-based measurements of fresh emissions from Japan, conducted on Fukue Island, Japan | Mar–Apr 207 | Shiraiwa, 2008 |
| Remote / background / continental / highly-aged | ~60[a] | 200–250 | ~days–wk | Ground-based measurements on Catalina Island (~70 km SW of Downtown LA) | 7–14 Sep 2017 | This study |
| | 130–300 | 60–80 | – | Ground-based measurements in Shanghai, China | 5–10 Dec 2013 | Gong, 2016 |
| | 37–93 | 200–260 | – | Ground-based measurements in Paris, France | 15 Jan–15 Feb 2010 | Laborde, 2013 |
| | 188±31 | 90-260 | – | Airborne measurements in the free troposphere | May 2010 | Metcalf, 2012 |
| | 75–100 | 150–200 | – | Ground-based measurements at the Pallas GAW (Finnish Arctic) | Dec 2011–Jan 2012 | Raatikainen, 2015 |
| | 90±5[b] | 180 | ~hours | Ground-based measurements in Mukteshwar, India | 9 Feb–31 Mar 2014 | Raatikainen, 2015 |
| | 48±14 | 190–210 | – | Airborne measurements over Houston and Dallas, TX | 20–26 Sep 2006 | Schwarz, 2008a |
| | < 30 nm | 190–210 | – | Airborne measurements over Costa Rica, 1-5 km | 6–9 Feb 2006 | Schwarz, 2008b |
| | 20–36 | 160–180 | – | Ground-based measurements in Alert, Nunavut, Canada (within Arctic Circle) | Mar 2011–Dec 2013 | Sharma, 2017 |
| | ~60 | 200 | ~days | Ground-based measurements of Asian continental air masses, conducted on Fukue Island, Japan | Mar–Apr 207 | Shiraiwa, 2008 |

[a] The range of values shown represent the approximate range of the mean $CT_{BC}$.

[b] The absolute coating thickness was calculated from the ratio of rBC core diameter to particle mobility diameter as presented in the study.

Note: A dash ("-") indicates that the value was not reported, or it could not be identified.

~~The SP2~~

## 4 Conclusion

This study investigates the concentration, size distribution, and mixing state of rBC on Catalina Island (~70 km southwest of Los Angeles) using a single-particle soot photometer (SP2). Measurements were taken during three separate campaigns with varying meteorological conditions and emission sources, in September 2017, December 2017, and November 2018. During the first campaign (7 to 14 September 2017), westerly winds dominated and thus the sampling location was upwind of the dominant regional sources of BC (i.e., urban emissions from the Los Angeles basin). The measurements from the first campaign were largely characteristic of ambient background levels of rBC over the Pacific Ocean, away from the broader urban Los Angeles plume. During the second and third campaigns (20 to 22 December 2017, 12 to 18 November 2018), atypical Santa Ana wind conditions caused measured rBC to include important contributions from large wildfires in California and urban emission from the Los Angeles basin. Furthermore, during the third campaign, rBC from the Camp Fire in Northern California was measured, allowing us to compare the mixing state of aged biomass burning particles (from Camp Fire) to fresher particles (from Southern California fires and urban Los Angeles emissions).

The measurements from these three campaigns showed that rBC physical properties (rBC core size and ~~coating thickness~~mixing state) were ~~strongly~~ influenced by (i~~1~~) emissions source type, and (ii~~2~~) atmospheric aging.

~~During periods when biomass burning emissions dominated measurements, weit was observedfound that the average rBC core size, $f_{BC}$, and BC coating thickness ($CT_{BC}$) increased compared to when fossil fuel (urban) emissions were dominant. rBC from air masses dominated by biomass burning emissions ($BC_{bb}$) were~~ generally had ~~found to have e the~~ larger ~~average~~ core diameters than ~~relative to rBC from air masses dominated by urban emissions (~~$BC_{ff}$~~)~~. The MMD ~~mass mean diameter~~ [CMD~~count mean diameter~~] of $BC_{bb}$ was observed to be ~180 nm [120 nm], while MMD [CMD] of $BC_{ff}$ was observed to be ~160 nm [100 nm]. ~~rBC from aged, continental air masses ($BC_{aged}$)~~ $BC_{aged,bg}$~~$BC_{cont}$~~ showed a bimodal rBC core size distribution, with MMD [CMD] peaks at ~170 nm [115 nm] for the ~~upper~~larger mode, and ~153 nm [109 nm] for the ~~lower~~smaller mode. The bimodal rBC core size distribution in the ~~well-aged~~aged background~~continental~~ air mass suggests that ~~continental-scale air masses~~background rBC~~aged rBC~~ above the Pacific Ocean during typical meteorological conditions are likely a mix of both urban (i.e., smaller rBC cores) and biomass burning (i.e., larger rBC cores) emissions. The larger CMD of the ~~lower~~smaller mode for $BC_{aged,bg}$~~$BC_{contaged}$~~ compared to the CMD of $BC_{ff}$ suggests that either (i) coagulation ~~is~~ increased~~sing~~ the size of $BC_{aged,bg}$~~$BC_{contaged}$~~ somewhere between the source and receptor, and/or (ii) the initial source and combustion conditions for $BC_{aged,bg}$~~$BC_{contaged}$~~ were different than for $BC_{ff}$ ~~specifically~~ in this study. More accurate methods of source apportionment would be needed to ~~definitively~~ quantify the relative contribution of each factor, but both factors likely

effect ~~well-~~aged urban rBC particles ~~to some degree~~. The ~~smaller~~ CMD [MMD] of the ~~upper~~larger mode for $BC_{aged,bg}$~~$BC_{cont}$~~~~cont~~ was smaller than~~,aged compared to~~ that of $BC_{bb}$, which suggest~~. larg~~s that (i) selective wet deposition of larger particles ~~during long-range transport~~, and/or (ii) increased wet scavenging of thickly-coated particles due to increased hygroscopicity, contributes to the shift in the rBC size distribution for biomass burning rBC-containing particles over long-range atmospheric transport.

Similar trends are ~~A similar trend is~~ observed for the impact of emissions source type on rBC mixing state. On average, $BC_{ff}$ ~~were~~was either uncoated or very thinly-coated, with mean coating thickness~~dian~~ ($CT_{BC}$) ranging from ~5 to ~~of less than~~ 15 nm~~,~~ and mean fraction of thickly coated particles (~~an average~~ $f_{BC}$) of less than 0.15. In contrast, $BC_{bb}$ was~~ere much~~ more thickly-coated, with mean $CT_{BC}$ ranging from ~40 to 70 nm~~,~~ and $f_{BC}$ ranging from ~0.23 to 0.47. $BC_{aged,bg}$~~$BC_{contaged}$~~ was characterized by a mean $CT_{BC}$ of ~60 nm and $f_{BC}$ ~~-~~of ~0.27, confirming that a mix of biomass ~~burning~~burning and urban emissions sources ~~are~~were likely entrained into these aged background~~, continental~~ air masses. ~~Just as~~

By estimating approximate source-to-receptor timescales (i.e., age) and also comparing the physical properties of fresh rBC~~emissions~~ to that of $BC_{aged,bg}$~~$BC_{contaged}$~~, we ~~were also able to identify~~assessed the ~~general~~ effect of aging on both $BC_{bb}$ and $BC_{ff}$. For $BC_{ff}$, we observed that timescales of less than one day were not ~~long enough~~sufficient for urban rBC particles to become thickly coated. This is in direct contrast to biomass burning rBC, which has been shown in previous studies to acquire thick coatings within hours or even minutes, near the source of emissions. For $BC_{bb}$, we observed higher values of $f_{BC}$ and $CT_{BC}$ during ~~impacts~~periods that included contributions from the Camp Fire in Northern California, compared to periods of fresh biomass burning impacts from local Southern California fires (e.g., L3). The average $CT_{BC}$ during the Camp Fire impacted period was ~18 nm higher than the average $CT_{BC}$ ~~In general, aging~~ during L3, when we identified Southern California fires as the main emission source. Likewise, we also observed an increase in the urban rBC-containing particles by comparing the aged urban mode of the ~~September 2017 rBC~~$BC_{aged,bg}$~~$BC_{cont}$~~ distribution~~, and compare its mixing state to~~~~of~~ fresh $BC_{ff}$ during periods ~~of direct impactd from the~~when emissions from the LA basin dominated.~~during Santa Ana wind conditions.~~ We found that coatings on ~~the~~ aged urban particles within ~~the continental air masses~~ $BC_{aged,bg}$~~$BC_{cont}$~~ were ~35 nm thicker than $BC_{ff}$ from fresh LA basin emissions. Overall, our measurements suggest ~~we confirm~~ that aging increases the coating thickness on both $BC_{ff}$ and $BC_{bb}$, which is consistent with previous research. ~~although w~~We did not quantify the rate of change of coating ~~formation~~thickness since we ~~could had no means to~~were unable track the evolution of the mixing state during source-to-receptor transport.~~in transport.~~

The measurements reported in this study agree ~~well~~ with ~~similar~~ past ~~studies~~research~~,~~ that investigates ~~and they also confirm the~~ impacts of source type and aging on rBC physical properties ~~reported in that a number of previous studies that have been~~

conducted also observed in various other locations. various other settings. This study , along with previous studies, further highlights the complexity of rBC mixing state and demonstrates how meteorology, emissions source type, and atmospheric aging can drastically affect the size distribution and mixing state of BC, even within the same region. Further measurements of rBC physical properties, along with chemicalpollutant measurements for a more that allow for robust source apportionment, willwould serve to improve our understanding of BC mixing state in various regions- with different atmospheric contextsand consequently help narrow the range of uncertainty for both BC lifetime and radiative absorption enhancement from BC coating.the aggregate effect of BC coating mixing state coating on the regional to global radiative budget. Given that there are less than 20 studies that quantify $CT_{BC}$ using the LEO method, this study confirms that further measurements are necessary in order to narrow the quantitative bounds of rBC mixing state in our climate system, particularly since it which has important implications on BC absorption enhancement and atmospheric lifetime. We also suggest that future studiess also further examine the BC mixing state as a function of heightaltitude, as well as the role of combustion conditions on mixing state (e.g., flaming versus smoldering), especially in real-world field measurements.

For the first campaign (September 2017), rBC concentrations remained relatively constant throughout the sampling period, and the mean concentration (0.04 μg $m^{-3}$) was about an order of magnitude lower than previous ground-based measurements of rBC concentrations in the Los Angeles basin (~ 0.14 μg $m^{-3}$) (Krasowsky et al., 2016). The mean number fraction of thickly coated rBC particles ($f_{BC}$) was 0.27 for this period, slightly lower than the lower end of $f_{BC}$ calculated from flight basedairborne measurements (Metcalf et al., 2012) and slightly higher than the upper end of $f_{BC}$ calculated from ground-based measurements (Krasowsky et al., 2016), all in the Los Angeles basin. The background, ambient population of rBC-containing aerosols off the coast of Los Angeles was characterized by a median coating thickness ($CT_{BC}$) of ~ 6306 nm. Measurements from this period show that rBC-containing particles over the Pacific Ocean during typical meteorological conditions are well-aged, based on the mean $f_{BC}$ and $CT_{BC}$ values.

In contrast, the measurements from the second and third campaigns (December 2017, November 2018) had much larger variability in meteorological conditions and BC sources, compared to the first campaign (September 2017). The Santa Ana wind conditions (northerly to easterly winds), along with large wildfire events across California, directly influenced which BC sources contributed to our measurements. During the second campaign, we measured rBC from urban emissions and wildfires in Southern California (Thomas Fire). In addition to urban and wildfire emissions from Southern California, rBC from Northern California (Camp Fire) was measured during the third campaign. The wide variety of meteorological conditions and BC sources resulted in a wide range of rBC concentrations (~ 0 to 0.6 μg $m^{-3}$ for the second campaign and ~ 0 to 1.5 μg $m^{-3}$ for the third campaign) and hourly-averaged $f_{BC}$ (~ 0 to 0.14 for second campaign, ~ 0.02 to 0.48 for third campaign).

Using the lag-time method and the LEO method we show that rBC mixing state is highly variable, dependent on emission source and atmospheric aging. Based on source-to-receptor timescales approximated with HYSPLIT back-trajectories,

~~MODIS imagery, and meteorological data, we examine the relationship between atmospheric aging and mixing state. Notably, we find that fresh emissions (biomass burning and urban emissions) from the Southern California region with source-to-receptor timescales of less than a day are not significantly coated, with median $CT_{BC}$ ranging from 5.6 to 13.4 nm. In contrast, we observe elevated $f_{BC}$ (~ 0.23 to 0.47) and much higher median $CT_{BC}$ (40.7 to 68.6 nm) during periods of known impact from a long-range emission source (Camp Fire in Northern California). Previous studies have concluded that rBC acquire significant coating within hours after emission from the source, but our results suggest that rBC in the Los Angeles area do not get coated as quickly when emissions are blown towards the ocean during Santa Ana wind conditions. Additionally, we observe a modest positive correlation ($R^2$ = 0.36) between median $CT_{BC}$ and median rBC core diameter, which supports previous suggestions that rBC cores can coagulate as they age in the atmosphere (Laborde et al., 2013; Shiraiwa et al., 2008). We also observed larger median mass diameters for periods where biomass burning emissions were suspected to be the dominant source of rBC, confirming measurements reported in previous studies.~~

~~Our study, in conjunction with previous studies, confirms that rBC mixing state is highly influenced by ***emissions source (??)***atmospheric context (i.e., meteorology, chemical composition of regional atmosphere, and **emission sources**), which varies widely both spatially and temporally. More field campaigns are needed in a variety of sampling locations with different source contributions and atmospheric contexts to further reduce uncertainty associated with rBC mixing state and its influence on BC atmospheric lifetime, spatial distributions, and radiative forcing. Further measurements can serve as an indicator for how accurately models represent BC mixing state and also improve our understanding of BC global distributions, ultimately reducing uncertainties in BC radiative forcing predicted by climate models. Given that there are less than 20 studies that quantify $CT_{BC}$ using the LEO method, this study confirms that further measurements are necessary in order to narrow the quantitative bounds of rBC mixing state in our climate system, particularly since it has important implications on BC absorption enhancement and atmospheric lifetime.~~

**Data availability**

Processed data is available at the following Harvard Dataverse repository:
https://dataverse.harvard.edu/dataverse/catalina_rbc_2017_2018.

DOI citations to individual datasets:
Ko, Joseph, 2019, "Time Series Data for Catalina Island rBC Measurements 2017-2018",
https://doi.org/10.7910/DVN/UJAGHY, Harvard Dataverse, V1

Ko, Joseph, 2019, "rBC Coating Thickness from Catalina Island rBC Measurements 2017-2018",
https://doi.org/10.7910/DVN/AAYMHH, Harvard Dataverse, V2

Ko, Joseph, 2019, "rBC Size Distribution from Catalina Island rBC Measurements 2017-2018",
https://doi.org/10.7910/DVN/CIMVS4, Harvard Dataverse, V1

Due to the extremely large file sizes for the raw SP2 data, they are not publicly available but may be available upon request to the corresponding author.

## Video supplement

~~[DOI link to video supplement will be inserted once approved by TIB AV portal]~~CAMS model output showing the Camp Fire and Southern California plumes during the November 2017 campaign: ~~https://doi.org/10.5446/42893~~https://doi.org/10.5446/42893

NASA MODIS images showing the Camp Fire plume during the November 2017 campaign: https://doi.org/10.5446/42892

CAMS model output showing the Camp Fire plume reaching Southern California during the December 2018 campaign: https://doi.org/10.5446/42943

Large-scale circulation of aerosols off the California coast during the December 2018 Campaign: https://doi.org/10.5446/42942

## Supplement

[DOI link will be inserted once supplied by ACP]

## Competing interests

~~:~~The authors declare no competing interests.

## Acknowledgements

This research was supported by the National Science Foundation under CAREER grant CBET-1752522. This research was also funded in part by the Indo-US Science and Technology Forum.

We acknowledge the use of data from the European Centre for Medium-Range Weather Forecasts (ECMWF). Neither the European Commission nor ECMWF is responsible for any use that may be made of the information it contains.

We acknowledge the NOAA Air Resources Laboratory (ARL) for the provision of the HYSPLIT transport and dispersion model and/or READY website (http://www.ready.noaa.gov) used in this publication.

We acknowledge the use of imagery from the NASA Worldview application (https://worldview.earthdata.nasa.gov/), part of the NASA Earth Observing System Data and Information System (EOSDIS).

## References

Adachi, K., Chung, S. H. and Buseck, P. R.: Shapes of soot aerosol particles and implications for their effects on climate, J. Geophys. Res. Atmos., 115(15), 1–9, doi:10.1029/2009JD012868, 2010.

Adachi, K., Moteki, N., Kondo, Y. and Igarashi, Y.: Mixing states of light-absorbing particles measured using a transmission electron microscope and a single-particle soot photometer in Tokyo, Japan, J. Geophys. Res., 121(15), 9153–9164, doi:10.1002/2016JD025153, 2016.

Akagi, S. K., Craven, J. S., Taylor, J. W., McMeeking, G. R., Yokelson, R. J., Burling, I. R., Urbanski, S. P., Wold, C. E., Seinfeld, J. H., Coe, H., Alvarado, M. J. and Weise, D. R.: Evolution of trace gases and particles emitted by a chaparral fire in California, Atmos. Chem. Phys., 12(3), 1397–1421, doi:10.5194/acp-12-1397-2012, 2012.

Baumgardner, D., Kok, G. L. and Raga, G. B.: On the diurnal variability of particle properties related to light absorbing carbon in Mexico City, Atmos. Chem. Phys., 7(10), 2517–2526, doi:10.5194/acp-7-2517-2007, 2007.

Beccario, C.: earth.nullschool.net, last access: 26 August 2019.

Bond, T. C. and Bergstrom, R. W.: Light absorption by carbonaceous particles: An investigative review, Aerosol Sci. Technol., 40(1), 27–67, doi:10.1080/02786820500421521, 2006.

Bond, T. C., Doherty, S. J., Fahey, D. W., Forster, P. M., Berntsen, T., Deangelo, B. J., Flanner, M. G., Ghan, S., Kärcher, B., Koch, D., Kinne, S., Kondo, Y., Quinn, P. K., Sarofim, M. C., Schultz, M. G., Schulz, M., Venkataraman, C., Zhang, H., Zhang, S., Bellouin, N., Guttikunda, S. K., Hopke, P. K., Jacobson, M. Z., Kaiser, J. W., Klimont, Z., Lohmann, U.,

Schwarz, J. P., Shindell, D., Storelvmo, T., Warren, S. G. and Zender, C. S.: Bounding the role of black carbon in the climate system: A scientific assessment, J. Geophys. Res. Atmos., 118(11), 5380–5552, doi:10.1002/jgrd.50171, 2013.

CBS Los Angeles: Danielle Gersh's Weather Forecast (Dec. 20), https://youtu.be/p8dEJ-qoPwA, last access: 26 August 2019, 2017a.

CBS Los Angeles: Evelyn Taft's Weather Forecast (Dec. 20), https://youtu.be/gDH73gLbGDk, last access: 26 August 2019, 2017b.

CBS Los Angeles: Danielle Gersh's Weather Forecast (Dec. 21), https://youtu.be/j_0P09YZuKc, last access: 26 August 2019, 2017c.

CBS Los Angeles: Garth Kemp's Weather Forecast (Dec. 21), https://youtu.be/vpv65O1MP0A, last access: 26 August 2019, 2017d.

CBS Los Angeles: Evelyn Taft's Weather Forecast (Dec. 22), https://youtu.be/I7KkZiduQq4, last access: 26 August 2019, 2017e.

CBS Los Angeles: Markina Brown's Weather Forecast (Dec. 22), https://youtu.be/N7htXoFLVcw, last access: 26 August 2019, 2017f.

Cappa, C. D., Onasch, T. B., Massoli, P., Worsnop, D. R., Bates, T. S., Cross, E. S., Davidovits, P., Hakala, J., Hayden, K. L., Jobson, B. T., Kolesar, K. R., Lack, D. A., Lerner, B. M., Li, S. M., Mellon, D., Nuaaman, I., Olfert, J. S., Petäjä, T., Quinn, P. K., Song, C., Subramanian, R., Williams, E. J. and Zaveri, R. A.: Radiative absorption enhancements due to the mixing state of atmospheric black carbon, Science (80-. )., 337(6098), 1078–1081, doi:10.1126/science.1223447, 2012.

Cheng, Y., Li, S. M., Gordon, M. and Liu, P.: Size distribution and coating thickness of black carbon from the Canadian oil sands operations, Atmos. Chem. Phys., 18(4), 2653–2667, doi:10.5194/acp-18-2653-2018, 2018.

Dahlkötter, F., Gysel, M., Sauer, D., Minikin, A., Baumann, R., Seifert, P., Ansmann, A., Fromm, M., Voigt, C. and Weinzierl, B.: The Pagami Creek smoke plume after long-range transport to the upper troposphere over Europe ~~–~~ Aerosol properties and black carbon mixing state, Atmos. Chem. Phys., 14(12), 6111–6137, doi:10.5194/acp-14-6111-2014, 2014.

Gao, R. S., Schwarz, J. P., Kelly, K. K., Fahey, D. W., Watts, L. A., Thompson, T. L., Spackman, J. R., Slowik, J. G., Cross, E. S., Han, J. H., Davidovits, P., Onasch, T. B. and Worsnop, D. R.: A novel method for estimating light-scattering properties of soot aerosols using a modified single-particle soot photometer, Aerosol Sci. Technol., 41(2), 125–135, doi:10.1080/02786820601118398, 2007.

Garofalo, L. A., Pothier, M. A., Levin, E. J. T., Campos, T., Kreidenweis, S. M. and Farmer, D. K.: Emission and Evolution of Submicron Organic Aerosol in Smoke from Wildfires in the Western United States, ACS Earth Sp. Chem., 3(7), 1237–1247, doi:10.1021/acsearthspacechem.9b00125, 2019.

He, C., Liou, K. N., Takano, Y., Zhang, R., Levy Zamora, M., Yang, P., Li, Q. and Leung, L. R.: Variation of the radiative properties during black carbon aging: Theoretical and experimental intercomparison, Atmos. Chem. Phys., 15(20), doi:10.5194/acp-15-11967-2015, 2015.

Hughes, L. S., Allen, J. O., Bhave, P., Kleeman, M. J., Cass, G. R., Liu, D. Y., Fergenson, D. P., Morrical, B. D. and Prather, K. A.: Evolution of atmospheric particles along trajectories crossing the Los Angeles basin, Environ. Sci. Technol., 34(15), 3058–3068, doi:10.1021/es9908671, 2000.

IPCC: Climate Change 2013: The Physical Science Basis. Contribution of Working Group I to the Fifth Assessment Report of the Intergovernmental Panel on Climate Change, Cambridge University Press, Cambridge, United Kingdom and New York, NY, USA, https://doi.org/10.1017/CBO9781107415324, 2013.

Jaross, G.: OMPS-NPP L2 NM Ozone (O3) Total Column swath orbital V2, Greenbelt, MD, USA, Goddard Earth Sciences Data and Information Services Center (GES DISC), last access: 26 August 2019, doi:10.5067/0WF4HAAZ0VHK, 2017.

Johnson, G. R., Ristovski, Z. D., D'Anna, B. and Morawska, L.: Hygroscopic behavior of partially volatilized coastal marine aerosols using the volatilization and humidification tandem differential mobility analyzer technique, J. Geophys. Res. D Atmos., 110(20), 1–14, doi:10.1029/2004JD005657, 2005.

Justice, C. O., Giglio, L., Korontzi, S., Owens, J., Morisette, J., Roy, D., Descloitres, J., Alleaume, S., Petitcolin, F. and Kaufman, Y. J.: The MODIS fire products. Remote Sensing of Environment 83:244-262. doi:10.1016/S0034-4257(02)00076-7, 2002.

Knox, A., Evans, G. J., Brook, J. R., Yao, X., Jeong, C. H., Godri, K. J., Sabaliauskas, K. and Slowik, J. G.: Mass absorption cross-section of ambient black carbon aerosol in relation to chemical age, Aerosol Sci. Technol., 43(6), 522–532, doi:10.1080/02786820902777207, 2009.

Kondo, Y., Matsui, H., Moteki, N., Sahu, L., Takegawa, N., Kajino, M., Zhao, Y., Cubison, M. J., Jimenez, J. L., Vay, S., Diskin, G. S., Anderson, B., Wisthaler, A., Mikoviny, T., Fuelberg, H. E., Blake, D. R., Huey, G., Weinheimer, A. J., Knapp, D. J. and Brune, W. H.: Emissions of black carbon, organic, and inorganic aerosols from biomass burning in North America and Asia in 2008, J. Geophys. Res. Atmos., 116(8), 1–25, doi:10.1029/2010JD015152, 2011.

Krasowsky, T. S., McMeeking, G. R., Wang, D., Sioutas, C. and Ban-Weiss, G. A.: Measurements of the impact of atmospheric aging on physical and optical properties of ambient black carbon particles in Los Angeles, Atmos. Environ., 142, 496–504, doi:10.1016/j.atmosenv.2016.08.010, 2016.

Krasowsky, T. S., Mcmeeking, G. R., Sioutas, C. and Ban-Weiss, G.: Characterizing the evolution of physical properties and mixing state of black carbon particles: From near a major highway to the broader urban plume in Los Angeles, Atmos. Chem. Phys., 18(16), 11991–12010, doi:10.5194/acp-18-11991-2018, 2018.

Laborde, M., Mertes, P., Zieger, P., Dommen, J., Baltensperger, U. and Gysel, M.: Sensitivity of the Single Particle Soot Photometer to different black carbon types, Atmos. Meas. Tech., 5(5), 1031–1043, doi:10.5194/amt-5-1031-2012, 2012.

Laborde, M., Crippa, M., Tritscher, T., Jurányi, Z., Decarlo, P. F., Temime-Roussel, B., Marchand, N., Eckhardt, S., Stohl, A., Baltensperger, U., Prévôt, A. S. H., Weingartner, E. and Gysel, M.: Black carbon physical properties and mixing state in the European megacity Paris, Atmos. Chem. Phys., 13(11), 5831–5856, doi:10.5194/acp-13-5831-2013, 2013.

Liu, D., Allan, J. D., Young, D. E., Coe, H., Beddows, D., Fleming, Z. L., Flynn, M. J., Gallagher, M. W., Harrison, R. M., Lee, J., Prevot, A. S. H., Taylor, J. W., Yin, J., Williams, P. I. and Zotter, P.: Size distribution, mixing state and source apportionment of black carbon aerosol in London during winter time, Atmos. Chem. Phys., 14(18), 10061–10084, doi:10.5194/acp-14-10061-2014, 2014.

Lund, M. T., Samset, B. H., Skeie, R. B., Watson-Parris, D., Katich, J. M., Schwarz, J. P. and Weinzierl, B.: Short Black Carbon lifetime inferred from a global set of aircraft observations, npj Clim. Atmos. Sci., 1(1), 1–8, doi:10.1038/s41612-018-0040-x, 2018.

McMeeking, G. R., Hamburger, T., Liu, D., Flynn, M., Morgan, W. T., Northway, M., Highwood, E. J., Krejci, R., Allan, J. D., Minikin, A. and Coe, H.: Black carbon measurements in the boundary layer over western and northern Europe, Atmos. Chem. Phys., 10(19), 9393–9414, doi:10.5194/acp-10-9393-2010, 2010.

McMeeking, G. R., Good, N., Petters, M. D., McFiggans, G. and Coe, H.: Influences on the fraction of hydrophobic and hydrophilic black carbon in the atmosphere, Atmos. Chem. Phys., 11(10), 5099–5112, doi:10.5194/acp-11-5099-2011, 2011a.

McMeeking, G. R., Morgan, W. T., Flynn, M., Highwood, E. J., Turnbull, K., Haywood, J. and Coe, H.: Black carbon aerosol mixing state, organic aerosols and aerosol optical properties over the United Kingdom, Atmos. Chem. Phys., 11(17), 9037–9052, doi:10.5194/acp-11-9037-2011, 2011b.

Metcalf, A. R., Craven, J. S., Ensberg, J. J., Brioude, J., Angevine, W., Sorooshian, A., Duong, H. T., Jonsson, H. H., Flagan, R. C. and Seinfeld, J. H.: Black carbon aerosol over the Los Angeles Basin during CalNex, J. Geophys. Res. Atmos., 117(8), 1–24, doi:10.1029/2011JD017255, 2012.

Morgan, W. T., Allan, J. D., Bauguitte, S., Darbyshire, E., Flynn, M. J., Lee, J., Liu, D., Johnson, B., Haywood, J., Longo, K. M., Artaxo, P. E. and Coe, H.: Transformation and ageing of biomass burning carbonaceous aerosol over tropical South America from aircraft in situ measurements during SAMBBA, Atmos. Chem. Phys., 20(9), 5309–5326, doi:10.5194/acp-20-5309-2020, 2020.

Moteki, N., Kondo, Y., Miyazaki, Y., Takegawa, N., Komazaki, Y., Kurata, G., Shirai, T., Blake, D. R., Miyakawa, T. and Koike, M.: Evolution of mixing state of black carbon particles: Aircraft measurements over the western Pacific in March 2004, Geophys. Res. Lett., 34(11), doi:10.1029/2006GL028943, 2007.

Moteki, N. and Kondo, Y.: Method to measure time-dependent scattering cross sections of particles evaporating in a laser beam, J. Aerosol Sci., 39(4), 348–364, doi:10.1016/j.jaerosci.2007.12.002, 2008.

Moteki, N., Kondo, Y., Oshima, N., Takegawa, N., Koike, M., Kita, K., Matsui, H. and Kajino, M.: Size dependence of wet removal of black carbon aerosols during transport from the boundary layer to the free troposphere, Geophys. Res. Lett., 39(13), 2–5, doi:10.1029/2012GL052034, 2012.

Moteki, N., Kondo, Y., & Adachi, K.: Identification by single-particle soot photometer of black carbon particles attached to other particles: Laboratory experiments and ground observations in Tokyo. Geophys. Res. Lett., *119*(2), 1031–1043. ~~https://doi.org/10.1002/2013JD020655~~https://doi.org/10.1002/2013JD020655, 2014.

Pan, X., Kanaya, Y., Taketani, F., Miyakawa, T., Inomata, S., Komazaki, Y., Tanimoto, H., Wang, Z., Uno, I. and Wang, Z.: Emission characteristics of refractory black carbon aerosols from fresh biomass burning: A perspective from laboratory experiments, Atmos. Chem. Phys., 17(21), 13001–13016, doi:10.5194/acp-17-13001-2017, 2017.

~~Ramanathan, V. and Carmichael, G.: Global and regional climate changes due to black carbon, Nat. Geosci., 1(4), 221–227, doi:10.1038/ngeo156, 2008.~~

Perring, A. E., Schwarz, J. P., Markovic, M. Z., Fahey, D. W., Jimenez, J. L., Campuzano-Jost, P., Palm, B. D., Wisthaler, A., Mikoviny, T., Diskin, G., Sachse, G., Ziemba, L., Anderson, B., Shingler, T., Crosbie, E., Sorooshian, A., Yokelson, R. and Gao, R. S.: In situ measurements of water uptake by black carbon-containing aerosol in wildfire plumes, J. Geophys. Res., 122(2), doi:10.1002/2016JD025688, 2017.~~,~~

Ramanathan, V. and Carmichael, G.: Global and regional climate changes due to black carbon, Nat. Geosci., 1(4), 221–227, doi:10.1038/ngeo156, 2008.

Sahu, L. K., Kondo, Y., Moteki, N., Takegawa, N., Zhao, Y., Cubison, M. J., Jimenez, J. L., Vay, S., Diskin, G. S., Wisthaler, A., Mikoviny, T., Huey, L. G., Weinheimer, A. J. and Knapp, D. J.: Emission characteristics of black carbon in anthropogenic and biomass burning plumes over California during ARCTAS-CARB 2008, J. Geophys. Res. Atmos., 117(16), 1–20, doi:10.1029/2011JD017401, 2012.

Schwarz, J. P., Gao, R. S., Fahey, D. W., Thomson, D. S., Watts, L. A., Wilson, J. C., Reeves, J. M., Darbeheshti, M., Baumgardner, D. G., Kok, G. L., Chung, S. H., Schulz, M., Hendricks, J., Lauer, A., Kärcher, B., Slowik, J. G., Rosenlof, K. H., Thompson, T. L., Langford, A. O., Loewenstein, M. and Aikin, K. C.: Single-particle measurements of midlatitude black carbon and light-scattering aerosols from the boundary layer to the lower stratosphere, J. Geophys. Res. Atmos., 111(16), doi:10.1029/2006JD007076, 2006.

Schwarz, J. P., Gao, R. S., Spackman, J. R., Watts, L. A., Thomson, D. S., Fahey, D. W., Ryerson, T. B., Peischl, J., Holloway, J. S., Trainer, M., Frost, G. J., Baynard, T., Lack, D. A., de Gouw, J. A., Warneke, C. and Del Negro, L. A.:

Measurement of the mixing state, mass, and optical size of individual black carbon particles in urban and biomass burning emissions, Geophys. Res. Lett., 35(13), 1–5, doi:10.1029/2008GL033968, 2008a.

Schwarz, J. P., Spackman, J. R., Fahey, D. W., Gao, R. S., Lohmann, U., Stier, P., Watts, L. A., Thomson, D. S., Lack, D. A., Pfister, L., Mahoney, M. J., Baumgardner, D., Wilson, J. C. and Reeves, J. M.: Coatings and their enhancement of black carbon light absorption in the tropical atmosphere, J. Geophys. Res. Atmos., 113(3), 1–10, doi:10.1029/2007JD009042, 2008b.

Schwarz, J. P., Spackman, J. R., Gao, R. S., Perring, A. E., Cross, E., Onasch, T. B., Ahern, A., Wrobel, W., Davidovits, P., Olfert, J., Dubey, M. K., Mazzoleni, C. and Fahey, D. W.: The detection efficiency of the single particle soot photometer, Aerosol Sci. Technol., 44(8), 612–628, doi:10.1080/02786826.2010.481298, 2010.

Schroeder, W., Oliva, P., Giglio, L., & Csiszar, I. A.: The New VIIRS 375 m active fire detection data product: algorithm description and initial assessment. Remote Sensing of Environment, 143, 85-96. doi:10.1016/j.rse.2013.12.008, 2014.

Sedlacek, A. J., Lewis, E. R., Kleinman, L., Xu, J. and Zhang, Q.: Determination of and evidence for non-core-shell structure of particles containing black carbon using the Single-Particle Soot Photometer (SP2), Geophys. Res. Lett., 39(6), 2–7, doi:10.1029/2012GL050905, 2012.

Sedlacek, A. J., Lewis, E. R., Onasch, T. B., Lambe, A. T. and Davidovits, P.: Investigation of Refractory Black Carbon-Containing Particle Morphologies Using the Single-Particle Soot Photometer (SP2), Aerosol Sci. Technol., 49(10), 872–885, doi:10.1080/02786826.2015.1074978, 2015.

Sedlacek, A. J., Lewis, E. R., Onasch, T. B., Kleinman, L.: Improving our Understanding of Light Absorbing Aerosols from Biomass Burning. Abstract [A23E-02] presented at 2019 Fall Meeting, AGU, San Francisco, CA, 9-13 Dec., 2019.

Shiraiwa, M., Kondo, Y., Moteki, N., Takegawa, N., Miyazaki, Y. and Blake, D. R.: Evolution of mixing state of black carbon in polluted air from Tokyo, Geophys. Res. Lett., 34(16), 2–6, doi:10.1029/2007GL029819, 2007.

Shiraiwa, M., Kondo, Y., Moteki, N., Takegawa, N., Sahu, L. K., Takami, A., Hatakeyama, S., Yonemura, S. and Blake, D. R.: Radiative impact of mixing state of black carbon aerosol in Asian outflow, J. Geophys. Res. Atmos., 113(24), 1–13, doi:10.1029/2008JD010546, 2008.

Slowik, J. G., Cross, E. S., Han, J. H., Davidovits, P., Onasch, T. B., Jayne, J. T., Williams, L. R., Canagaratna, M. R., Worsnop, D. R., Chakrabarty, R. K., Moosmüller, H., Arnott, W. P., Schwarz, J. P., Gao, R. S., Fahey, D. W., Kok, G. L. and Petzold, A.: An Inter-Comparison of Instruments Measuring Black Carbon Content of Soot Particles, Aerosol Sci. Technol., 41(3), 295–314, doi:10.1080/02786820701197078, 2007.

Soleimanian, E., Mousavi, A., Taghvaee, S., Shafer, M. M. and Sioutas, C.: Impact of secondary and primary particulate matter (PM) sources on the enhanced light absorption by brown carbon (BrC) particles in central Los Angeles, Sci. Total Environ., 705, 135902, doi:10.1016/j.scitotenv.2019.135902, 2020.

Stein, A. F., Draxler, R. R., Rolph, G. D., Stunder, B. J. B., Cohen, M. D. and Ngan, F.: Noaa's hysplit atmospheric transport and dispersion modeling system, Bull. Am. Meteorol. Soc., 96(12), 2059–2077, doi:10.1175/BAMS-D-14-00110.1, 2015.

Stephens, M., Turner, N. and Sandberg, J.: Particle identification by laser-induced incandescence in a solid-state laser cavity, Appl. Opt., 42(19), 3726, doi:10.1364/ao.42.003726, 2003.

Subramanian, R., Kok, G. L., Baumgardner, D., Clarke, A., Shinozuka, Y., Campos, T. L., Heizer, C. G., Stephens, B. B., De Foy, B., Voss, P. B. and Zaveri, R. A.: Black carbon over Mexico: The effect of atmospheric transport on mixing state, mass absorption cross-section, and BC/CO ratios, Atmos. Chem. Phys., 10(1), 219–237, doi:10.5194/acp-10-219-2010, 2010.

Taylor, J. W., Allan, J. D., Allen, G., Coe, H., Williams, P. I., Flynn, M. J., Le Breton, M., Muller, J. B. A., Percival, C. J., Oram, D., Forster, G., Lee, J. D., Rickard, A. R., Parrington, M., and Palmer, P. I.: Size-dependent wet removal of black carbon in Canadian biomass burning plumes, Atmos. Chem. Phys., 14, 13755–13771, https://doi.org/10.5194/acp-14-13755-2014, 2014.

Todey, D. P., Herzmann, D. E., and Takle, G. S.: The Iowa Environmental Mesonet – combining networks into a single network, Preprints 6th Symposium on Integrated Observing Systems, Annual Meeting of the American Meteorological Society, 14–17 January 2002, Orlando, FL, USA, 2002

Torres, O.: OMI/Aura Near UV Aerosol Optical Depth and Single Scattering Albedo 1-orbit L2 Swath 13x24 km V003, Greenbelt, MD, USA, Goddard Earth Sciences Data and Information Services Center (GES DISC), last access: 26 August 2019, 10.5067/Aura/OMI/DATA2004, 2006.

Wang, Q., Huang, R. J., Cao, J., Han, Y., Wang, G., Li, G., Wang, Y., Dai, W., Zhang, R. and Zhou, Y.: Mixing state of black carbon aerosol in a heavily polluted urban area of China: Implications for light absorption enhancement, Aerosol Sci. Technol., 48(7), 689–697, doi:10.1080/02786826.2014.917758, 2014.

Wang, Q., Cao, J., Han, Y., Tian, J., Zhang, Y., Pongpiachan, S., Zhang, Y., Li, L., Niu, X., Shen, Z., Zhao, Z., Tipmanee, D., Bunsomboonsakul, S., Chen, Y. and Sun, J.: Enhanced light absorption due to the mixing state of black carbon in fresh biomass burning emissions, Atmos. Environ., 180(December 2017), 184–191, doi:10.1016/j.atmosenv.2018.02.049, 2018.

World Health Organization (WHO): Health effects of black carbon, ISBN: 9789289002653, available at: http://www.euro.who.int/__data/assets/pdf_file/0004/162535/e96541.pdf, last access: 26 August 2019, 2012.

Zhang, J., Liu, J., Tao, S. and Ban-Weiss, G. A.: Long-range transport of black carbon to the Pacific Ocean and its dependence on aging timescale, Atmos. Chem. Phys., 15(20), 11521–11535, doi:10.5194/acp-15-11521-2015, 2015.